

UC Riverside

UC Riverside Electronic Theses and Dissertations

Title

Identifying and Characterizing TANGLED1 Protein Interactions and Their Roles in Division Plane Orientation in Arabidopsis thaliana

Permalink

<https://escholarship.org/uc/item/66x9v06w>

Author

Mills, Alison Margaret

Publication Date

2022

Copyright Information

This work is made available under the terms of a Creative Commons Attribution-NonCommercial-NoDerivatives License, available at <https://creativecommons.org/licenses/by-nc-nd/4.0/>

Peer reviewed|Thesis/dissertation

UNIVERSITY OF CALIFORNIA
RIVERSIDE

Identifying and Characterizing TANGLED1 Protein Interactions and Their Roles
in Division Plane Orientation in *Arabidopsis thaliana*

A Dissertation submitted in partial satisfaction
of the requirements for the degree of

Doctor of Philosophy

in

Biochemistry and Molecular Biology

by

Alison Margaret Mills

June 2022

Dissertation Committee:

Dr. Carolyn Rasmussen, Chairperson

Dr. Patricia Springer

Dr. Meng Chen

Copyright by
Alison Margaret Mills
2022

The Dissertation of Alison Margaret Mills is approved by:

Committee Chairperson

University of California, Riverside

ACKNOWLEDGEMENTS

In accordance with graduate program guidelines, Chapter 2, in full, is a reprint of a published article in the Journal of Microbiology & Biology Education (<https://journals.asm.org/journal/jmbe>): Mills, A., Jaganatha, V., Cortez, A., Guzman, M., Burnette, J.M., Collin, M., Lopez-Lopez, B., Wessler, S.R., Van Norman, J.M., Nelson, D.C., and Rasmussen, C.G. (2021). A Course-Based Undergraduate Research Experience in CRISPR-Cas9 Experimental Design to Support Reverse Genetic Studies in *Arabidopsis thaliana*. Journal of Microbiology & Biology Education 22. DOI: 10.1128/jmbe.00155-21. This article is licensed under an Open Access (CC BY-NC-ND) license. To view a copy of this license, visit <https://creativecommons.org/licenses/by-nc-nd/4.0/>.

Initial Research Evaluation Committee:

Carolyn G. Rasmussen

Paul Larsen

Meng Chen

Qualifying Exam Committee:

Carolyn G. Rasmussen

Seán O'Leary

Meng Chen

Julia Bailey-Serres

Patricia Springer

Dissertation Committee:

Carolyn G. Rasmussen

Patricia Springer

Meng Chen

Funding:

NSF 1716972

NSF-CAREER-MCB 1942734

USDA-NIFA-CA-R-BPS-5108-H

AUTHOR CONTRIBUTIONS

CHAPTER 1

Alison Mills wrote this chapter with comments and edits from Carolyn G. Rasmussen.

CHAPTER 2

Alison Mills wrote this manuscript with comments and edits from all authors. Initial protocols for guide RNA design and cloning of CRISPR-Cas9 constructs were developed by David C. Nelson. Michael Guzman created Figure 1. Alison Mills, Venkateswari Jagantha, James M. Burnette III, and Alejandro Cortez implemented the CURE in BIOL 020 Dynamic Genome classes at UC Riverside.

CHAPTER 3

Alison Mills and Carolyn G. Rasmussen designed research. Victoria Morris designed and created TANGLED1 alanine scanning mutagenesis constructs for yeast two-hybrid. Alison Mills performed research. Alison Mills and Carolyn G. Rasmussen wrote and edited this manuscript.

CHAPTER 4

Alison Mills and Carolyn G. Rasmussen designed research. Alison Mills performed research and wrote this manuscript with comments and edits from Carolyn G. Rasmussen.

ABSTRACT OF THE DISSERTATION

Identifying and Characterizing TANGLED1 Protein Interactions and Their Roles
in Division Plane Orientation in *Arabidopsis thaliana*

by

Alison Margaret Mills

Doctor of Philosophy, Graduate Program in Biochemistry and Molecular Biology
University of California, Riverside, June 2022
Dr. Carolyn G. Rasmussen, Chairperson

TANGLED1 (TAN1) is a microtubule binding, division-site-localized protein that plays a role in division plane orientation in plants. Although many potential TAN1 interacting proteins have been identified, how TAN1 interacts with other proteins to ensure correct division positioning is not well understood. *Arabidopsis thaliana tan1* single mutants have very weak division plane orientation defects. However mutating a second gene that encodes the unrelated, division-site-localized protein AUXIN-INDUCED-IN-ROOT-CULTURES9 (AIR9), results in strong synthetic phenotypes in the *tan1 air9* double mutant including stunted growth, misoriented divisions, and increased cell file rotation. I designed a course-based undergraduate research experience as a high-throughput strategy to screen for TAN1 interactors. Students participated in a sensitized mutagenesis screen by learning how to use CRISPR-Cas9 technology to create gene knockouts of

candidate TAN1 interactor genes in *air9* single mutant Arabidopsis plants. I also investigated the functional role of TAN1 interaction with the division-site-localized kinesin PHRAGMOPLAST ORIENTING KINESIN1 (POK1). I found that POK1 was mislocalized in the *tan1 air9* double mutant, which suggests that AIR9 and TAN1 are involved in POK1 localization to the division site. Using a yeast two-hybrid screen, I identified POK1 interaction sites within the first 132 highly conserved amino acids of TAN1. When mutagenized TAN1 that lost interaction with POK1 in the yeast two-hybrid system was introduced into the *tan1 air9* double mutant, it failed to fully rescue phragmoplast positioning defects and disrupted TAN1 and POK1 recruitment to the division site during metaphase and early telophase. This demonstrated that TAN1 interaction with POK1 is important for stabilizing both proteins at the division site to ensure correct phragmoplast guidance during telophase, and that there are likely other unidentified proteins that further stabilize TAN1 and POK1 at the division site. Finally, I investigated the cause of defects in the nondividing cells of *tan1 air9* double mutants, by driving *TAN1* expression in the *tan1 air9* double mutant using the well characterized G2/M-phase specific promoter of the *KNOLLE* gene. *KNOLLE* driven *TAN1* fully rescued the *tan1 air9* phenotypes, suggesting that defects that occur during mitosis can influence the organization of nondividing cells.

TABLE OF CONTENTS

Chapter 1: Protein-protein interactions with division site localized proteins are crucial for correct division plane orientation in plants 1

Abstract	1
Introduction	1
Research outline	10
References	11

Chapter 2: A Course-Based Undergraduate Research Experience in CRISPR-Cas9 Experimental Design to Support Reverse Genetic Studies in *Arabidopsis thaliana*..... 17

Abstract	17
Introduction	18
Intended audience.....	24
Prerequisite knowledge	24
Learning time	25
Learning outcomes.....	25
Procedure.....	28
Student and faculty instructions	28
Remote-learning CURE	28
In-person CURE.....	31
Safety concerns	34

Discussion	35
Evidence of student learning.....	35
Possible modifications	37
Challenges specific to remote-learning classes	38
Acknowledgments	38
Supplemental materials.....	39
References.....	40
 Chapter 3: The localization of PHRAGMOPLAST ORIENTING KINESIN1 at the division site depends on two microtubule binding proteins TANGLED1 and AUXIN-INDUCED-IN-ROOT-CULTURES9 in Arabidopsis	 44
Abstract.....	44
Introduction	45
Results	49
Either TAN1 or AIR9 is sufficient to recruit and maintain POK1 at the division site	49
Amino acids 1-132 of TAN1 Rescue the <i>tan1 air9</i> Double Mutant.....	55
Disrupting TAN1-POK1 interaction alters TAN1 and POK1 localization to the division site and reduces <i>tan1 air9</i> rescue	60
Discussion.....	75
Materials and methods.....	84
Acknowledgements	92

Supplemental figures and tables	93
References.....	103
Chapter 4: Action at a distance: Defects in division plane positioning in the root meristematic zone affect cell organization in the differentiation zone	108
Abstract.....	108
Introduction	108
Results and discussion.....	113
Materials and methods.....	128
Acknowledgements	134
Supplemental figures and tables	135
References.....	140
Chapter 5: Discussion and Future Directions	149
Teaching students molecular biology while conducting a high throughput screen for TAN1 interactors	150
Live cell imaging of fluorescent tagged proteins in the <i>tan1 air9</i> double mutant	152
Yeast two-hybrid as a tool to identify protein interaction motifs.....	158
Determining if defects in the nondividing cells of the <i>tan1 air9</i> double mutant are caused by cell wall integrity responses	164
References.....	167

LIST OF FIGURES

Figure 2.1: Strategy to identify genetic modifiers through CRISPR-Cas9.....	21
Figure 2.2: Timeline of the CURE.....	23
Figure 3.1: TAN1 and AIR9 together promote POK1 maintenance at the division site.....	53
Figure 3.2: <i>p35S:TAN1₁₋₁₃₂-YFP</i> rescues Arabidopsis <i>tan1 air9</i> double mutant phenotypes.....	58
Figure 3.3: Division site localization during telophase is common for TAN1 ₁₋₁₃₂ -YFP but rare for TAN1(28-33A) ₁₋₁₃₂ -YFP in <i>tan1 air9</i> double mutants.....	59
Figure 3.4: <i>p35S:TAN1(28-33A)₁₋₁₃₂-YFP</i> partially rescues <i>tan1 air9</i> double mutant phenotypes.....	63
Figure 3.5: Full length <i>TAN1</i> with alanine substitutions replacing amino acids 28 to 33 (<i>p35S:YFP-TAN1(28-33A)</i>) mostly rescues the <i>tan1 air9</i> double mutant. .	67
Figure 3.6: CFP-TAN1(28-33A) and YFP-POK1 exhibit impaired recruitment to the division site in the <i>tan1 air9</i> double mutant.....	71
Figure 3.7: A speculative model on TAN1, AIR9, and POK1 interactions to ensure correct division plane orientation.....	78
Supplementary Figure 3.1. <i>p35S:TAN1₁₋₁₃₂-YFP tan1 air9</i> lines show significant rescue compared to untransformed <i>tan1 air9</i> double mutants.....	94
Supplementary Figure 3.2. Yeast two-hybrid interactions between POK1 (C-terminal amino acids 1683-2066, as previously described (Müller et al., 2006; Rasmussen et al., 2011; Lipka et al., 2014)) and TAN1 ₁₋₁₃₂ alanine scanning constructs.....	95
Supplementary Figure 3.3. Yeast two-hybrid interactions between TAN1 and POK1 (C-terminal amino acids 1683-2066, as previously described (Müller et al., 2006; Rasmussen et al., 2011; Lipka et al., 2014)) and TAN1(28-33A).	96
Supplementary Figure 3.4. <i>p35S:YFP-TAN1(28-33A) tan1 air9</i> lines show significant rescue compared to untransformed <i>tan1 air9</i> , but less accumulation of YFP-TAN1(28-33A) during telophase.....	97

Supplementary Figure 3.5. YFP-TAN1(28-33A) localizes to the division site in preprophase or prophase and with reduced fluorescence during telophase in <i>tan1 air9</i> mutants.....	99
Supplementary Figure 3.6. A model of POK1 localization in <i>tan1</i> and <i>air9</i> single mutants.....	100
Supplementary Figure 3.7. Alignments of amino acids 1-55 of <i>A. thaliana</i> TAN1 with TAN1 homologs from other plant species.....	101
Figure 4.1: The TAN1 native promoter fused to TAN1 (<i>pTAN:CFP-TAN1</i>) rescues the <i>tan1 air9</i> double mutant.....	116
Figure 4.2: Full rescue of the <i>tan1 air9</i> double mutant with the G2/M-specific <i>KNOLLE</i> promoter fused to TAN1 (<i>pKN:TAN1-YFP</i>).....	121
Figure 4.3: Comparison between <i>KNOLLE</i> promoter driven (<i>pKN:TAN1-YFP</i>) and 35S driven TAN1 (<i>p35S:TAN1-YFP</i>) rescue of the <i>tan1 air9</i> double mutants. .	123
Figure 4.4: Comparison of TAN1-YFP fluorescence intensity when driven by the constitutive 35S promoter (<i>p35S:TAN1-YFP</i>) and G2/M-specific <i>KNOLLE</i> promoter (<i>pKN:TAN1-YFP</i>) in <i>tan1 air9</i> roots.....	125
Supplementary Figure 4.1. <i>TAN1-YFP</i> expressed by its native promoter (<i>pTAN:TAN1-YFP</i>) rescues <i>tan1 air9</i> double mutant root growth.....	135
Supplementary Figure 4.2. <i>pKN:TAN1-YFP tan1 air9</i> lines show significant rescue compared to untransformed <i>tan1 air9</i>	137
Supplementary Figure 4.3. Division site localization of TAN1-YFP driven by the <i>KNOLLE</i> promoter (<i>pKN:TAN1-YFP</i>) and CFP-TAN1 driven by the <i>TAN1</i> promoter (<i>pTAN:CFP-TAN1</i>) in <i>tan1 air9</i> double mutants.....	138
Figure 5.1: TAN1 and AIR9 promote POK2 maintenance at the division site...	156
Figure 5.2: Yeast two-hybrid testing pAD- <i>POK2</i> 2083-2771 interaction with pBD- <i>TAN1</i> and alanine scanning pAS- <i>TAN1</i> ₁₋₁₃₂ constructs.....	159
Figure 5.3: TAN1(58-63A) partly rescues the <i>tan1 air9</i> double mutant and localizes to the division site during preprophase/prophase, and telophase.....	163

LIST OF TABLES

Table 2.1: Assessment of key learning outcomes.	26
Table 3.1: YFP-POK1 division site and phragmoplast midline accumulation in wild-type, <i>tan1</i> , <i>air9</i> , and <i>tan1 air9</i> double mutant plants.	54
Table 3.2. POK1 and TAN1 or TAN1(28-33) localization to the division site in <i>tan1 air9</i> double mutants.	72
Supplementary Table 3.1. Primers used for cloning and genotyping.	102
Supplementary Table 4.1. Primers used for cloning and genotyping.....	139

Chapter 1: Protein-protein interactions with division site localized proteins are crucial for correct division plane orientation in plants

ABSTRACT

Tight regulation of division plane orientation is critical in plants because their cells are confined by cell walls. Land plants have additional division structures compared to animals to establish the placement of and then correctly construct cell walls during cell division. Numerous proteins, including many that colocalize with division structures and/or the division site, play key roles in division plane orientation. Many of these proteins interact with one another and are dependent on protein-protein interactions for their correct localization and/or function. The mechanism by which precise protein-protein interactions preserve and convey the correct location for the new cell wall established in preprophase to the cell wall building machinery in telophase is an active area of investigation. Here I outline a strategy for dissecting protein-protein interactions involved in division plane orientation by identifying and investigating interactors of the key division-site-localized protein, TANGLED1.

INTRODUCTION

The morphology, development, and growth of multicellular organisms relies on the correct placement of cell divisions. This is especially critical in plants where the shape and position of cells is dependent on their cell walls, which in turn

influences tissue and organ morphology (Rasmussen and Bellinger, 2018; Livanos and Müller, 2019; Facette et al., 2019). During symmetric proliferative divisions, the division plane is typically the minimal area that equally divides the cell volume, although cell shape and mechanical stresses also influence the precise positioning of the division plane (Martinez et al. 2018; Besson and Dumais 2011; Hamant et al. 2008; Landrein and Hamant 2013). Asymmetric division positioning, responsible for generating daughter cells with different cell fates, is controlled by polarity cues that are dependent on mechanical cues from neighboring cells and hormonal signals, which are perceived by receptor-like kinases (Facette et al. 2015; Yi and Goshima 2022; Bringmann and Bergmann 2017; Lucas et al. 2013). Nuclear migration during S and G2 also plays a role in division plane determination (Mineyuki et al. 1991; Wada 2018; Yi and Goshima 2020).

Cellular structures unique to land plants also function to ensure the correct placement and construction of nascent cell walls when undergoing cell division. The preprophase band (PPB) defines the position of the new cell wall during G2. The PPB is a ring of microtubules, microfilaments, and proteins that form at the cortex of the cell around the premitotic nucleus (Smertenko et al., 2017). Although the PPB marks the predicted location of the new cell wall, evidence suggests that the PPB is not required for division site determination (Schaefer et al. 2017). The microtubule ring of the PPB disassembles upon entry into

prometaphase, however a number of division site localized proteins, including TANGLED1 (TAN1), PHRAGMOPLAST ORIENTING KINESIN1 (POK1), POK2, MICROTUBULE-ASSOCIATED PROTEIN 65-4 (MAP65-4), RAN GTPase ACTIVATING PROTEIN (RAN-GAP), and KINESIN-LIKE CALMODULIN BINDING PROTEIN (KCBP) remain at the division site throughout cell division (Rasmussen and Bellinger, 2018; Walker et al., 2007; Lipka et al., 2014; Herrmann et al., 2018; Li et al., 2017; Buschmann et al., 2015; Xu et al., 2008). Proteins associated with the cortical division site are thought to preserve the “molecular memory” of the correct cell wall location. During telophase and cytokinesis the phragmoplast, an anti-parallel array of microtubules, directs vesicles carrying cell plate components to construct the new cell wall beginning in the middle of the cell and expanding outwards to contact the cortical division site originally marked by the PPB (Müller and Jürgens, 2016).

TAN1 plays a role in guiding the phragmoplast to the correct division site. In maize, TAN1 and other division site localized proteins organize the telophase cortical microtubule array, which is incorporated into the phragmoplast to direct its movement along the cortical division site (Bellinger et al., 2021). It is likely that this process is mediated by direct TAN1 interaction with microtubules because TAN1 was demonstrated to bind and bundle microtubules in vitro (Martinez et al., 2020). TAN1 recruitment to the division site is dynamic and is mediated by different regions of the TAN1 protein. Amino acids 126-229 of TAN1 specifically

localize to the PPB while the highly conserved first 132 amino acids of TAN1 (*TAN1*₁₋₁₃₂) localize to the division site during telophase (Rasmussen et al., 2011). *tan1* maize mutants have stunted growth and misoriented divisions (Cleary and Smith, 1998). However, *tan1 Arabidopsis thaliana* (*Arabidopsis*) mutants grow as well as wild-type plants and have very minor division plane defects (Walker et al., 2007). AUXIN-INDUCED-IN-ROOT-CULTURES9 (AIR9), a microtubule-associated protein that is localized to the division site, is unrelated to TAN1. AIR9 was initially identified in a screen for auxin-inducible genes, although the relevance of its auxin inducibility remains unknown (Neuteboom et al., 1999). AIR9 was later isolated again in a proteomic experiment to identify plant microtubule-associated proteins. AIR9 associates with cortical microtubules, and during cell division AIR9 colocalizes with the PPB but is lost from the division site after PPB disassembly. AIR9 then reappears at the division site as the cell plate fuses with the cortical division site (Buschmann et al., 2006). Even though *air9 Arabidopsis* single mutants have no discernible phenotypic defects, AIR9 is likely a key component of the cortical division site. AIR9 interacts with division-site-localized KCBP, and AIR9 fails to localize to ectopic cell plate fusion sites outside of the division site predicted by the PPB (Buschmann et al. 2015). *tan1 air9 Arabidopsis* double mutants have strong synthetic mutant phenotypes including stunted growth, division plane orientation defects, and increased cell file twisting in nondividing cells (Mir et al., 2018). Division plane orientation defects in maize *tan1* single mutants and *Arabidopsis tan1 air9*

double mutants are at least partially due to phragmoplast guidance defects where the phragmoplast fails to construct the new cell wall at the location predicted by the PPB (Martinez et al. 2017; Mir et al. 2018). The *tan1 air9* double mutant has been an invaluable tool for studying TAN1 in Arabidopsis by allowing a variety of TAN1 constructs to be examined for changes in localization and ability to rescue double mutant phenotypes. Both full-length *TAN1-YFP* or a truncated protein containing only the first 132 amino acids of TAN1 (*TAN1₁₋₁₃₂-YFP*) driven by the constitutively active viral Cauliflower mosaic *CaMV35S* promoter are sufficient to rescue the *tan1 air9* double mutant (Mills et al., 2022; Mir et al., 2018). These results suggest that TAN1₁₋₁₃₂ and its presence at the division site during telophase are critical for TAN1 function.

In addition to being the most conserved region of TAN1, *TAN1₁₋₁₃₂* has also been shown to mediate TAN1 interaction with many other proteins. A yeast two-hybrid screen of an Arabidopsis cDNA library showed that TAN1₁₋₁₃₂ reliably interacts with RAB GTPase-activating protein, CALCIUM-DEPENDENT PROTEIN KINASE1 ADAPTOR PROTEIN2, and MYOSIN BINDING PROTEIN3 (Su, 2012). POK1 and POK2 are division-site localized kinesin-12 proteins that were identified through their interaction with full-length TAN1 and TAN1₁₋₁₃₂ (Müller et al. 2006; Rasmussen et al. 2011; unpublished data). This suggests that TAN1₁₋₁₃₂ may be a hub for protein interactions that are involved in division plane

orientation. The significance of these protein-protein interactions and whether they are essential for correct division plane orientation requires further study.

In addition to known TAN1 interacting proteins, there are over 100 proteins that are candidate TAN1 interactors based on their function in division plane orientation or localization to the division site. This makes identifying novel TAN1 interactors a daunting task. Crossing in or generating mutants for candidate genes in the *air9* single mutant can be done as a sensitized screen for TAN1 interactors. If a double mutant combination with *air9* and a loss-of-function candidate gene exhibits division plane defects similar to the *tan1 air9* double mutant, it would suggest that the candidate gene functions closely with TAN1 in division plane orientation. However, the large number of candidates makes conducting such a screen difficult.

Having undergraduates assist in generating mutant combinations is one potential solution to make screening for TAN1 interacting proteins higher throughput. In partnership with BIOL 020 Dynamic Genome at UC Riverside, we successfully implemented a course-based undergraduate research experience (CURE) where students designed gene knockouts for candidate genes (Mills et al., 2021). Students were taught how CRISPR-Cas9 can be used to create gene deletions and how to design guide RNAs that target a single gene. The students then cloned their guide RNAs into a CRISPR-Cas9 construct and introduced the

construct into *air9* single mutants by *Agrobacterium*-mediated floral dip. During the Fall quarter of 2021, two class sections of 45 students total successfully dipped CRISPR-Cas9 constructs for 39 candidate TAN1 interactor genes. There is also the potential for future classes, or undergraduate researchers, to screen the seeds of these dipped plants for transformants and identify and characterize the double mutant phenotypes. Identifying genes that function in the same pathway as TAN1 will further our understanding of TAN1 function and potentially reveal proteins that have a yet uncharacterized role in division plane orientation.

Of the known TAN1 interacting proteins, POK1 and POK2 are of particular interest because they are involved in correct phragmoplast guidance and maintaining TAN1 at the division site. *pok1 pok2* double mutants have severe phragmoplast guidance defects and fail to maintain TAN1 at the division site after PPB disassembly (Lipka et al. 2014). Similarly, POK1 and POK2 colocalize with the PPB in the *tan1 air9* double mutant but are then lost from the division site after PPB disassembly (Mills et al., 2022; unpublished data). Together these data suggest that POK1, POK2, AIR9, and TAN1 interact to stabilize one another at the division site to ensure correct division plane orientation. I investigated TAN1 and POK1 interaction by identifying regions within TAN1₁₋₁₃₂ that mediate interaction with POK1 using alanine scanning mutagenesis followed by screening for loss of TAN1₁₋₁₃₂-POK1 interaction using a yeast two-hybrid assay. Introducing TAN1₁₋₁₃₂ with a mutagenized interaction site into the *tan1 air9*

double mutant resulted in intermediate rescue of root growth but failed to rescue phragmoplast positioning. Mutagenized TAN1₁₋₁₃₂-YFP also showed reduced accumulation at the division site during telophase. However, full-length TAN1 with the same mutation fully rescued the *tan1 air9* double mutant, except for minor phragmoplast positioning defects. POK1 and mutagenized full-length TAN1 also failed to be maintained at the division site in some *tan1 air9* metaphase and early telophase cells. This suggests that TAN1 and POK1 interaction promotes, but is not strictly necessary for, stabilization of both proteins at the division site in the absence of AIR9. This observation also suggests that there are other unidentified protein(s) that interact with TAN1 and POK1 and are involved in the maintenance and/or recruitment of TAN1 and POK1 to the division site. These results highlight the need to identify and determine how proteins interact with one another at the division site.

Finally, I investigated the cause of increased cell file twisting in the nondividing cells in the differentiation zone of *tan1 air9* double mutant roots. The relationship between phragmoplast guidance defects and the organization of nondividing cells, as well as the overall growth of *tan1 air9* double mutants was unclear. Cell file rotation defects are often associated with mutations that alter the stability of tubulin (Abe et al., 2004; Buschmann and Borchers, 2020; Ishida et al., 2007; Nakajima et al., 2004; Sedbrook et al., 2004; Shoji et al., 2004), although there are some examples of cell file twisting in mutants caused by misplaced divisions

(Cnops et al., 2000; Goff and Van Norman). Additionally, *tan1 air9* double mutants are sensitive to the microtubule destabilizing drug, propyzamide (Mir et al., 2018). Together this suggested that TAN1 may have a direct role in microtubule stability or organization in nondividing cells. However, TAN1 is highly expressed in dividing tissues and has a clearly defined role during mitosis (Walker et al. 2007; Smith et al. 2001). To address whether or not defects in nondividing cells of *tan1 air9* double mutants is caused by loss of interphase TAN1, *TAN1* expression was driven in the *tan1 air9* double mutant using the well characterized G2/M-phase specific *KNOLLE* promoter (Menges et al., 2005; Lukowitz et al., 1996). *KNOLLE* is a syntaxin/Qa-SNARE that promotes vesicle fusion at the forming cell plate during telophase and cytokinesis (Strompen et al., 2002; Völker et al., 2001). *TAN1* driven by its native promoter or the *KNOLLE* promoter fully rescued the *tan1 air9* double mutant despite the absence of TAN1 in the differentiation zone of roots (Mills and Rasmussen, 2022). This suggested that defects in nondividing cells are the consequence of defects that occurred during mitosis and not due to lack of TAN1 in interphase cells. I hypothesized that cell wall stresses caused by misoriented divisions in *tan1 air9* double mutants trigger stress responses that alter growth and cell morphogenesis (Caño-Delgado et al., 2003; Gonneau et al., 2018; Hématy et al., 2007; Wolf et al., 2014). These findings emphasize the importance of division plane orientation for overall plant patterning and growth, perhaps by indirectly triggering stress response pathways.

RESEARCH OUTLINE

In this dissertation work, I develop strategies to identify TANGLED1 interactors and clarify how interactions between TAN1, POK1, POK2, and AIR9 promote correct division plane orientation. In chapter 2, I describe the implementation of a course-based undergraduate research experience to perform a reverse genetic screen by creating CRISPR-Cas9 gene knockouts in a sensitized mutant background. In chapter 3, I show that POK1 maintenance at the division site requires either TAN1 or AIR9 and demonstrate that TAN1-POK1 interaction stabilizes both proteins at the division site in the absence of AIR9. In chapter 4, I demonstrate that defects observed in some nondividing cells of the *tan1 air9* double mutant are the consequence of mitotic defects. In chapter 5, I briefly summarize the research presented and how it informs future experiments.

REFERENCES

- Abe, T., Thitamadee, S., and Hashimoto, T.** (2004). Microtubule defects and cell morphogenesis in the *lefty1lefty2* tubulin mutant of *Arabidopsis thaliana*. *Plant Cell Physiol.* 45: 211–220.
- Bellinger, M.A., Uyehara, A.N., Martinez, P., McCarthy, M.C., and Rasmussen, C.G.** (2021). Cell cortex microtubules contribute to division plane positioning during telophase in maize. *bioRxiv* 2021.01.11.426230; doi: <https://doi.org/10.1101/2021.01.11.426230>.
- Besson, S., Dumais, J.** (2011). Universal rule for the symmetric division of plant cells. *PNAS* 108: 6294–99
- Bringmann, M., Bergmann, D.C.** (2017). Tissue-wide mechanical forces influence the polarity of stomatal stem cells in *Arabidopsis*. *Curr. Biol.* 27: 877–83
- Buschmann, H. and Borchers, A.** (2020). Handedness in plant cell expansion: a mutant perspective on helical growth. *New Phytol.* 225: 53–69.
- Buschmann, H., Chan, J., Sanchez-Pulido, L., Andrade-Navarro, M. A., Doonan, J. H. and Lloyd, C. W.** (2006). Microtubule-associated AIR9 recognizes the cortical division site at preprophase and cell-plate insertion. *Curr. Biol.* 16, 1938–1943.
- Buschmann, H., Dols, J., Kopischke, S., Pen, E.J., Andrade-Navarro, M.A., Heinlein, M., Szymanski, D.B., Zachgo, S., Doonan, J.H., and Lloyd, C.W.** (2015). *Arabidopsis* KCBP interacts with AIR9 but stays in the cortical division zone throughout mitosis via its MyTH4-FERM domain.: 2033–2046.
- Caño-Delgado, A., Penfield, S., Smith, C., Catley, M., and Bevan, M.** (2003). Reduced cellulose synthesis invokes lignification and defense responses in *Arabidopsis thaliana*. *Plant J.* 34: 351–362.
- Cleary, A.L. and Smith, L.G.** (1998). The *Tangled1* gene is required for spatial control of cytoskeletal arrays associated with cell division during maize leaf development. *Plant Cell* 10: 1875–1888.

- Cnops, G., Wang, X., Linstead, P., Van Montagu, M., Van Lijsebettens, M., and Dolan, L.** (2000). Tornado1 and tornado2 are required for the specification of radial and circumferential pattern in the Arabidopsis root. *Development* 127: 3385–3394.
- Facette, M.R., Park, Y., Sutimantanapi, D., Luo, A., Cartwright, H.N., et al.** (2015). The SCAR/WAVE complex polarizes PAN receptors and promotes division asymmetry in maize. *Nat. Plants* 1: 14024
- Facette, M.R., Rasmussen, C.G., and Van Norman, J.M.** (2019). A plane choice: coordinating timing and orientation of cell division during plant development. *Curr. Opin. Plant Biol.* 47: 47–55.
- Goff, J. and Van Norman, J. M.** (2021). Polarly localized receptor-like kinases PXC2 and IRK act redundantly during Arabidopsis root development in the radial axis. *bioRxiv*. 2021.02.11.429611.
- Gonneau, M. et al.** (2018). Receptor Kinase THESEUS1 Is a Rapid Alkalinization Factor 34 Receptor in Arabidopsis. *Curr. Biol.* 28: 2452–2458.e4.
- Hamant O, Heisler MG, Jönsson H, Krupinski P, Uyttewaal M, et al.** 2008. Developmental patterning by mechanical signals in Arabidopsis. *Science* 322: 1650–55.
- Hématy, K., Sado, P.-E., Van Tuinen, A., Rochange, S., Desnos, T., Balzergue, S., Pelletier, S., Renou, J.-P., and Höfte, H.** (2007). A Receptor-like Kinase Mediates the Response of Arabidopsis Cells to the Inhibition of Cellulose Synthesis. *Current Biology* 17: 922–931.
- Herrmann, A., Livanos, P., Lipka, E., Gadeyne, A., Hauser, M.-T., Van Damme, D., and Müller, S.** (2018). Dual localized kinesin-12 POK2 plays multiple roles during cell division and interacts with MAP65-3. *EMBO Rep.* 19.
- Ishida, T., Kaneko, Y., Iwano, M., and Hashimoto, T.** (2007). Helical microtubule arrays in a collection of twisting tubulin mutants of Arabidopsis thaliana. *Proceedings of the National Academy of Sciences* 104: 8544–8549.
- Landrein B, Hamant O.** (2013). How mechanical stress controls microtubule behavior and morphogenesis in plants: history, experiments and revisited theories. *Plant J.* 75: 324–38.

- Li, H., Sun, B., Sasabe, M., Deng, X., Machida, Y., Lin, H., Lee, Y.J., and Liu, B.** (2017). Arabidopsis MAP 65-4 plays a role in phragmoplast microtubule organization and marks the cortical cell division site. *New Phytologist* 215: 187–201.
- Lipka, E., Gadeyne, A., Stöckle, D., Zimmermann, S., De Jaeger, G., Ehrhardt, D.W., Kirik, V., Van Damme, D., and Müller, S.** (2014). The Phragmoplast-Orienting Kinesin-12 Class Proteins Translate the Positional Information of the Preprophase Band to Establish the Cortical Division Zone in Arabidopsis thaliana. *Plant Cell* 26: 2617–2632.
- Livanos, P. and Müller, S.** (2019). Division Plane Establishment and Cytokinesis. *Annu. Rev. Plant Biol.* 70: 239–267.
- Lucas, M., Kenobi, K., von Wangenheim, D., Voß, U., Swarup, K., et al.** (2013). Lateral root morphogenesis is dependent on the mechanical properties of the overlying tissues. *PNAS* 110: 5229–34.
- Lukowitz, W., Mayer, U., and Jürgens, G.** (1996). Cytokinesis in the Arabidopsis embryo involves the syntaxin-related KNOLLE gene product. *Cell* 84: 61–71.
- Martinez, P., Allsman, L.A., Brakke, K.A., Hoyt, C., Hayes, J., et al.** (2018). Predicting division planes of three-dimensional cells by soap-film minimization. *Plant Cell* 30: 2255–66.
- Martinez, P., Dixit, R., Balkunde, R.S., Zhang, A., O’Leary, S.E., Brakke, K.A., and Rasmussen, C.G.** (2020). TANGLED1 mediates microtubule interactions that may promote division plane positioning in maize. *J. Cell Biol.* 219.
- Martinez, P., Luo, A., Sylvester, A., and Rasmussen, C.G.** (2017). Proper division plane orientation and mitotic progression together allow normal growth of maize. *Proc. Natl. Acad. Sci. U. S. A.* 114: 2759–2764.
- Menges, M., de Jager, S.M., Gruitsem, W., and Murray, J.A.H.** (2005). Global analysis of the core cell cycle regulators of Arabidopsis identifies novel genes, reveals multiple and highly specific profiles of expression and provides a coherent model for plant cell cycle control. *Plant J.* 41: 546–566.

- Mills, A., Jaganatha, V., Cortez, A., Guzman, M., Burnette, J.M., Collin, M., Lopez-Lopez, B., Wessler, S.R., Van Norman, J.M., Nelson, D.C., and Rasmussen, C.G.** (2021). A Course-Based Undergraduate Research Experience in CRISPR-Cas9 Experimental Design to Support Reverse Genetic Studies in *Arabidopsis thaliana*. *Journal of Microbiology & Biology Education*. **22**, (2) e00155-21.
- Mills, A.M., Morris, V.H., and Rasmussen, C.G.** (2022). The localization of PHRAGMOPLAST ORIENTING KINESIN1 at the division site depends on two microtubule binding proteins TANGLED1 and AUXIN-INDUCED-IN-ROOT-CULTURES9 in *Arabidopsis*. *bioRxiv*. doi.org/10.1101/2022.04.27.489732
- Mills, A.M. and Rasmussen, C.G.** (2022). Action at a distance: Defects in division plane positioning in the root meristematic zone affect cell organization in the differentiation zone. *bioRxiv* doi.org/10.1101/2021.04.30.442137
- Mineyuki Y, Murata T, Wada M.** (1991). Experimental obliteration of the preprophase band alters the site of cell division, cell plate orientation, and phragmoplast expansion in *Adiantum protonemata*. *J. Cell Sci.* **100**: 551–57.
- Mir, R., Morris, V.H., Buschmann, H., and Rasmussen, C.G.** (2018). Division Plane Orientation Defects Revealed by a Synthetic Double Mutant Phenotype. *Plant Physiol.* **176**: 418–431.
- Müller, S., Han, S., and Smith, L.G.** (2006). Two Kinesins Are Involved in the Spatial Control of Cytokinesis in *Arabidopsis thaliana*. *Curr. Biol.* **16**: 888–894.
- Müller, S. and Jürgens, G.** (2016). Plant cytokinesis—No ring, no constriction but centrifugal construction of the partitioning membrane. *Seminars in Cell & Developmental Biology* **53**: 10–18.
- Nakajima, K., Furutani, I., Tachimoto, H., Matsubara, H., and Hashimoto, T.** (2004). SPIRAL1 encodes a plant-specific microtubule-localized protein required for directional control of rapidly expanding *Arabidopsis* cells. *Plant Cell* **16**: 1178–1190.
- Neuteboom, L.W., Ng, J.M., Kuyper, M., Clijdesdale, O.R., Hooykaas, P.J., van der Zaal, B.J.** (1999). Isolation and characterization of cDNA clones corresponding with mRNAs that accumulate during auxin-induced lateral root formation. *Plant Mol. Biol.* **39**: 273-287.

- Rasmussen, C.G. and Bellinger, M.** (2018). An overview of plant division-plane orientation. *New Phytol.* **219**: 505–512.
- Rasmussen, C.G., Sun, B., and Smith, L.G.** (2011). Tangled localization at the cortical division site of plant cells occurs by several mechanisms. *J. Cell Sci.* **124**: 270–279.
- Schaefer, E., Belcram, K., Uyttewaal, M., Duroc, Y., Goussot, M., Pastuglia, M., and Bouchez, D.** (2017). The preprophase band of microtubules controls the robustness of division orientation in plants. *Science.* **189**: 186–189.
- Sedbrook, J.C., Ehrhardt, D.W., Fisher, S.E., Scheible, W.-R., and Somerville, C.R.** (2004). The *Arabidopsis* sku6/spiral1 gene encodes a plus end-localized microtubule-interacting protein involved in directional cell expansion. *Plant Cell* **16**: 1506–1520.
- Shoji, T., Narita, N.N., Hayashi, K., Asada, J., Hamada, T., Sonobe, S., Nakajima, K., and Hashimoto, T.** (2004). Plant-specific microtubule-associated protein SPIRAL2 is required for anisotropic growth in *Arabidopsis*. *Plant Physiol.* **136**: 3933–3944.
- Smertenko, A. et al.** (2017). Plant Cytokinesis: Terminology for Structures and Processes. *Trends Cell Biol.* **27**: 885–894.
- Smith L.G., Gerttula S.M., Han S., Levy J.** (2001). TANGLED1: a microtubule binding protein required for the spatial control of cytokinesis in maize. *J Cell Biol.* **152**:231–236
- Strompen, G., El Kasmi, F., Richter, S., Lukowitz, W., Assaad, F.F., Jürgens, G., and Mayer, U.** (2002). The *Arabidopsis* HINKEL gene encodes a kinesin-related protein involved in cytokinesis and is expressed in a cell cycle-dependent manner. *Curr. Biol.* **12**: 153–158.
- Su, T.** (2012). Proteins that Interact with *Arabidopsis* TANGLED. UC San Diego. ProQuest ID: Su_ucsd_0033M_12339. Merritt ID: ark:/20775/bb3926230d. Retrieved from <https://escholarship.org/uc/item/5bx9v4v9>
- Völker, A., Stierhof, Y.D., and Jürgens, G.** (2001). Cell cycle-independent expression of the *Arabidopsis* cytokinesis-specific syntaxin KNOLLE results in mistargeting to the plasma membrane and is not sufficient for cytokinesis. *J. Cell Sci.* **114**: 3001–3012.

- Wada, M.** (2018). Nuclear movement and positioning in plant cells. *Semin. Cell Dev. Biol.* **82**, 17–24.
- Walker, K.L., Müller, S., Moss, D., Ehrhardt, D.W., and Smith, L.G.** (2007). Arabidopsis TANGLED identifies the division plane throughout mitosis and cytokinesis. *Curr. Biol.* **17**: 1827–1836.
- Wolf, S. et al.** (2014). A receptor-like protein mediates the response to pectin modification by activating brassinosteroid signaling. *Proc. Natl. Acad. Sci. U. S. A.* **111**: 15261–15266.
- Xu, X.M., Zhao, Q., Rodrigo-Peiris, T., Brkljacic, J., He, C.S., Müller, S., and Meier, I.** (2008). RanGAP1 is a continuous marker of the Arabidopsis cell division plane. *Proc. Natl. Acad. Sci. U. S. A.* **105**: 18637–18642.
- Yi, P. and Goshima, G.** (2020). Rho of Plants GTPases and Cytoskeletal Elements Control Nuclear Positioning and Asymmetric Cell Division during *Physcomitrella patens* Branching. *Curr. Biol.* **30**, 2860–2868.e3.
- Yi, P. and Goshima, G.** (2022). Division site determination during asymmetric cell division in plants. *Plant Cell.* **34**, 6, 2120-2139.

**Chapter 2: A Course-Based Undergraduate Research Experience in
CRISPR-Cas9 Experimental Design to Support Reverse Genetic Studies
in *Arabidopsis thaliana***

ABSTRACT

Gene-editing tools such as CRISPR-Cas9 have created unprecedented opportunities for genetic studies in plants and animals. We designed a course-based undergraduate research experience (CURE) to train introductory biology students in the concepts and implementation of gene-editing technology as well as develop their soft skills in data management and scientific communication. We present two versions of the course that can be implemented with twice-weekly meetings over a 5-week period. In the remote-learning version, students performed homology searches, designed guide RNAs (gRNAs) and primers, and learned the principles of molecular cloning. This version is appropriate when access to laboratory equipment or in-person instruction is limited, such as during closures that have occurred in response to the COVID-19 pandemic. In person, students designed gRNAs, cloned CRISPR-Cas9 constructs, and performed genetic transformation of *Arabidopsis thaliana*. Students learned how to design effective gRNA pairs targeting their assigned gene with an 86% success rate. Final exams tested students' ability to apply knowledge of an unfamiliar genome database to characterize gene structure and to properly design gRNAs. Average final exam scores of ~73% and ~84% for in-person and remote-learning CUREs, respectively, indicated that students met learning outcomes. The highly parallel

nature of the CURE makes it possible to target dozens to hundreds of genes, depending on the number of sections. Applying this approach in a sensitized mutant background enables focused reverse genetic screens for genetic suppressors or enhancers. The course can be adapted readily to other organisms or projects that employ gene editing.

INTRODUCTION

Course-based undergraduate research experiences (CUREs) are credit-based classes in which students investigate an unresolved research question rather than carry out predetermined experiments with a well-defined outcome (Auchincloss et al., 2014). CUREs can have powerful positive impacts on students by providing a more accurate representation of the process of science and introducing them to problem solving required to answer open-ended questions (Brewer and Smith, 2011; Linn et al., 2015). Students that experience CUREs are more likely to remain in science, technology, engineering, and mathematics (STEM) during college, enter STEM graduate programs, and identify as scientists (Hernandez et al., 2018; Seymour et al., 2004). CUREs can increase diversity in STEM by promoting higher levels of retention of traditionally underrepresented students (Bangera and Brownell, 2014). Because CUREs require few or no prerequisites, they provide unique opportunities to students from diverse backgrounds to experience research, serving more students than do traditional undergraduate research experiences (Rowland et al., 2012). Despite

the benefits, CUREs are not yet widely implemented for several reasons. CUREs require flexibility and coordination between lab instructors and the researcher(s) providing the research project. Further, CUREs lack the predictability of traditional lab courses because the outcomes of experiments are unknown (Weaver et al., 2008; Gormally et al., 2009).

Several strategies are recommended to promote a successful CURE. The direct participation of professors and graduate students who are knowledgeable about the research project encourages students to learn the scientific process (Brewer and Smith, 2011; Hensel, 2018). Using simple laboratory techniques and building redundancy within or between class sections ensures that research goals are met (Kloser et al., 2011). Frequently monitoring student understanding with quizzes, lab notebook entries, and writing assignments highlights when concepts need clarification (Shortlidge and Brownell, 2016).

We envisioned a CURE enabling high-throughput mutagenesis of genes using simple gene-editing techniques. Our goals were to discover genes that function in division-plane orientation or in karrikin signaling (Nelson et al., 2012; Waters et al., 2017; Rasmussen and Bellinger, 2018). Here, we describe a reverse genetic approach to characterize a set of candidate genes associated with a gene of interest by biochemical screens for protein interactors. Vast collections of defined *Arabidopsis thaliana* mutants have been generated through insertional

mutagenesis (Alonso et al., 2003; O'Malley and Ecker, 2010). Mutant collections are enviable resources for reverse genetic studies but are not well-suited to high-throughput tests for genetic modifiers, which would require extensive crossing and isolation of double or higher-order combinations of mutants. In contrast, clustered regularly interspaced short palindromic repeats and CRISPR-associated protein 9 (CRISPR-Cas9) can introduce mutations into two or more related genes at once. Biallelic or homozygous mutations are common in the first transformed generation (Minkenberg et al., 2017). Much effort in CRISPR-Cas9 approaches goes toward identification of useful alleles and deriving homozygous mutant lines. We reasoned that this effort could be reduced by applying a forward genetics strategy where the pooled progeny of CRISPR-Cas9 transgenic plants are screened for phenotypes and then focusing further studies on individuals with phenotypes and their targeted candidate gene(s) ([Fig. 2.1](#)).

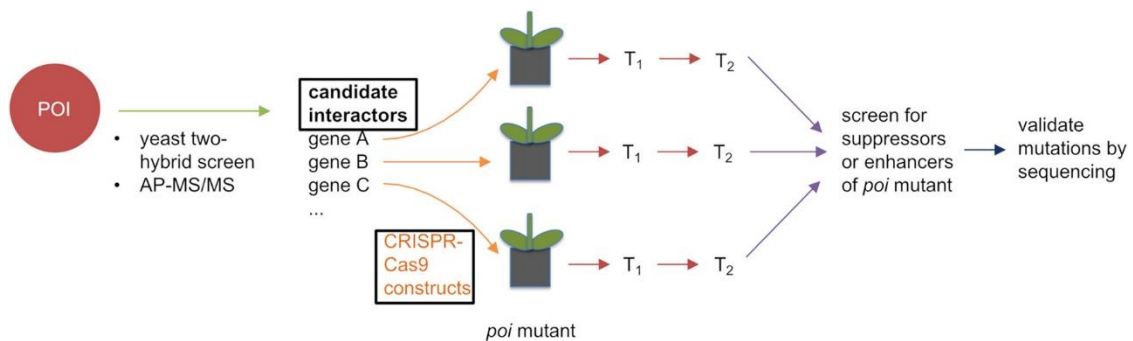


Figure 2.1: Strategy to identify genetic modifiers through CRISPR-Cas9.

Proteins that potentially interact with a protein of interest (POI) are identified through yeast two-hybrid library screens or affinity-purification mass spectrometry. Each candidate interactor gene is assigned to two students. Students identify homologs that may be functionally redundant with a candidate interactor and select two guide RNA (gRNA) sequences to target the candidate and its close homologs, if any. Students use PCR and Golden Gate cloning to insert both gRNAs into a CRISPR-Cas9 construct. Correct constructs are identified after *E. coli* transformation with colony PCR, plasmid preparation, and sequencing. Constructs are then transformed into the *Arabidopsis thaliana poi* mutant background. Transformed seed (T1) are selected and selfed to produce T2 seed. Pooled T2 seed from different T1 lines carrying a single construct are phenotyped for either suppression or synthetic enhancement of the *poi* mutant phenotype. CRISPR-induced mutations are then validated by sequencing of the target gene(s). Black boxes around “candidate interactors” and “CRISPR-Cas9 constructs” indicate CURE contributions specific to this research.

We adopted this approach to evaluate a list of proteins identified as candidate interactors with TANGLED1 (TAN1) or KARRIKIN UPREGULATED F-BOX1 (KUF1) through yeast two-hybrid library screens, affinity-purification mass spectrometry, or predicted function (Nelson et al., 2010; Mir et al., 2018). In the in-person CURE, students were asked to use CRISPR-Cas9 to target 64 genes encoding candidate protein interactors of KUF1. Students designed guide RNAs (gRNAs), generated CRISPR-Cas9 constructs, and transformed *A. thaliana kuf1* mutants. In the remote-learning CURE, we asked students to design gRNAs to mutate 46 target genes encoding potential TAN1 interactors. Later, these gRNAs will be cloned into vectors and transformed into plants to generate mutants as part of the independent research project. Here, we provide detailed protocols to implement either version of the CURE depending upon the availability of laboratory facilities ([Fig. 2.2](#)). This innovative CURE uses a reverse genetics approach to generate higher-order mutants in a sensitized mutant background using CRISPR-Cas9 gene editing.

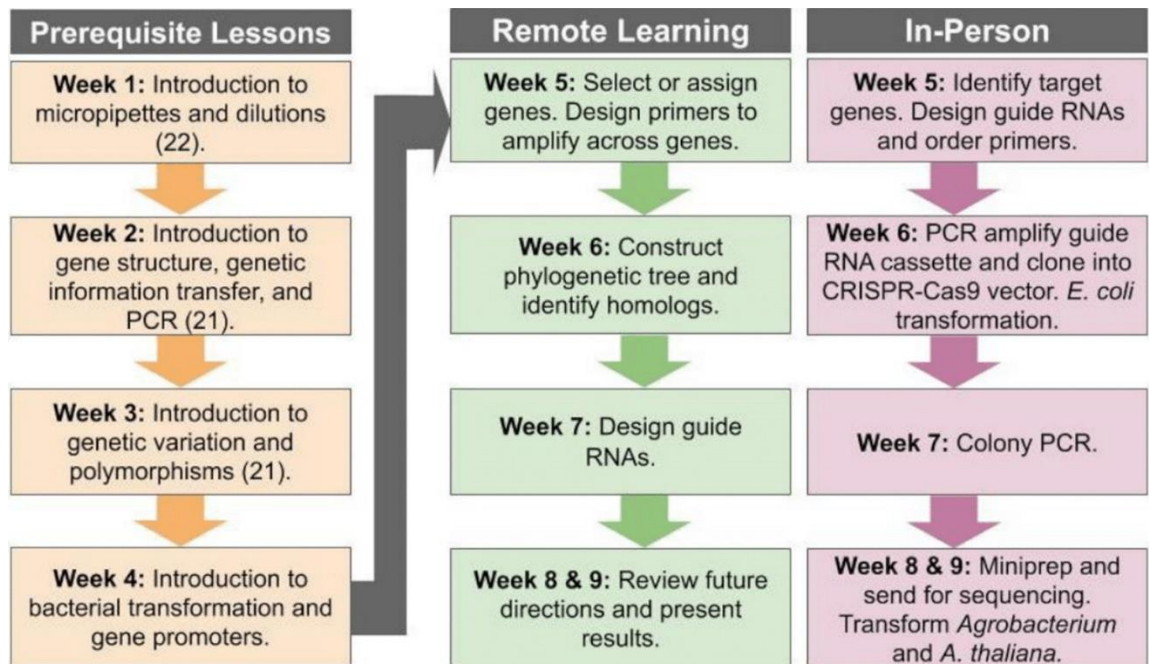


Figure 2.2: Timeline of the CURE. Steps shown in the left column are recommended prerequisite lessons before beginning the research project. Middle column steps outline the remote-learning CURE while right column steps outline the in-person CURE and require laboratory facilities.

INTENDED AUDIENCE

This course is intended for first-year biology students or other STEM majors. It was implemented in-person in Spring 2019 for 6 sections and online in Spring 2020 for 8 sections with 18 to 24 students enrolled in each section. Student demographics were ~50% Asian and ~25% Hispanic for both courses (see Appendix S1 in the supplemental material). The CURE is a long-running course offered to first-year biology students as an alternative to the traditional first-year lab course (Burnette and Wessler, 2013). During the first 4 to 5 weeks of the 10-week quarter, class instructors introduce students to common laboratory techniques and basic biological concepts. University of California, Riverside faculty then offer 5- to 6-week-long CUREs in the second half of the class while course administration, grading, and most technical support are handled by instructors, teaching assistants, and staff. This organization allows faculty to deliver a focused research project experience. The remote-learning option was a direct result of the cancelation of in-person instruction due to the COVID-19 pandemic. However, instructions presented here can be applied to online courses or used in settings where laboratory space for students is unavailable.

PREREQUISITE KNOWLEDGE

Students are first-year undergraduates. Students are introduced to basic experimental and computational genomics techniques during the first 4 to 5 weeks. Structured lab activities include pipetting and dilutions (Burnette et al.,

2016), PCR, bacterial transformation, and introduction to gene structure and polymorphisms (Burnette and Wessler, 2013). Videos demonstrating techniques were provided for remote instruction. Because the class is for first-year students, techniques and concepts taught before the start of the CURE are necessary for students to perform the experiments and understand the key concepts of genetic information transfer and genome organization.

LEARNING TIME

The course is 10 weeks, with a 5-week CURE consisting of class meetings twice a week on either Mondays and Wednesdays or Tuesdays and Thursdays. Online classes' meetings are 1 to 1.5 h each. For in-person classes, lab periods are 3 h each. Because students cannot access the laboratory outside class, all protocols are designed to fit in 3-h sessions.

LEARNING OUTCOMES

Three of six core competencies (the ability to apply the process of science, the ability to tap into the interdisciplinary nature of science, and the ability to use modeling and simulation) and three of five core concepts for biological literacy (information flow, exchange, and storage, evolution, and systems) outlined by the Vision and Change framework are addressed ([Table 2.1](#); Appendix S22).

Table 2.1: Assessment of key learning outcomes. Assessment of learning outcomes from 10 random exams taken in Spring 2020. A full list of learning outcomes can be found in Appendix S2, and mapping of learning outcomes to other exam questions can be found in Appendix S42.

Learning Outcomes	Exam Question	Rubric		Outcomes
		Points	Examples	
(9) Design gRNAs to specifically target different regions of a gene to create a null mutation. (10) Evaluate and select gRNAs based on a given set of criteria to selectively target a single gene.	Design gRNAs that will remove the whole gene. Draw a diagram with gRNA locations indicated and show the size of the deletion. Justify why you chose those guides.	14	gRNAs shown with location, target whole gene, PCR primers shown, gRNAs are inside the PCR priming sites, deletion shown and size is correct. Diagram is drawn correctly.	Points possible: 14 Mean: 13.6 (97%) Standard dev.: 1.26
		7	gRNAs are wrong, outside PCR primers and/or do not target whole gene.	
		1	Much is missing, weak attempt.	
(2) Design PCR primers with the aid of online tools and databases to amplify their assigned gene. (11) Design PCR experiment to detect successful gRNA guided deletions.	Design a PCR experiment that would show that the CRISPR gRNAs were effective in making the deletion.	6	Prediction that the genomic DNA size will be smaller in the deletion plant, mRNA from wild type and mutant, mRNA copied to cDNA by reverse transcriptase (RT), PCR with primers, run gel.	Points possible: 6 Mean: 5.1 (85%) Standard dev.: 0.32
		3	Prediction is missing or RT is missing.	
		1	Incomplete description of setting up the reactions is given.	

By the end of the CURE, students should be able to

1. Use online resources and databases to research genes from *A. thaliana* or another organism.
2. Design PCR primers with the aid of online tools and databases to amplify their assigned *A. thaliana* gene.
3. Identify homologs of their gene and design gRNAs targeting their gene and any close homologs.
4. Define homology and identify gene homologs through DNA database searches.
5. Discuss the evolutionary relationships between paralogs and orthologs.
6. Create a phylogenetic tree for a gene family using online tools and identify paralogs and orthologs for their assigned gene.
7. Discuss the mechanism of CRISPR-Cas9 mutagenesis.
8. Form a hypothesis about the potential consequences of mutating a gene and what that suggests about the gene's function.
9. Design gRNAs to specifically target different regions of a gene to create a null mutation.
10. Evaluate and select gRNAs based on a given set of criteria to selectively target a single gene.
11. Design PCR experiment to detect successful gRNA guided deletions in *A. thaliana*.

PROCEDURE

Student and faculty instructions

To promote peer learning and replicability, students work in pairs on a single gene. This increases the likelihood of meeting research goals by producing multiple unique gRNAs to target each gene and CRISPR-Cas9 constructs in case one student is not successful in their cloning. All other lab work and assignments are completed individually by students. We present an overview of the remote-learning and in-person workflow (see Appendix S3, remote learning, and Appendix S4, in person, in the supplemental material). The in-person timeline differs from the online version because gRNA selection is done during the first week; however, students write a report, record their results in an online lab notebook, complete quizzes, and present their results as described in the remote-learning version.

Remote-learning CURE

Week 1. A video provides background information and the scientific rationale for the project (Appendix S5). Specific guidelines are provided for the written project report due at the end of the course (Appendix S6). Because one common error in student-generated reports is lack of familiarity with formatting and terminology, examples of published papers relating to the project are provided for students and discussed in class to help students conceptualize how to format and write a scientific report. Students start working on a draft of their report introduction,

which is due at the end of the week. Teaching assistants grade the draft and offer guidance on formatting in their feedback, providing opportunities for students to improve their scientific writing.

Primer design concepts are introduced, emphasizing using primers to detect insertions and deletions (indels). A step-by-step guide for primer design is provided using the maize ACTIN-1 gene (Appendix S7). Students are assigned their genes and asked to create primers to amplify the coding sequence using online resources (Appendix S8). Students record their primer design results in an online lab notebook, which is graded for completeness by teaching assistants who also monitor the quality of the results obtained (rubric in Appendix S9 and example notebook entry in Appendix S10). We used WordPress to keep all lab notebook entries in a single, accessible place (Robb et al., 2015). Student understanding of the project goals and how to use BLAST to examine gene structure is assessed with Quiz 1 (Appendix S11, answer key Appendix S12).

Week 2. The concepts of gene evolution and homologs are explored with a prerecorded lecture (Appendix S5). Students create a phylogenetic tree for their assigned gene using Plaza 4.0 (https://bioinformatics.psb.ugent.be/plaza/versions/plaza_v4_dicots/) (Appendix S13). Students use their phylogenetic tree to identify homologs for their assigned

gene and record their findings in an electronic lab notebook entry (example in Appendix S14).

Week 3. CRISPR-Cas9 methodologies are explained and students design dual gRNAs for their assigned genes using the E-CRISP (<http://www.e-crisp.org/E-CRISP/>) tool (Appendix S15). The instructor explains features of acceptable gRNAs, including location of the gRNAs within the gene, the presence of a protospacer-adjacent motif (PAM) sequence, and lack of off-target sequences. To gain experience designing gRNAs, students create two pairs targeting a small region of their gene and two pairs targeting the entire gene for deletion. In their notebooks, students identify which gRNA pairs likely render their assigned gene nonfunctional (example in Appendix S16). Students then add their best gRNA pairs into a class spreadsheet (example in Appendix S17). Students begin working on a draft for the methods and data sections of their reports to be turned in for feedback at the start of the following week (Appendix S6). Teaching assistants address common pitfalls such as writing bullet points instead of using complete sentences. Student understanding of how to create a phylogenetic tree and design gRNAs is assessed with Quiz 2 (Appendix S18, answer key Appendix S19).

Weeks 4 and 5. Students practice communicating scientific ideas by preparing a 5-min presentation about the project rationale, their assigned gene, and their

results that is presented to the class in week 5 (presentation guidelines in Appendix S20, presentation rubric in Appendix S21, example score sheet in Appendix S22, and example presentation slides in Appendix S23). Presentations are scored by the instructor and teaching assistants. Future project plans are discussed in class (Appendix S24). Students are then expected to complete their project report by writing conclusions and future directions (example in Appendix S25 and rubric in Appendix S26). The report helps solidify their understanding of the experiments and form their own hypothesis about the next steps and potential project outcomes. Additionally, scientific writing improves students' overall academic performance and critical thinking skills (Gupta et al., 2015). During their final exam, students are asked to locate the gene sequence and design gRNAs of an assigned rice gene (Appendix S27, answer key Appendix S28, and exam rubric Appendix S29).

In-person CURE

Week 1. Students are introduced to the project with a slide presentation. This is followed by an introduction to *Arabidopsis thaliana* as a genetic model and use of forward and reverse genetic strategies to understand gene function. The metaphor “how a biologist would fix a radio” makes these concepts accessible to introductory biology students (Lazebnik, 2002). We introduce CRISPR-Cas9 as a gene-editing tool, and each student is assigned a target gene. Students use BLAST and phylogenetic comparisons to identify close homologs of their gene

that may be functionally redundant (Appendix S30). Students use CRISPR-P 2.0 to select two gRNA sequences that target their assigned gene and its homolog(s) (Appendix S31) (Liu et al., 2017). Students submit their selected 23-nucleotide guide plus protospacer-adjacent motif (PAM) sequence with their gRNA selection rationale to an online form. Instructors order four oligonucleotide primers for each student that will be used to incorporate the two guide sequences into a CRISPR-Cas9 construct in the following week (Appendix S32). A materials and equipment list is provided (Appendix S33).

Week 2. A brief lecture introduces students to CRISPR-Cas9 components and the PCR product they will generate (Xing et al., 2014; Wang et al., 2015). PCRs are performed using four primers to incorporate both the RNA-encoding sequences into a cassette containing a U6-26 terminator and a U6-29 promoter (Appendix S34). After students check them for successful amplification, the PCR products are purified and quantified. This is followed by a Golden Gate cloning reaction to incorporate the gRNA cassette into a CRISPR-Cas9 vector backbone such as pHEE401E or pYUU (Wang et al., 2015; Cermak et al., 2011; Angulo et al., 2020). If time permits, students transform *Escherichia coli* with the Golden Gate reaction (Appendix S35).

Week 3. If not completed during week 2, students transform *E. coli* with the Golden Gate reaction. A short lecture is given on selectable markers and

transformation approaches (e.g., electroporation and infection with *Agrobacterium tumefaciens*) for bacteria and plants. The next lab day, students use colony PCR to confirm insertion of the gRNA cassette into the plant transformation vector (Appendix S36).

Week 4. Teaching assistants inoculate two PCR-positive colonies for overnight cultures the evening before the first lab day. During class, students prepare glycerol stocks and plasmid miniprep isolations from the cultures (Appendix S37). After the plasmid DNA concentration is measured, the constructs are sent for sequencing. The next class period, *A. tumefaciens* (e.g., strain GV3101) (Hellens et al., 2000) is transformed, as it requires 2 days to grow colonies (Appendix S38). Rather than wait for the results of sequencing, it may be expedient to transform all constructs, discarding those with errors later after sequencing results are available. Sequences are visualized using chromatograms and compared to a template sequence using free tools provided by Benchling (Appendix S39) to ensure that both guide sequences are incorporated without errors. We typically observe a high rate of success from PCR-positive colonies. If some students are unable to generate clones, they use other students' constructs to participate in *Arabidopsis* transformation the following week.

Week 5. *A. tumefaciens* cultures for each construct are initiated by teaching assistants the evening before the first lab day. We used the floral dip

transformation method (Clough and Bent, 1998) because it is simple, effective, and tolerant of experimental variation with modifications for small culture volumes (Appendix S40). Students transform one pot of five healthy, flowering *A. thaliana* plants each. We typically obtained about 16 transformants. Because the students' transformations will not be ready for several weeks, a demonstration sample can be prepared in advance to show students what will happen next to their samples.

Safety concerns

No additional safety training is required when the course is conducted remotely.

For in-person activities, the course instructors review lab safety protocols on the first day. Students are instructed how to appropriately dispose of hazardous and biohazardous waste, and the locations of biohazard waste bins and fire extinguishers are reviewed. In the lab, students wear proper personal protective equipment at all times, including lab coat, eye protection, gloves, closed-toe shoes, and long pants or skirts. Because the mutagen ethidium bromide is incorporated into agarose gels, all ethidium bromide-contaminated materials (gels, gloves, pipette tips) are collected and disposed of by environmental health and safety personnel. Materials containing transgenic *E. coli* and *A. tumefaciens* are classified as BSL-1 and are placed in biohazard bins and later autoclaved. Bleach is added to bacterially contaminated solutions. Finally, after

each laboratory session, students disinfect bench surfaces with antibacterial wipes.

DISCUSSION

Evidence of student learning

Assessment of this CURE and dissemination of the data were performed in accordance with UC Riverside Institutional Review Board (IRB) approval (HS-14-085). Student learning outcomes were assessed by open-answer exam questions. We randomly selected 10 final exams each from one in-person CURE (Spring 2019) and two remote-learning CURES (Spring 2020 and Fall 2020), representing ~6% of total exams, to measure mastery of learning outcomes. During the Spring 2020 exam, students demonstrated their understanding of the principles of guide RNA design by applying what they learned in the CURE to a new organism (rice) and using an unfamiliar, yet similar, genome database to acquire gene information and sequences. Students scored $\geq 85\%$ on related questions, demonstrating mastery of key learning outcomes 2, 9, 10, and 11 (Table 2.1). For all exams analyzed, average scores were between 75 and 100% for each question (see Appendix S42 in the supplemental material), and total exam scores were ~73% and ~84% for in-person and remote-learning CURES, respectively (Appendix S41), demonstrating that students learned the course material.

Likert-style surveys designed by course instructors focused on student perceptions of learning are completed at the beginning and end of the course (Appendix S43). For those completing either the in-person or the remote-learning CURE, results indicate increased interest in participating in research on campus, with values rising from ~24% presurvey to an impressive ~90% postsurvey. When asked to rate perceptions of their understanding of certain lab skills (on a scale of 1 to 7, where 1 is strongly disagree and 7 is strongly agree), overall scores increased 1 point from the presurveys to the postsurveys for both CUREs. Additionally, student perceptions of the online project were favorable (ratings of 5 to 7), with 84% reporting that the project was enjoyable and the research meaningful. Taken together, these results indicate that participation in primary research (whether in-person or remote) increased student understanding of modern lab techniques and their likely future participation in research.

During the Spring 2020 quarter, 8 sections containing 142 students total participated in the remote-learning CURE by designing gRNAs for 46 *A. thaliana* genes. Students generated a total of 285 gRNA pairs. A total of 245 pairs correctly and specifically targeted the assigned genes, representing an 86% success rate for gRNA design. All assigned genes had at least one correctly designed pair of gRNAs. The most common error made by students was selecting overlapping gRNA pairs (9/285 guide RNA pairs overlapped). In the future, instructors will mention a minimum expected deletion size so students will

not select guides that overlap. In two instances, gRNAs were predicted to target both the gene of interest and a different gene. Altogether, successful gRNA design demonstrates that first-year undergraduates learned how to use free online software to identify homologs and design gRNAs.

Possible modifications

Specific goals and organisms used in the project can be modified, making this type of CURE adaptable and generalizable. This CURE is best suited to organisms with sequenced and annotated genomes that are amenable to gene editing and transformation. To identify candidate genes and potential interactors, genome databases are available for other organisms such as zebrafish (<http://zfin.org>) or *Drosophila* (<http://flybase.org>). Other online tools such as STRING (<http://string-db.org>) may be used to identify interacting proteins.

There are many free gRNA design programs available online that do not require downloads. The program chosen for the in-person course was CRISPR-P 2.0 (<http://crispr.hzau.edu.cn/CRISPR2/>). The CRISPR-P 2.0 output shows all potential gRNAs, which is useful if the goal of the project includes mutating more than one gene per gRNA. The program chosen for the remote-learning course was E-CRISP (<http://www.e-crisp.org/E-CRISP/index.html>). The interface, including simple bar graphs that show the specificity, annotation score, and

efficiency of each gRNA, provides intuitively simple parameters for judging gRNAs.

Challenges specific to remote-learning classes

Remote learning has several unique challenges. Students may occasionally experience technical issues, including slow Internet connection or lack of computers altogether. To promote inclusion, we identified online tools supported across multiple platforms, including tablets and Chromebooks. We provided detailed protocols for students to follow and demonstrated the protocols with example genes. Online polls are useful to determine whether students need more time to complete steps. Online quiz tools such as Kahoot can be used to assess conceptual understanding. We offered additional one-on-one help from teaching assistants or instructors during office hours to clarify concepts and help students with activities missed due to absence or technical issues.

ACKNOWLEDGMENTS

We thank BIOL20 students, teaching assistants, undergraduate lab assistants, and laboratory preparation staff at the University of California, Riverside (UCR) for their hard work, dedication, and feedback. We thank undergraduate students Dorothy Nguyen and Kruti Seethammagari for allowing us to use their exceptional work as examples. We thank Lindy Allsman (UCR) and Aimee Uyehara (UCR) for helpful manuscript comments. We thank Tarek Azzam (UC

Santa Barbara) for survey information. We gratefully acknowledge funding from the National Science Foundation (CAREER MCB-1942734 to C.G.R., IOS-1856741 to D.C.N., CAREER IOS-1751385 to J.M.V.N., IOS-1027542 to S.R.W.), HHMI Institutional Grant (52008110) to S.R.W., and Neil and Rochelle Campbell Presidential Chair for Innovation in Science Education to S.R.W.

We declare no conflicts of interest.

SUPPLEMENTAL MATERIALS

Supplemental materials available at:

<https://journals.asm.org/doi/10.1128/jmbe.00155-21#supplementary-materials>

ASM does not own the copyrights to Supplemental Material that may be linked to, or accessed through, an article. The authors have granted ASM a non-exclusive, world-wide license to publish the Supplemental Material files. Please contact the corresponding author directly for reuse.

REFERENCES

- Alonso, J.M., Stepanova, A.N., Leisse, T.J., Kim, C.J., Chen, H., Shinn, P., Stevenson, D.K., Zimmerman, J., Barajas, P., Cheuk, R., Gadrinab, C., Heller, C., Jeske, A., Koesema, E., Meyers, C.C., Parker, H., Prednis, L., Ansari, Y., Choy, N., Deen H, Geralt M, Hazari N, Hom E, Karnes M, Mulholland C, Ndubaku R, Schmidt I., Guzman, P., Aguilar-Henonin, L., Schmid, M., Weigel, D., Carter, D.E., Marchand, T., Risseuw, E., Brogden, D., Zeko, A., Crosby, W.L., Berry, C.C., Ecker, J.R.** (2003). Genome-wide insertional mutagenesis of *Arabidopsis thaliana*. *Science* **301**:653–657.
- Angulo, J., Astin, C.P., Bauer, O., Blash, K.J., Bowen, N.M., Chukwudinma, N.J., Dinofrio, A.S., Faletti, D.O., Ghulam, A.M., Gusinde-Duffy, C.M., Horace, K.J., Ingram, A.M., Isaack, K.E., Jeong, G., Kiser, R.I., Kobylanski, J.S., Long, M.R., Manning, G.A., Morales, J.M., Nguyen, K.H., Pham, R.T., Phillips, M.H., Reel, T.W., Seo, J.E., Vo, H.D., Wukuson, A.M., Yeary, K.A., Zheng, G.Y., Lukowitz, W.** (2020). Targeted mutagenesis of the *Arabidopsis* GROWTH-REGULATING FACTOR (GRF) gene family suggests competition of multiplexed sgRNAs for Cas9 apoprotein. *bioRxiv*. doi.org/10.1101/2020.08.16.253203.
- Auchincloss, L.C., Laursen, S.L., Branchaw, J.L., Eagan, K., Graham, M., Hanauer, D.I., Lawrie, G., McLinn, C.M., Pelaez, N., Rowland, S., Towns, M., Trautmann, N.M., Varma-Nelson, P., Weston, T.J., Dolan, E.L.** (2014). Assessment of course-based undergraduate research experiences: a meeting report. *CBE Life Sci Educ* **13**:29–40.
- Bangera, G., Brownell, S.E.** (2014). Course-based undergraduate research experiences can make scientific research more inclusive. *CBE Life Sci Educ* **13**:602–606.
- Burnette, J., Kanizay, L., Chester, N., Wessler, S.R.** (2016). Dilution and pipetting lesson using food dyes. *Cs 3*.
- Burnette, J.M., 3rd, Wessler, S.R.** (2013). Transposing from the laboratory to the classroom to generate authentic research experiences for undergraduates. *Genetics* **193**:367–375.
- Brewer, C.A., Smith, D.** (2011). *Vision and change in undergraduate biology education: a call to action. 2009 National Conference by AAAS, Washington, DC, USA*. American Association for the Advancement of Science, Washington, DC.

- Cermak, T., Doyle, E.L., Christian, M., Wang, L., Zhang, Y., Schmidt, C., Baller, J.A., Somia, N.V., Bogdanove, A.J., Voytas, D.F.** (2011). Efficient design and assembly of custom TALEN and other TAL effector-based constructs for DNA targeting. *Nucleic Acids Res* **39**:e82.
- Clough, S.J., Bent, A.F.** (1998). Floral dip: a simplified method for Agrobacterium-mediated transformation of *Arabidopsis thaliana*. *Plant J* **16**:735–743.
- Gupta, T., Burke, K.A., Mehta, A., Greenbowe, T.J.** (2015). Impact of guided-inquiry-based instruction with a writing and reflection emphasis on chemistry students' critical thinking abilities. *J Chem Educ* **92**:32–38.
- Gormally, C., Brickman, P., Hallar, B., Armstrong, N.** (2009). Effects of inquiry-based learning on students' science literacy skills and confidence. *IJ-SoTL* **3**:16.
- Hellens, R., Mullineaux, P., Klee, H.** (2000). Technical focus: a guide to Agrobacterium binary Ti vectors. *Trends Plant Sci* **5**:446–451.
- Hensel, N.H.** (2018). *Course-based undergraduate research: educational equity and high-impact practice*. Stylus Publishing, LLC.
- Hernandez, P.R., Woodcock, A., Estrada, M., Schultz, P.W.** (2018). Undergraduate research experiences broaden diversity in the scientific workforce. *Bioscience* **68**:204–211.
- Kloser, M.J., Brownell, S.E., Chiariello, N.R., Fukami, T.** (2011). Integrating teaching and research in undergraduate biology laboratory education. *PLoS Biol* **9**:e1001174.
- Lazebnik, Y.** (2002). Can a biologist fix a radio?—Or, what I learned while studying apoptosis. *Cancer Cell* **2**:179–182.
- Linn, M.C., Palmer, E., Baranger, A., Gerard, E., Stone, E.** (2015). Education. Undergraduate research experiences: impacts and opportunities. *Science* **347**:1261757.
- Liu, H., Ding, Y., Zhou, Y., Jin, W., Xie, K., Chen, L.-L.** (2017). CRISPR-P 2.0: an improved CRISPR-Cas9 tool for genome editing in plants. *Mol Plant* **10**:530–532.

- Minkenberg, B., Xie, K., Yang, Y.** (2017). Discovery of rice essential genes by characterizing a CRISPR-edited mutation of closely related rice MAP kinase genes. *Plant J* **89**:636–648.
- Mir, R., Morris, V.H., Buschmann, H., Rasmussen, C.G.** (2018). Division plane orientation defects revealed by a synthetic double mutant phenotype. *Plant Physiol* **176**:418–431.
- Nelson, D.C., Flematti, G.R.-A., Riseborough, J., Ghisalberti, E.L., Dixon, K.W., Smith, S.M.** (2010). Karrikins enhance light responses during germination and seedling development in *Arabidopsis thaliana*. *Proc Natl Acad Sci U S A* **107**:7095–7100.
- Nelson, D.C., Flematti, G.R., Ghisalberti, E.L., Dixon, K.W., Smith, S.M.** (2012). Regulation of seed germination and seedling growth by chemical signals from burning vegetation. *Annu Rev Plant Biol* **63**:107–130.
- O'Malley, R.C., Ecker, J.R.** (2010). Linking genotype to phenotype using the *Arabidopsis* unimutant collection. *Plant J* **61**:928–940.
- Rasmussen, C.G., Bellinger, M.** (2018). An overview of plant division-plane orientation. *New Phytol* **219**:505–512.
- Robb S., Burnette, J.M., III, Chapovskya, A., Palmer, K., Wessler, S.R.** (2015). An open source, collaborative electronic notebook for undergraduate laboratory classes. *CourseSource* **2**.
- Rowland, S.L., Lawrie, G.A., James, B.Y., Gillam, E.M.J.** (2012). Is the undergraduate research experience (URE) always best?: The power of choice in a bifurcated practical stream for a large introductory biochemistry class. *Biochem Mol Biol Educ* **40**:46–62.
- Seymour, E., Hunter, A.-B., Laursen, S.L., DeAntoni, T.** (2004). Establishing the benefits of research experiences for undergraduates in the sciences: first findings from a three-year study. *Sci Ed* **88**:493–534.
- Shortlidge, E.E., Brownell, S.E.** (2016). How to assess your CURE: a practical guide for instructors of course-based undergraduate research experiences. *J Microbiol Biol Educ* **17**:399–408.
- Wang, Z.-P., Xing, H.-L., Dong, L., Zhang, H.-Y., Han, C.-Y., Wang, X.-C., Chen, Q.-J.** (2015). Egg cell-specific promoter-controlled CRISPR/Cas9 efficiently generates homozygous mutants for multiple target genes in *Arabidopsis* in a single generation. *Genome Biol* **16**:144.

Waters, M.T., Gutjahr, C., Bennett, T., Nelson, D.C. (2017). Strigolactone signaling and evolution. *Annu Rev Plant Biol* **68**:291–322.

Weaver, G.C., Russell, C.B., Wink, D.J. (2008). Inquiry-based and research-based laboratory pedagogies in undergraduate science. *Nat Chem Biol* **4**:577–580.

Xing, H.-L., Dong, L., Wang, Z.-P., Zhang, H.-Y., Han, C.-Y., Liu, B., Wang, X.-C., and Chen, Q.-J. (2014). A CRISPR/Cas9 toolkit for multiplex genome editing in plants. *BMC Plant Biol.* **14**: 327.

Chapter 3: The localization of PHRAGMOPLAST ORIENTING KINESIN1 at the division site depends on two microtubule binding proteins TANGLED1 and AUXIN-INDUCED-IN-ROOT-CULTURES9 in Arabidopsis

ABSTRACT

Proper plant growth and development requires spatial coordination of cell divisions. Two unrelated microtubule-binding proteins, TANGLED1 (TAN1) and AUXIN-INDUCED-IN-ROOT-CULTURES9 (AIR9), are together required for normal growth and division-plane orientation in Arabidopsis. *tan1 air9* double mutants have synthetic growth and division-plane orientation defects while single mutants lack obvious defects. Here we show that the division-site localized protein, PHRAGMOPLAST-ORIENTING-KINESIN1 (POK1), was aberrantly lost from the division site during metaphase and telophase in *tan1 air9* mutants. Since TAN1 and POK1 interact via the first 132 amino acids of TAN1 (TAN1₁₋₁₃₂), we assessed its localization and function in the *tan1 air9* double mutant. TAN1₁₋₁₃₂ rescued *tan1 air9* mutant phenotypes and localized to the division site in telophase. However, replacing six amino-acid residues within TAN1₁₋₁₃₂ that disrupts POK1-TAN1 interaction in the yeast two-hybrid system caused loss of both rescue and division-site localization of TAN1₁₋₁₃₂ in *tan1 air9* mutants. Full-length TAN1 with the same alanine substitutions had defects in phragmoplast guidance and reduced TAN1 and POK1 localization at the division site but rescued most *tan1 air9* mutant phenotypes. Together, these data suggest that

TAN1 and AIR9 are required for POK1 localization, and yet unknown proteins may stabilize TAN1-POK1 interactions.

INTRODUCTION

Division plane orientation is important for many aspects of plant, microbial, and animal development, particularly growth and patterning. Division plane orientation is especially relevant for plant cells which are encased in cell walls, and unable to migrate (Rasmussen and Bellinger, 2018; Livanos and Müller, 2019; Facette et al., 2018; Wu et al., 2018). Positioning and construction of the new cell wall (cell plate) during cytokinesis involves two microtubule- and microfilament-rich cytoskeletal structures, the preprophase band (PPB) and the phragmoplast respectively (Smertenko et al., 2017). The PPB is a ring of microtubules, microfilaments, and proteins that forms at the cell cortex just beneath the plasma membrane during G2: this region is defined as the cortical division zone (Van Damme, 2009; Smertenko et al., 2017; Li et al., 2015). The cortical division zone is characterized by active endocytosis mediated by TPLATE-clathrin coated vesicles that may deplete actin and the actin-binding kinesin like-protein KCA1/KAC1 (Vanstraelen et al., 2004; Suetsugu et al., 2010; Karahara et al., 2009; Kojo et al., 2013; Panteris, 2008; Hoshino et al., 2003). After nuclear envelope breakdown, the PPB disassembles and the metaphase spindle, an antiparallel microtubule array with its plus-ends directed toward the middle of the cell, forms (Dixit and Cyr, 2002). After the chromosomes are

separated, the phragmoplast is constructed from spindle remnants to form another antiparallel array of microtubules (Lee and Liu, 2019). The phragmoplast microtubules are tracks for the movement of vesicles containing cell wall materials towards the forming cell plate (McMichael and Bednarek, 2013; Müller and Jürgens, 2016). The phragmoplast expands by nucleation of new microtubules on pre-existing microtubules (Murata et al., 2013; Smertenko et al., 2018) and is partially dependent on the mitotic microtubule binding protein ENDOSPERM DEFECTIVE1 and the augmin complex to recruit gamma tubulin to phragmoplast microtubules (Lee et al., 2017; Nakaoka et al., 2012). Finally, the phragmoplast reaches the cell cortex and the cell plate and associated membranes fuse with the mother cell membranes at the cell plate fusion site previously specified by the PPB (van Oostende-Triplet et al., 2017).

TANGLED1 (TAN1, AT3G05330) was the first protein identified to localize to the plant division site throughout mitosis and cytokinesis (Walker et al., 2007). In maize, the *tan1* mutant has defects in division plane orientation caused by phragmoplast guidance defects (Cleary and Smith, 1998; Martinez et al., 2017). TAN1 bundles and crosslinks microtubules in vitro (Martinez et al., 2020). In vivo, TAN1 promotes microtubule pausing at the division site (Bellinger et al., 2021). TAN1, together with other division site localized proteins, is critical for the organization of an array of cell cortex localized microtubules that is independent from the phragmoplast. These cortical-telophase microtubules accumulate at the

cell cortex during telophase and are subsequently incorporated into the phragmoplast to direct its movement towards the division site (Bellinger et al., 2021). Other important division site localized proteins were identified through their interaction with TAN1, such as the division site localized kinesin-12 proteins PHRAGMOPLAST ORIENTING KINESIN1 (POK1) and POK2 (Müller et al., 2006; Lipka et al., 2014). Similar to other kinesin-12 proteins, PHRAGMOPLAST ASSOCIATED KINESIN RELATED PROTEIN (PAKRP1) and PAKRPL1 (Lee et al., 2007; Pan et al., 2004), POK2 localizes to the phragmoplast midline during telophase and plays a unique role in phragmoplast expansion (Herrmann et al., 2018). Together, POK1 and POK2 are required to guide the phragmoplast to the division site (Herrmann et al., 2018; Müller et al., 2006). *pok1 pok2 Arabidopsis thaliana* (*Arabidopsis*) double mutants have stunted growth and misplaced cell walls as a result of phragmoplast guidance defects (Müller et al., 2006). The *pok1 pok2* double mutants also fail to maintain TAN1 at the division site after entry into metaphase (Lipka et al., 2014). This suggests that TAN1 maintenance at the division site after metaphase is dependent on POK1 and POK2.

In *Arabidopsis*, *tan1* mutants have very minor phenotypes (Walker et al., 2007). However, combination of *tan1* with *auxin-induced-in-root-cultures9* (*air9*), a mutant with no obvious defects (Buschmann et al., 2015), resulted in a synthetic phenotype consisting of reduced root growth, increased root cell file rotation and phragmoplast guidance defects (Mir et al., 2018). TAN1 and AIR9 are unrelated

microtubule-binding proteins that both localize to the division site (Walker et al., 2007; Buschmann et al., 2006). Both TAN1 and AIR9 colocalize with the PPB. TAN1 remains at the division site throughout cell division, while AIR9 is lost from the division site upon PPB disassembly and then reappears at the division site during cytokinesis when the phragmoplast contacts the cortex. When full length *TAN1* fused to *YELLOW FLUORESCENT PROTEIN (TAN1-YFP)* and driven either by the constitutive viral cauliflower mosaic *CaMV35S* promoter (*p35S:TAN1-YFP*) or the native promoter with the fluorescent protein as either N- or C-terminal fusion (*pTAN1:TAN1-YFP* or *pTAN1:CFP-TAN1*) was transformed into the *tan1 air9* double mutant, the phenotype was rescued such that plants looked similar to and grew as well as wild-type plants (Mir et al., 2018; Mills and Rasmussen, 2022).

TAN1 is an intrinsically disordered protein with no well-defined domains. It was divided into five conserved regions based on alignments of amino acid similarity across plant species. Region I, which covers the first ~130 amino acids of *TAN1*, is the most highly conserved, and mediates *TAN1* localization to the division site during telophase. This ~130 amino acid region also mediates interactions between *TAN1* and *POK1* in the yeast two-hybrid system (Rasmussen et al., 2011). When *TAN1* missing the first ~130 amino acids was transformed into the *tan1 air9* double mutant, no rescue was observed (Mir et al., 2018). This

suggests that the first ~130 amino acids of the TAN1 protein are critical for function in root growth and division plane positioning.

Here, we show that both AIR9 and TAN1 are required for POK1 to remain at the division site after PPB disassembly. We identified TAN1-POK1 interaction motifs within the first 132 amino acids using the yeast two-hybrid system. Interestingly, the first 132 amino acids of TAN1 (TAN1₁₋₁₃₂) are sufficient to rescue the *tan1 air9* double mutant, but not when a TAN1-POK1 interaction motif was disrupted. We found that when full-length TAN1 with the same mutated motif was used, substantial rescue was observed, except defects in phragmoplast guidance and loss of POK1 and TAN1 at the division site during metaphase and telophase. Together, this suggests that interactions between POK1 and AIR9, and TAN1 and POK1, as well as other yet unknown proteins, are important for division plane orientation and plant growth.

RESULTS

Either TAN1 or AIR9 is sufficient to recruit and maintain POK1 at the division site

To understand how known division-site localized proteins interact at the division site, we examined POK1 fused to YELLOW FLUORESCENT PROTEIN (YFP-POK1 (Lipka et al., 2014)) localization in wild type, *tan1 air9* double mutants and single mutants expressing the microtubule marker *UBQ10:mScarlet-MAP4* (Pan

et al., 2020). Our hypothesis was that POK1 localization would not be contingent on TAN1 or AIR9, and would therefore be unaltered in the *tan1 air9* double mutant. In contrast to our hypothesis, YFP-POK1 was lost from the division site during metaphase and telophase and also accumulated less frequently during preprophase and prophase. In wild-type cells, YFP-POK1 colocalized with PPBs in 71% of preprophase/prophase cells (n = 50/70 cells, 15 plants, Figure 3.1A) consistent with previous observations (Schaefer et al., 2017). In the *tan1 air9* double mutant, YFP-POK1 colocalized with 50% of PPBs during preprophase/prophase, which was not significantly different than wild-type (n = 27/54 cells, 15 plants, Figure 3.1D; Table 3.1; Fisher's exact test, P-Value = 0.0165, ns with Bonferroni correction). In wild-type cells, YFP-POK1 remained at the division site in all observed metaphase (n = 13/13 cells, Figure 3.1B) and telophase cells (n = 31/31 cells, Figure 3.1C), similar to previous studies (Lipka et al., 2014). In rare instances, YFP-POK1 also accumulated in the phragmoplast midline in wild-type cells (13%, n = 4/31, 11 plants, Table 3.1). In contrast, in *tan1 air9* mutants, YFP-POK1 was lost from the division site in metaphase (n = 0/21 cells, Figure 3.1E; Table 3.1) and telophase (n = 0/44, Figure 3.1F). Interestingly, in *tan1 air9* double mutants, although YFP-POK1 did not accumulate at the division site, it accumulated at the phragmoplast midline in 77% of cells (n = 34/44), significantly more frequent midline accumulation than the 13% observed in wild-type plants (n = 4/31 cells, Table 3.1; Fisher's exact test, P-value < 0.00001). Together, this shows that POK1 is not maintained at the division site

after PPB disassembly and that instead it accumulates in the phragmoplast midline. We hypothesize that mislocalized phragmoplast midline accumulation of YFP-POK1 in *tan1 air9* mutants occurs because YFP-POK1 is not maintained at the division site.

Next, we examined YFP-POK1 localization in *tan1* and *air9* single mutants. YFP-POK1 localized to the division site during all mitotic stages, but aberrantly accumulated in the phragmoplast midline in *tan1* single mutants. Similar to wild-type plants, YFP-POK1 colocalized with PPBs during preprophase or prophase in *tan1* mutants (Figure 3.1G) and *air9* mutants (Figure 3.1H), and remained at the division site during metaphase and telophase (Figure 3.1G-L, Table 3.1). In *tan1* single mutants, YFP-POK1 localized both to the division site and the phragmoplast midline in 44% of telophase cells (Figure 3.1I, n = 12/27), which is significantly more midline accumulation compared to wild-type plants (13%, n = 4/31, 10 plants, Fisher's exact test, P-value = 0.0094) or *air9* single mutants (Figure 3.1L, 10%, n = 4/40). Aberrant phragmoplast midline accumulation of YFP-POK1 in the *tan1* single mutants suggested that POK1-TAN1 interaction might be required to maintain POK1 at the division site. This prompted us to examine their interaction more closely.

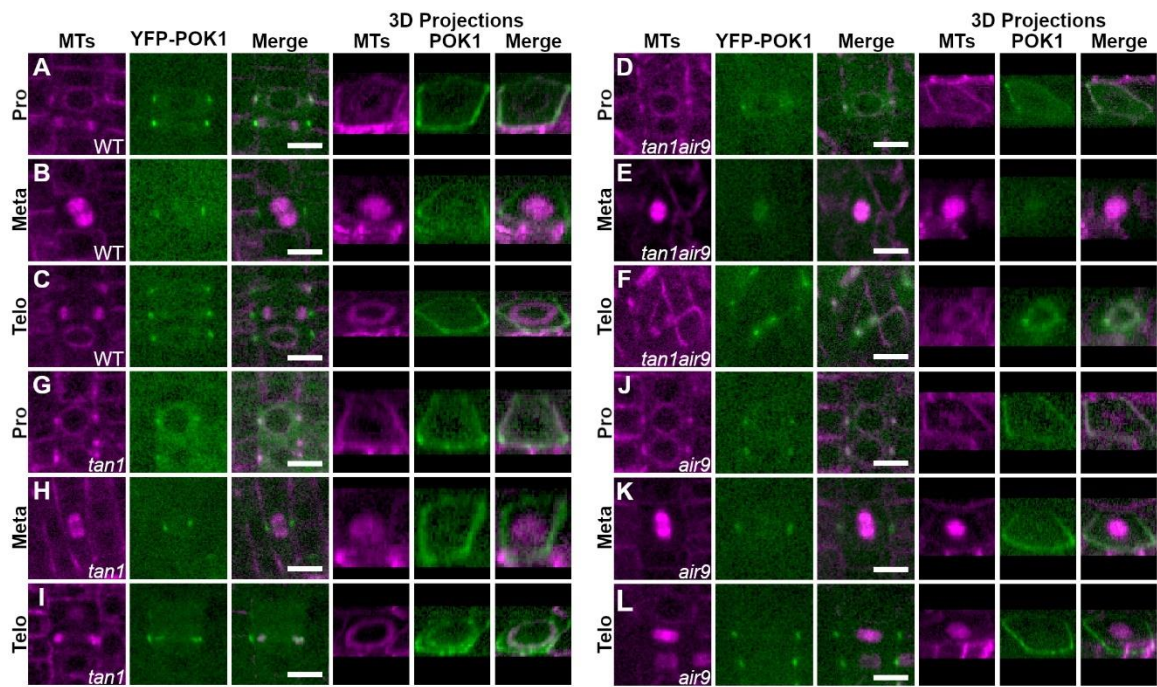
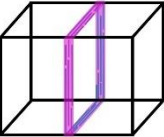
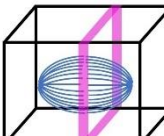
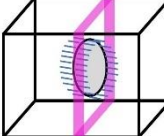
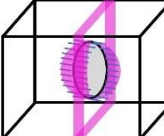
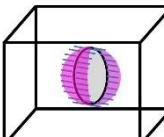


Figure 3.1: TAN1 and AIR9 together promote POK1 maintenance at the division site. YFP-POK1 localization in Col-0 wild-type plants, *tan1* single mutants, *air9* single mutants, and *tan1 air9* double mutants expressing UBQ10:mScarlet-MAP4 to mark microtubules and pPOK1:YFP-POK1. Scale bars = 10 μ m. A-C) YFP-POK1 localization in Col-0 wild-type plants, N = 15 plants. A) YFP-POK1 localization during preprophase/prophase. In 71% of cells (50/70) YFP-POK1 colocalized with the PPB. B) YFP-POK1 was observed to be maintained at the division site in metaphase and anaphase cells in Col-0 plants (n = 13/13 metaphase cells, n = 3/3 anaphase cells). C) YFP-POK1 remains clearly visible at the division site in Col-0 telophase cells (n = 31/31 cells). D-F) YFP-POK1 localization in *tan1 air9* double mutant plants, N = 19 plants. D) YFP-POK1 localization during preprophase/prophase. In 50% of cells (27/54) YFP-POK1 colocalized with the PPB. E) YFP-POK1 was observed to be lost from the division site upon entry into metaphase (n = 0/21 cells) and was absent in anaphase cells (n = 0/4 cells). F) In *tan1 air9* telophase cells YFP-POK1 was absent from the division site and accumulated in the phragmoplast midline (n = 34/44 cells). G-I) YFP-POK1 localization in *tan1* single mutants, N = 17 plants. G) YFP-POK1 localization during preprophase/prophase. In 64% of cells (54/85) YFP-POK1 colocalized with the PPB. H) YFP-POK1 was observed to be maintained at the division site in metaphase and anaphase cells in *tan1* plants (n = 17/17 metaphase cells, n = 6/6 anaphase cells). I) YFP-POK1 remains clearly visible at the division site in *tan1* telophase cells (n = 27/27 cells). J-L) YFP-POK1 localization in *air9* single mutant plants (N = 15 plants). J) YFP-POK1 localization during preprophase/prophase. In 64% of cells (46/72) YFP-POK1 colocalized with the PPB. K) YFP-POK1 was maintained at the division site in metaphase and anaphase cells in *air9* plants (n = 24/24 metaphase cells, n = 4/4 anaphase cells). L) YFP-POK1 remains clearly visible at the division site in *air9* telophase cells (n = 40/40 cells).

Table 3.1: YFP-POK1 division site and phragmoplast midline accumulation in wild-type, *tan1*, *air9*, and *tan1 air9* double mutant plants. Statistically significant differences were determined using Fisher's exact test with Bonferroni correction - for 4 sample types, $P < 0.0125$ is significant. P-values are in parentheses. Stars indicate significant differences; ns indicates not significant. Magenta represents YFP-POK1, blue represents microtubules, and light gray represents the cell plate in schematics.

Schematic	Description	Wild-type, N = 15 plants	<i>tan1 air9</i> , N = 19 plants	<i>tan1</i> , N = 17 plants	<i>air9</i> , N = 15 plants
	PPB, POK1 at the division site	71%, n = 50/70	50%, n = 27/54 (p = 0.0165, ns with Bonferroni correction)	64%, n = 54/85 (ns)	64%, n = 46/72 (ns)
	Metaphase, POK1 at the division site	100%, n = 13/13	0%, n = 0/21*** (p < 0.00001)	100%, n = 17/17 (ns)	100%, n = 24/24 (ns)
	Telophase, POK1 at the division site only	87%, n = 27/31	0%, n = 0/44 *** (p < 0.00001)	56%, n = 15/27** (p = 0.0094)	90%, n = 36/40 (ns)
	Telophase, POK1 at the division site and in the phragmoplast midline	13%, n = 4/31	0%, n = 0/44 (p = 0.0259, ns with Bonferroni correction)	44%, n = 12/27** (p = 0.0094)	10%, n = 4/40 (ns)
	Telophase, POK1 in phragmoplast midline but NOT at the division site	0%, n = 0/31	77%, n = 34/44*** (p < 0.00001)	0%, n = 0/27 (ns)	0%, n = 0/40 (ns)

Amino acids 1-132 of TAN1 Rescue the *tan1 air9* Double Mutant

POK1 interacts with both full-length TAN1 and the first 132 amino acids of TAN1 using the yeast two-hybrid system (Rasmussen et al., 2011). In addition, TAN1 missing the first 126 amino acids failed to rescue the *tan1 air9* double mutant, suggesting that this part of the protein is critical for TAN1 function (Mir et al., 2018). To test the function of this region of the protein in Arabidopsis, the *TAN1* coding sequence for the first 132 amino acids was fused to YFP (*TAN1*₁₋₁₃₂-YFP) driven by the cauliflower mosaic *p35S* promoter and was then transformed into the *tan1 air9* double mutant. We used *p35S:TAN1-YFP* in the *tan1 air9* double mutant as our benchmark for rescue, as its ability to rescue the *tan1 air9* double mutant was demonstrated previously (Mir et al., 2018). The progeny of several independent *p35S:TAN1*₁₋₁₃₂-YFP lines rescued the *tan1 air9* double mutant, as described in more detail below. Overall root patterning of *tan1 air9* double mutants expressing either *p35S:TAN1*₁₋₁₃₂-YFP or full-length *p35S:TAN1-YFP* was restored, while untransformed *tan1 air9* double mutant roots had misoriented divisions (Figure 3.2A, Supplementary Figure 3.1). Cell file rotation, which skews left and has large variance in the *tan1 air9* double mutant (Figure 3.2B & 3.2C), was significantly rescued in both *p35S:TAN1*₁₋₁₃₂-YFP and *p35S:TAN1-YFP tan1 air9* lines (n = 37 and 41 plants respectively), compared to the untransformed *tan1 air9* control (Levene's test used due to non-normal distribution, P-value < 0.0001). Root length at 8 days after stratification was also restored (Figure 3.2D). Interestingly, although *TAN1*₁₋₁₃₂-YFP rarely co-localizes with PPBs in wild-type

plants (Rasmussen et al., 2011) or in *tan1 air9* double mutants (10%, n = 9/89 cells, Figure 3.3A), PPB angles of *p35S:TAN1₁₋₁₃₂-YFP* and *p35S:TAN1-YFP tan1 air9* plants had significantly less variance compared to the untransformed control (Figure 3.2E). Phragmoplast positioning defects of the *tan1 air9* double mutant were also significantly rescued by *p35S:TAN1₁₋₁₃₂-YFP*. Altogether, *p35S:TAN1₁₋₁₃₂-YFP* rescued the phenotypes of the double mutant similar to full-length *p35S:TAN1-YFP*. This indicates that most functions that affect phenotypes assessed here are encoded by the first section of the *TAN1* gene.

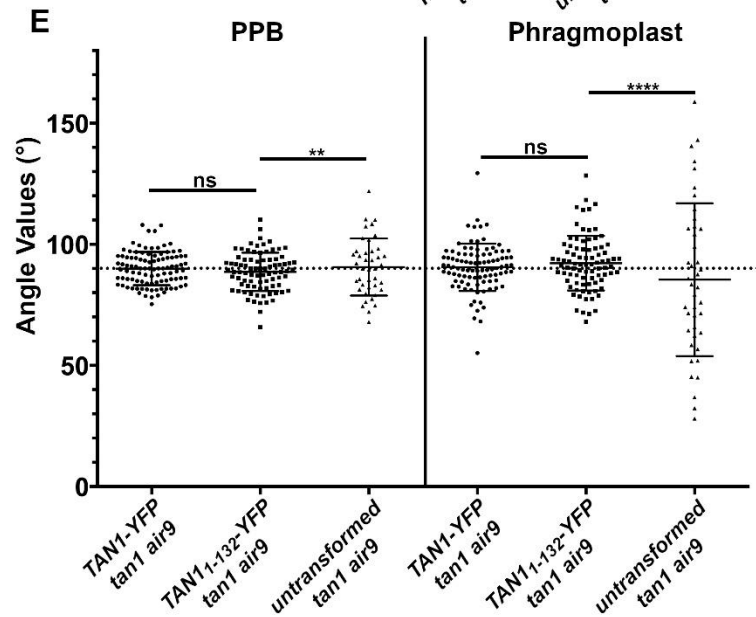
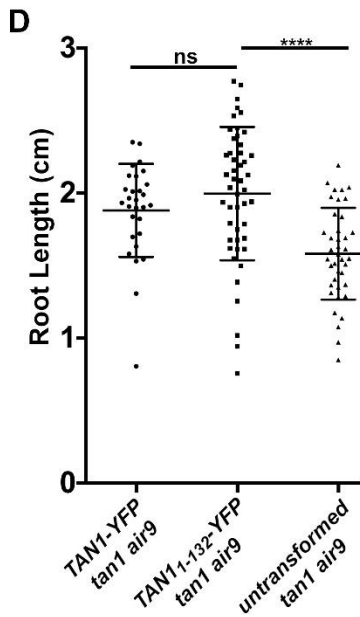
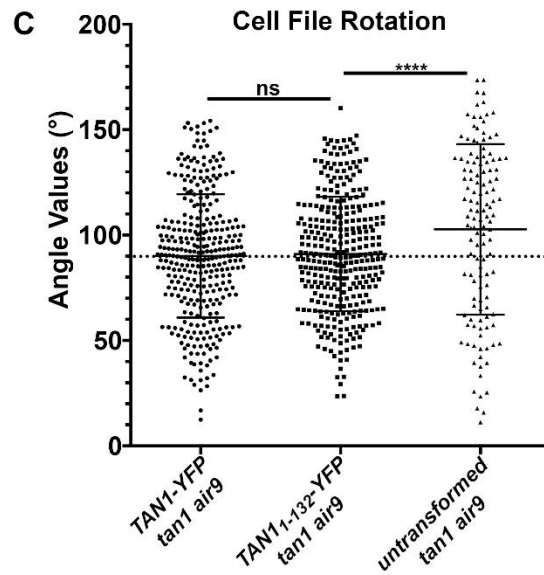
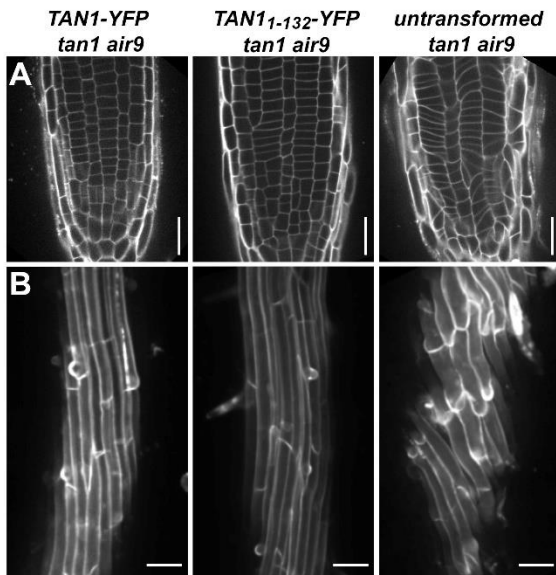


Figure 3.2: *p35S:TAN1₁₋₁₃₂-YFP* rescues *Arabidopsis tan1 air9* double mutant phenotypes. A) Cell walls stained with propidium iodide (PI) of *tan1 air9* double mutant root tips expressing *p35S:TAN1-YFP* (left), *p35S:TAN1₁₋₁₃₂-YFP* (middle), and untransformed *tan1 air9* double mutants (right). Bars = 25 μ m. B) Maximum projections of 10 1- μ m Z-stacks of PI-stained differentiation zone root cell walls. Scale bars = 50 μ m. C) Cell file rotation angles of *tan1 air9* double mutants expressing *p35S:TAN1-YFP* (left), *p35S:TAN1₁₋₁₃₂-YFP* (middle) and untransformed plants (right), n > 13 plants for each genotype. Each dot represents an angle measured from the left side of the long axis of the root to the transverse cell wall. Angle variances were compared with Levene's test due to non-normal distribution. D) Root length measurements from 8 days after stratification of *tan1 air9* double mutants expressing *p35S:TAN1-YFP* (left), *p35S:TAN1₁₋₁₃₂-YFP* (middle) and untransformed plants (right), n > 28 plants for each genotype, compared by two-tailed t-test with Welch's correction. E) PPB and phragmoplast angle measurements in *tan1 air9* double mutant cells expressing *p35S:TAN1-YFP* (left), *p35S:TAN1₁₋₁₃₂-YFP* (middle) and untransformed plants (right), n > 20 plants for each genotype. Angle variations compared with F-test. ns indicates not significant, ** P-value <0.01, **** P-value <0.0001.

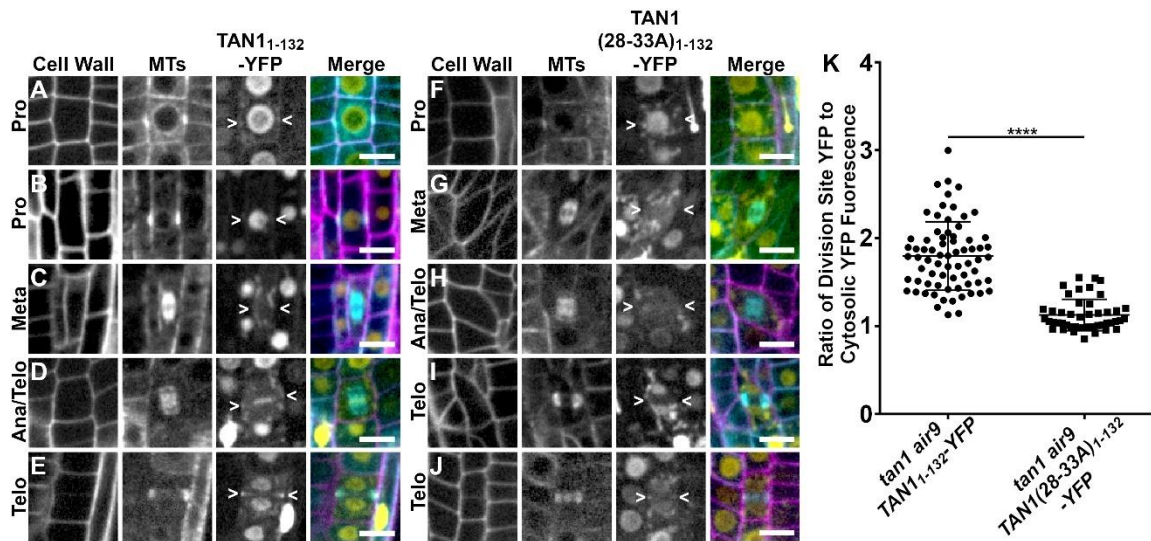


Figure 3.3: Division site localization during telophase is common for TAN1₁₋₁₃₂-YFP but rare for TAN1(28-33A)₁₋₁₃₂-YFP in *tan1 air9* double mutants. A-E) Propidium iodide stained *tan1 air9* plants expressing *p35S:TAN1₁₋₁₃₂-YFP* during mitosis (n = 29 plants). The division site is indicated by arrowheads in the YFP panels. Scale bars = 10 μ m. A) Rare prophase division site accumulation of TAN1₁₋₁₃₂-YFP, (10%, n = 9/89 cells), (B) common prophase TAN1₁₋₁₃₂-YFP nuclear accumulation without division site localization (90%, n = 80/89 cells), (C) no specific TAN1₁₋₁₃₂-YFP division site accumulation in metaphase (100%, n = 28/28 cells), (D) faint TAN1₁₋₁₃₂-YFP division site accumulation accompanied by midline accumulation in late anaphase/early telophase (80%, n = 16/20 cells) and (E) TAN1₁₋₁₃₂-YFP division site accumulation during telophase (100%, n = 58/58 cells). F-H) *tan1 air9* plants expressing *p35S:TAN1(28-33A)₁₋₁₃₂-YFP* during mitosis (n = 13 plants). The division site is indicated by arrowheads in the YFP panels. F) No specific TAN1(28-33A)₁₋₁₃₂-YFP prophase division site accumulation during prophase (100%, n = 20/20 cells), (G) no specific TAN1(28-33A)₁₋₁₃₂-YFP division site accumulation during metaphase (100%, n = 12/12 cells), (H) no TAN1(28-33A)₁₋₁₃₂-YFP division site or midline accumulation in late anaphase/early telophase (100%, n = 8/8 cells), (I) no specific TAN1(28-33A)₁₋₁₃₂-YFP division site accumulation during telophase (68%, n = 15/22 cells) and (J) faint TAN1(28-33A)₁₋₁₃₂-YFP division site accumulation during telophase (32%, n = 7/22 cells). K) Ratio of TAN1₁₋₁₃₂-YFP (left) or TAN1(28-33A)₁₋₁₃₂-YFP (right) fluorescence at the division site to cytosolic fluorescence from *tan1 air9* plants expressing *p35S:TAN1₁₋₁₃₂-YFP* or *p35S:TAN1(28-33A)₁₋₁₃₂-YFP* during telophase, n >23 plants for each genotype. Asterisks indicate a significant difference as determined by Mann-Whitney U test, P-value <0.0001.

Disrupting TAN1-POK1 interaction alters TAN1 and POK1 localization to the division site and reduces *tan1 air9* rescue

To further understand how TAN1 functions, we disrupted its ability to interact with the kinesin POK1 using alanine scanning mutagenesis. Alanine scanning mutagenesis was used to replace six amino acids with six alanines across the first ~120 amino acids of TAN1₁₋₁₃₂ (described in materials and methods). After testing their interaction with POK1 using the yeast two-hybrid system, we identified seven constructs that lost interaction with POK1 (Supplementary Figure 3.2). Reasoning that highly conserved amino acids would be more likely to play critical roles in TAN1-POK1 interaction, we selected TAN1₁₋₁₃₂ with alanine substitutions replacing the highly conserved amino acids 28-33 (INKVDK) with six alanines (TAN1(28-33A)₁₋₁₃₂) for analysis in Arabidopsis. Our hypothesis was that the mutated form of TAN1₁₋₁₃₂ (TAN1(28-33A)₁₋₁₃₂) would not rescue the *tan1 air9* mutant due to lack of POK1 and TAN1 interaction. TAN1(28-33A)₁₋₁₃₂ was cloned into a plant transformation vector to generate *p35S:TAN1(28-33A)₁₋₁₃₂-YFP* and transformed into the *tan1 air9* double mutant. The *p35S:TAN1(28-33A)₁₋₁₃₂-YFP* construct partially rescued the *tan1 air9* double mutant (Figure 3.4). *p35S:TAN1(28-33A)₁₋₁₃₂-YFP* in the *tan1 air9* double mutant did not rescue cell file rotation defects (Figure 3.4B, D) or phragmoplast angle defects (Figure 3.4F). However, overall plant growth (Figure 3.4C) and root length (Figure 3.4E) showed intermediate rescue compared to unaltered *p35S:TAN1₁₋₁₃₂-YFP* in the *tan1 air9* double mutant. PPB angles in *tan1 air9* double mutants expressing

either *p35S:TAN1(28-33A)₁₋₁₃₂-YFP* or *p35S:TAN1₁₋₁₃₂-YFP* were similar, suggesting that TAN1-POK1 interaction may not be required for PPB placement (Figure 3.4F). These results suggest that the first 132 amino acids of TAN1 perform several vital functions, some of which are contingent or partially contingent on a likely interaction with POK1 in Arabidopsis.

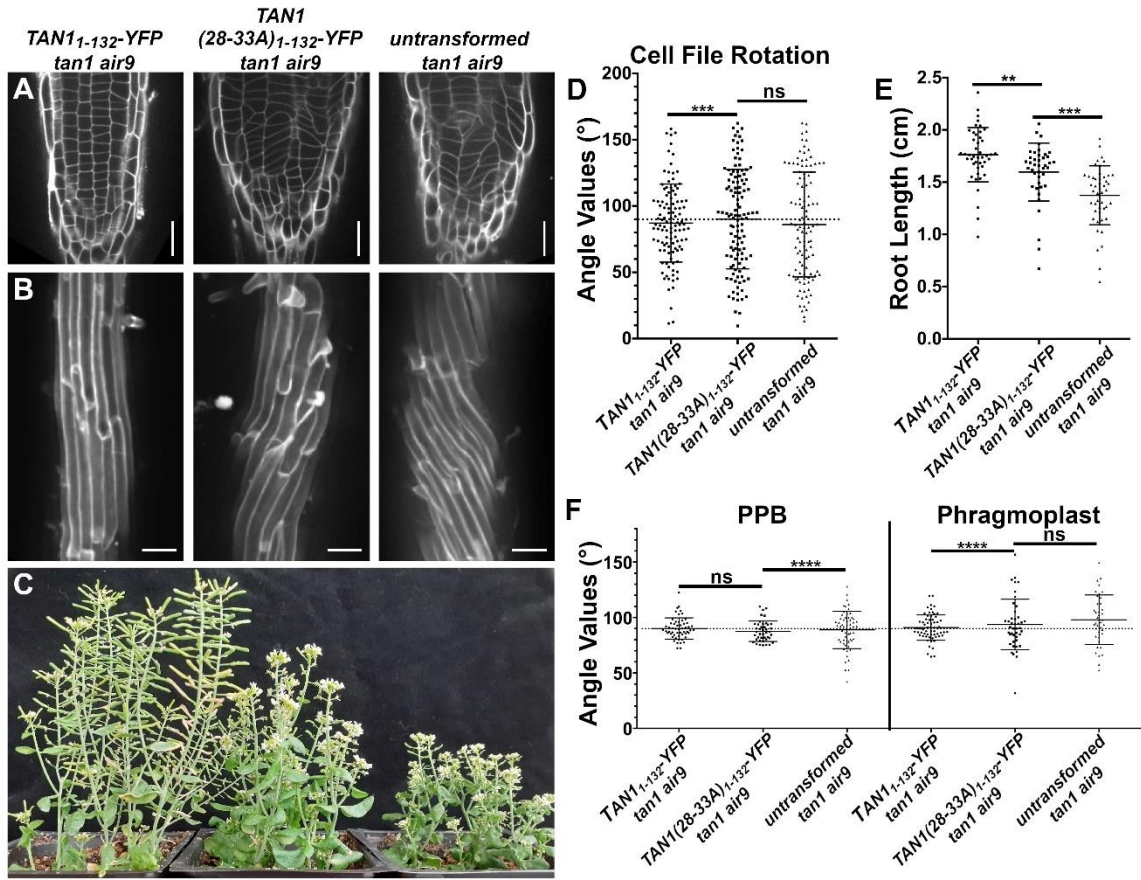


Figure 3.4: *p35S:TAN1(28-33A)₁₋₁₃₂-YFP* partially rescues *tan1 air9* double mutant phenotypes. A) Cell walls of Arabidopsis *tan1 air9* double mutant root tips stained with propidium iodide (PI) of plants expressing *p35S:TAN1₁₋₁₃₂-YFP* (left), *p35S:TAN1(28-33A)₁₋₁₃₂-YFP* (middle), and untransformed *tan1 air9* double mutants (right). Scale bars = 25 μ m. B) Maximum projections of 10 1- μ m Z-stacks of PI-stained differentiation zone root cell walls. Scale bars = 50 μ m. C) 58-day old *tan1 air9* double mutants expressing *p35S:TAN1₁₋₁₃₂-YFP* (left), *p35S:TAN1(28-33A)₁₋₁₃₂-YFP* (middle), and untransformed *tan1 air9* double mutants (right). D) Cell file rotation angles of *tan1 air9* double mutants expressing *p35S:TAN1₁₋₁₃₂-YFP* (left), *p35S:TAN1(28-33A)₁₋₁₃₂-YFP* (middle), and untransformed *tan1 air9* double mutants (right) $n > 27$ plants for each genotype. Variances were compared with Levene's test. E) Root length measurements from 8 days after stratification of *tan1 air9* double mutants expressing *p35S:TAN1₁₋₁₃₂-YFP* (left), *p35S:TAN1(28-33A)₁₋₁₃₂-YFP* (middle), and untransformed *tan1 air9* double mutants (right), $n > 40$ plants for each genotype, two-tailed t-test with Welch's correction. F) PPB and phragmoplast angle measurements in dividing root cells of *tan1 air9* double mutants expressing *p35S:TAN1₁₋₁₃₂-YFP* (left), *p35S:TAN1(28-33A)₁₋₁₃₂-YFP* (middle), and untransformed plants (right), $n > 17$ plants for each genotype. Angle variance compared with F-test. ns indicates not significant, ** P-value < 0.01 , *** P-value < 0.001 , **** P-value < 0.0001 .

To understand how this mutation within TAN1₁₋₁₃₂ affected localization, we analyzed TAN1(28-33A)₁₋₁₃₂-YFP in the *tan1 air9* double mutant. Localization of TAN1(28-33A)₁₋₁₃₂-YFP to the division site in *tan1 air9* double mutants was significantly reduced compared to unaltered TAN1₁₋₁₃₂-YFP, which localized to the division site during telophase 100% of the time (n = 58/58 cells, 29 plants, Figures 3.3E, (Rasmussen et al., 2011)). TAN1(28-33A)₁₋₁₃₂-YFP showed no obvious division site localization 68% of the time (n = 15/22 cells, Figure 3.3I) or faint division site accumulation in 32% of telophase cells (n = 7/22 cells, Figure 3.3J). When the fluorescence intensity of TAN1(28-33A)₁₋₁₃₂-YFP at the division site during telophase was compared to the cytosolic fluorescence intensity in the same cell, the median ratio was ~1.1 indicating little preferential accumulation of TAN1(28-33A)₁₋₁₃₂-YFP at the division site (Figure 3.3K). In contrast, the median ratio of unaltered TAN1₁₋₁₃₂-YFP at the division site was ~1.8 compared to cytosolic fluorescence, indicating its preferential accumulation at the division site. This suggests that TAN1 requires the motif in amino acids 28-33 to localize properly to the division site during telophase. Our hypothesis is that this reduced localization is due to disruptions in TAN1₁₋₁₃₂-POK1 interaction.

Next, we generated a construct that introduced alanines at amino acids 28-33 in full-length YFP-TAN1 constructs (*p35S:YFP-TAN1(28-33A)*) to assess whether *p35S:YFP-TAN1(28-33A)* would rescue the *tan1 air9* double mutant. In contrast to the modest partial rescue provided by *p35S:TAN1(28-33A)₁₋₁₃₂-YFP*, full-length

p35S:YFP-TAN1(28-33A) significantly rescued the defects in the *tan1 air9* double mutant, as described below. First, we assessed whether full-length TAN1(28-33A) interacted with POK1 via the yeast two-hybrid system, and it did not (Supplementary Figure 3.3). Next, we analyzed rescue in Arabidopsis expressing *p35S:YFP-TAN1(28-33A)*. Most defects except phragmoplast angle variance (Figure 3.5, Supplementary Figure 3.4) were fully rescued in the *p35S:YFP-TAN1(28-33A) tan1 air9* lines, including cell file rotation (Figure 3.5C), root length (Figure 3.5D) and PPB angles (Figure 3.5E). Similar to TAN1-YFP, YFP-TAN1(28-33A) localized to the division site in preprophase, prophase and telophase (Supplementary Figure 3.5).

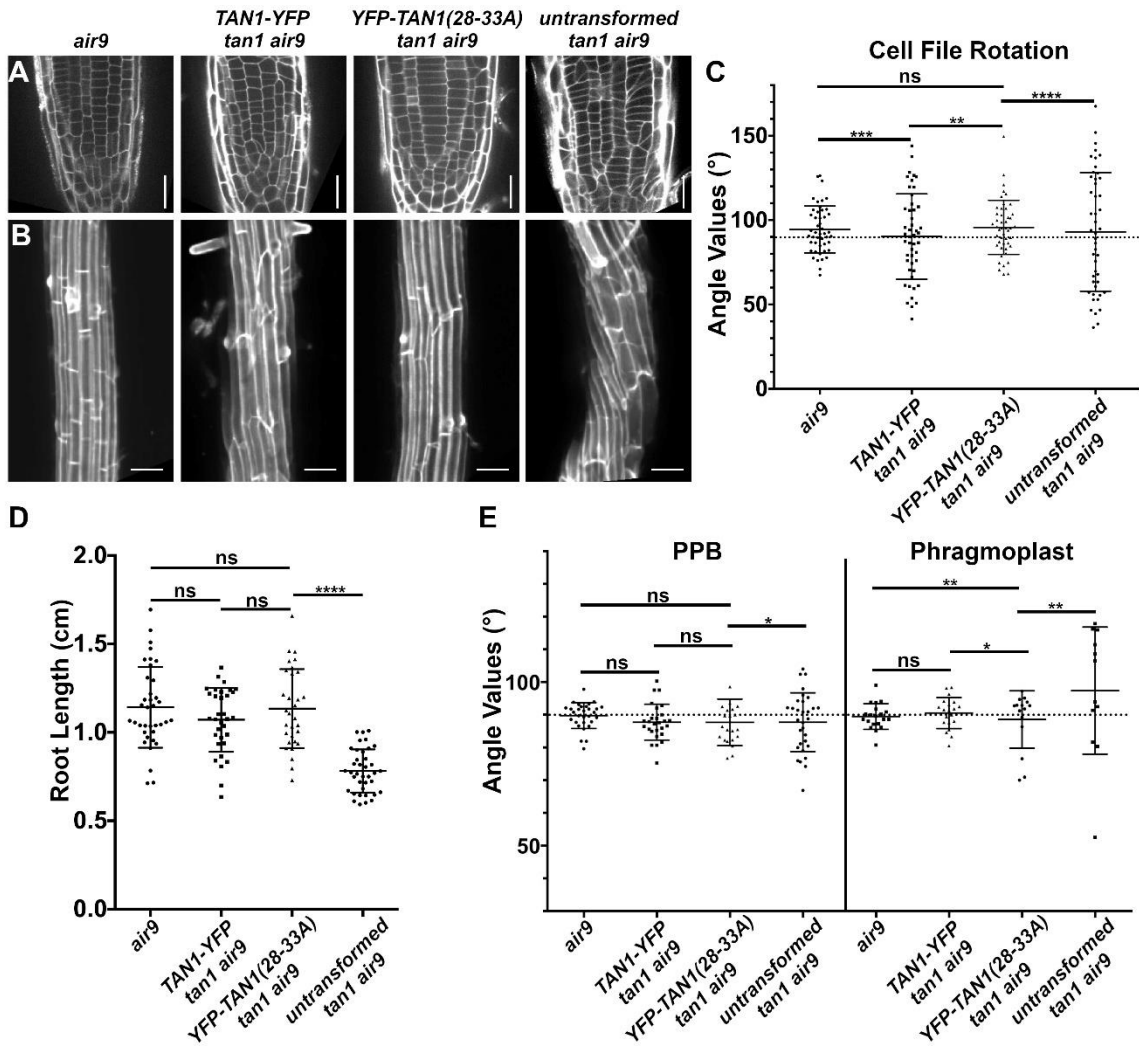


Figure 3.5: Full length *TAN1* with alanine substitutions replacing amino acids 28 to 33 (*p35S:YFP-TAN1(28-33A)*) mostly rescues the *tan1 air9* double mutant. A) Propidium iodide stained root tips of an *air9* single mutant (left) and *tan1 air9* double mutants expressing *p35S:TAN1-YFP* (center left) or *p35S:YFP-TAN1(28-33A)* (center right), and an untransformed *tan1 air9* plant (right). Scale bars = 25 μm . B) Maximum projections of 10 1- μm Z-stacks of PI-stained cell walls in the root differentiation zone. Scale bars = 50 μm . C) Cell file rotation angles of *air9* single mutants (left), *tan1 air9* double mutant plants expressing *p35S:TAN1-YFP* (center left) or *p35S:YFP-TAN1(28-33A)* (center right), and untransformed *tan1 air9* plants (right), $n > 9$ plants for each genotype. Variances were compared with Levene's test. D) Root length measurements from 8 days after stratification of *air9* single mutants (left) and *tan1 air9* double mutants expressing *p35S:TAN1-YFP* (center left) or *p35S:YFP-TAN1(28-33A)* (center right), and untransformed *tan1 air9* plants (right), $n > 30$ plants of each genotype, compared by two-tailed t-test with Welch's correction. E) PPB and phragmoplast angle measurements in dividing root cells of *air9* single mutants (left) and *tan1 air9* double mutant plants expressing *p35S:TAN1-YFP* (center left) or *p35S:YFP-TAN1(28-33A)* (center right), and untransformed *tan1 air9* plants (right), PPB measurements $n > 15$ plants for each genotype; phragmoplast measurements $n > 8$ plants for each genotype. Angle variance compared with F-test. ns indicates not significant, * P-value < 0.05 , ** P-value < 0.01 , *** P-value < 0.001 , **** P-value < 0.0001 .

To determine if full-length YFP-TAN1(28-33A) had reduced accumulation at the division site during telophase similar to TAN1(28-33A)₁₋₁₃₂-YFP, fluorescence intensity levels were measured. During prophase, YFP-TAN1(28-33A) fluorescence intensity at the division site compared to the cytosol was comparable to TAN1-YFP fluorescence intensity ratios. In contrast, YFP-TAN1(28-33A) fluorescence intensity ratios during telophase were reduced to ~1.6 compared with unaltered TAN1-YFP (~2.1) indicating that YFP-TAN1(28-33A) accumulated less at the division site during telophase (Supplementary Figure 3.5). Together, these data suggest that TAN1 is recruited to the division site during prophase without interaction with POK1. Defects in phragmoplast positioning may be due specifically to the disruption of TAN1-POK1 interaction, or due to the lower accumulation of TAN1 at the division site that would normally be mediated by POK1 during telophase.

To better understand how these alanine substitutions affect both POK1 and TAN1 localization we examined *tan1 air9* double mutants expressing a microtubule marker (*UBQ10:mScarlet-MAP4* (Pan et al., 2020)), *pTAN1:CFP-TAN1(28-33A)* and *pPOK1:YFP-POK1* (Lipka et al., 2014). Both CFP-TAN1(28-33A) and YFP-POK1 had reduced accumulation at the division site in the *tan1 air9* double mutant. CFP-TAN1(28-33A) and YFP-POK1 colocalized with the PPB in 41% of cells (n = 32/79) which is significantly less frequent when compared to 72% of cells (n=58/82 cells, 20 plants) with PPBs in *tan1 air9*

mutants containing unaltered CFP-TAN1 and YFP-POK1 (Figure 3.6A, Table 3.2; Fisher's exact test, P-value = 0.0001). Unaltered CFP-TAN1 fully rescued the *tan1 air9* double mutant (Mills and Rasmussen, 2022), and serves here as a control. Unaltered CFP-TAN1 and YFP-POK1 localized and were maintained at the division site similar to wild type in metaphase (Figure 3.6B, n=13/13), while CFP-TAN1(28-33A) and YFP-POK1 in *tan1 air9* mutants were sometimes absent from the division site in metaphase with only 58% of metaphase cells maintaining both proteins at the division site (n = 11/19 cells, Figure 3.6F, Table 3.2). During early telophase, unaltered CFP-TAN1 and YFP-POK1 were always at the division site (n = 14/14, Figure 3.6C), but CFP-TAN1(28-33A) and YFP-POK1 were maintained at the division site in only 65% of early telophase cells (n = 20/31 cells, Figure 3.6G, Table 3.2). Interestingly, YFP-POK1 accumulated in the phragmoplast midline in 26% of early telophase cells (n = 8/31 cells, Table 3.2) but was not observed in the phragmoplast midline in early telophase cells of plants expressing unaltered CFP-TAN1 (n = 0/14 cells, Table 3.2). During late telophase, when the phragmoplast has contacted the cell cortex in at least one location, CFP-TAN1 and POK1 always localized to the division site (100%, n = 63/63 cells, Figure 3.6D). Interestingly, although not observed in earlier stages, YFP-POK1 and CFP-TAN1(28-33A) recruitment to the division site increased to 90% of late telophase cells (n = 53/59 cells, Figure 3.6H). In the remainder of cells, neither CFP-TAN1(28-33) nor YFP-POK1 localized to the division site (3%, n = 2/59), or only CFP-TAN1(28-33) accumulated at the division site (7%, n =

4/59 cells). Together, these data suggest that TAN1-POK1 interactions play a critical role in stabilizing them together at the division site. Additionally, it suggests that other, yet unidentified proteins may recruit both TAN1 and POK1 to the division site, particularly during late telophase, in the absence of both AIR9 and TAN1-POK1 interaction.

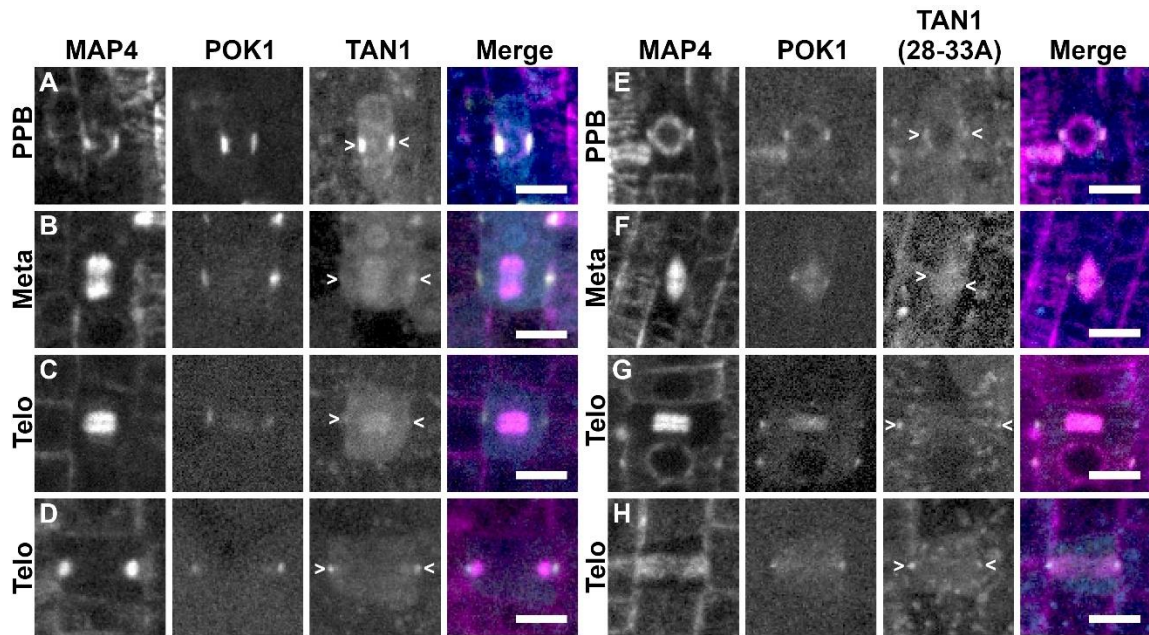
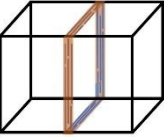
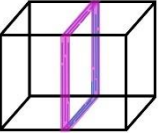
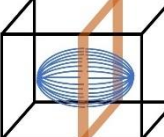
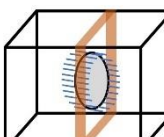
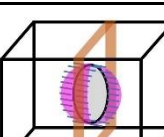
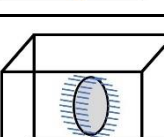
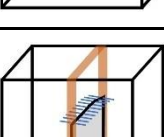
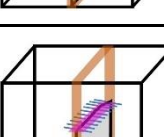
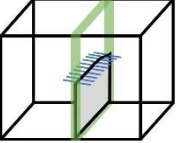
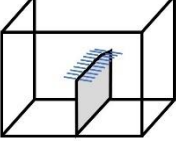


Figure 3.6: CFP-TAN1(28-33A) and YFP-POK1 exhibit impaired recruitment to the division site in the *tan1 air9* double mutant. YFP-POK1 localization in *tan1 air9* double mutants expressing *UBQ10:mScarlet-MAP4* and either (A-D) *pTAN1:CFP-TAN1* (n = 20 plants) or (E-I) *pTAN1:CFP-TAN1(28-33A)* (n = 22 plants). Maximum projections of 3 1- μ m Z-stacks. Scale bars = 10 μ m. Some bleed through from the mScarlet channel can be seen in the YFP-POK1 panels. A) YFP-POK1 and CFP-TAN1 colocalized with the PPB in 72% of cells (n = 59/82 cells). B) YFP-POK1 and CFP-TAN1 were maintained at the division site in metaphase 13/13 and anaphase 4/4 cells. C) YFP-POK1 and CFP-TAN1 were maintained at the division site in all early telophase cells (n = 14/14 cells) and late telophase (n = 63/63 cells). E) YFP-POK1 and CFP-TAN1(28-33A) colocalized with the PPB in 41% of cells (n = 32/79 cells). F) YFP-POK1 and CFP-TAN1(28-33A) were maintained at the division site in 58% of metaphase cells (n = 11/19 cells). CFP-TAN1(28-33A) was faint at the division site. G) Both YFP-POK1 and CFP-TAN1(28-33A) were observed at the division site in 65% of early telophase cells (n = 20/31 cells). H) YFP-POK1 and CFP-TAN1(28-33A) were recruited to the division site in 90% of late telophase cells (n = 53/59 cells). Some late telophase cells were observed to have CFP-TAN1(28-33A) but not YFP-POK1 at the division site (7%, n = 4/59 cells) or neither CFP-TAN1(28-33A) or YFP-POK1 at the division site (3% n = 2/59 cells).

Table 3.2. POK1 and TAN1 or TAN1(28-33) localization to the division site in *tan1 air9* double mutants. Statistically significant differences were determined using Fisher's exact test. NS indicates not significant. Brown represents dual localization of YFP-POK1 and either CFP-TAN1 or CFP-TAN1(28-33A), magenta is YFP-POK1 alone, green is CFP-TAN1(28-33A) alone, blue lines are microtubules, and light gray represents the cell plate in schematics.

Schematic	Description	<i>tan1 air9</i> CFP-TAN1, N = 20 plants	<i>tan1 air9</i> CFP-TAN1(28-33A), N = 22 plants
	PPB, Both POK1 and TAN1	72%, n = 59/82	41%, n = 32/79 *** (p = 0.001)
	PPB, POK1 only	6%, n = 5/82	16%, n = 13/79* (p = 0.461)
	Metaphase, Both POK1 and TAN1 at the division site	100%, n = 13/13	58%, n = 11/19** (p = 0.0104)
	Early Telophase, Both POK1 and TAN1 at the division site	100%, n = 14/14	39%, n = 12/31*** (p = 0.0001)
	Early Telophase, Both POK1 and TAN1 at the division site, POK1 in the phragmoplast midline	0%, n = 0/14	26%, n = 8/31* (p = 0.0436)
	Early Telophase, NO POK1 or TAN1 at division site or phragmoplast midline	0%, n = 0/14	35%, n = 11/31** (p = 0.098)
	Late Telophase, Both POK1 and TAN1 at the division site only	95%, n = 60/63	71%, n = 42/59*** (p = 0.0004)
	Late Telophase, POK1 and TAN1 at the division site and POK1 in the phragmoplast midline	5%, n = 3/63	19%, n = 11/59* (p = 0.022)

	<p>LateTelophase, TAN1 only at the division site</p>	<p>0%, n = 0/63</p>	<p>7%, n = 4/59 (NS, p = 0.0518)</p>
	<p>Late Telophase, Neither TAN1 or POK1 at division site or in the phragmoplast midline</p>	<p>0%, n = 0/63</p>	<p>3%, n = 2/59 (NS, p = 0.2318)</p>

DISCUSSION

In *tan1* and *air9* single mutants, POK1 localizes to the division site and there are no discernable division plane defects (Model in Supplementary Figure 3.6). However, in the *tan1 air9* double mutant, POK1 co-localizes with the PPB but is lost from the division site during metaphase (Model in Figure 3.7). First, this suggests that TAN1 and AIR9 are not essential for POK1 co-localization with the PPB. Second, it suggests that POK1 is maintained at the division site after PPB disassembly via direct or indirect interactions with TAN1 or AIR9. We provide evidence that TAN1 interacts with POK1 through motifs within the first 132 amino acids of TAN1, as identified using the yeast two-hybrid system. Alignments of TANGLED1 proteins from representative monocots and dicots, such as *Solanum lycopersium*, *Oryza sativa*, *Sorghum bicolor*, *Zea mays*, and *Brassica napus*, showed that amino acids 28-33 (INKVDK) are highly conserved across plant species (Supplementary Figure 3.7). Amino acids 30-32 (VDK) are identical and the remaining residues within the motif have similar properties across these plant species. The high degree of conservation suggests that these amino acids are likely important for TAN1 function. When alanine substitutions of these amino acids were introduced into TAN1 and transformed into *Arabidopsis tan1 air9* double mutants, we observed reduced TAN1 and POK1 localization at the division site, as well as defects in phragmoplast positioning. Here we hypothesize that amino acids 28-33 are essential for TAN1 and POK1 interaction in both yeast two-hybrid and in *Arabidopsis*. In addition to several reports showing that

TAN1 and POK1 interact using the yeast two-hybrid system (Müller et al., 2006; Rasmussen et al., 2011), bimolecular fluorescence complementation has also been used to show TAN1-POK1 interactions in Arabidopsis protoplasts (Lipka et al., 2014). Alanine substitutions at positions 28-33 of TAN1 may disrupt TAN1-POK1 interaction through misfolding that blocks the POK1 interaction site or by affecting the amino acids that directly mediate POK1 binding. Regardless of the exact mechanism(s) of POK1-TAN1 physical interactions or the possibility that yeast two-hybrid interactions do not reflect equivalent POK1-TAN1 physical interactions in Arabidopsis, we show that these TAN1 amino acids are involved in mediating TAN1 and POK1 localization to the division site.

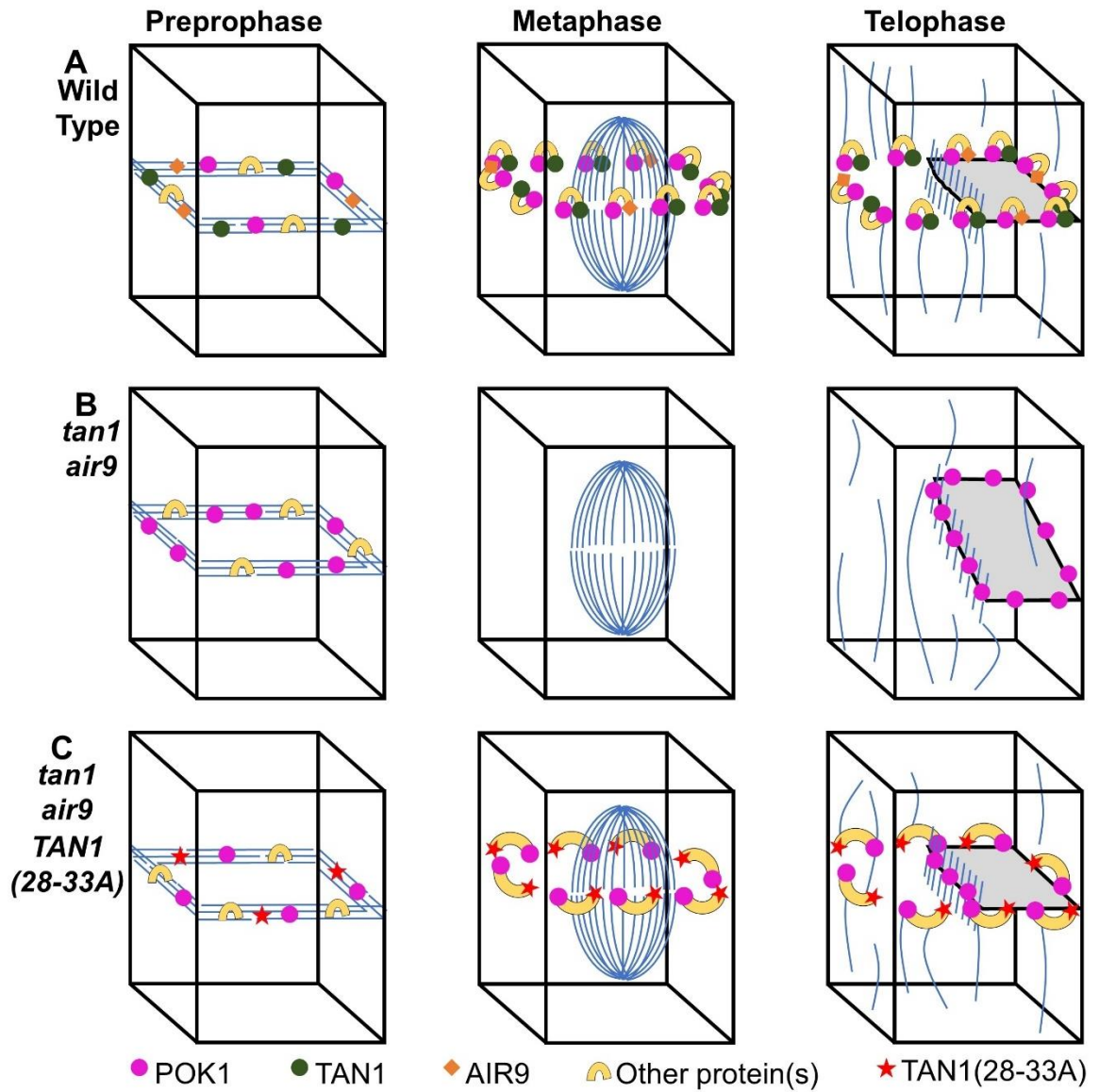


Figure 3.7: A speculative model on TAN1, AIR9, and POK1 interactions to ensure correct division plane orientation. A) In wild-type (WT) cells, AIR9, TAN1, and POK1 are recruited independently of one another to the PPB. Interaction between TAN1 and POK1 maintain both proteins at the division site through telophase, with AIR9 being re-recruited to the division site in late telophase. B) In the *tan1 air9* double mutant, TAN1, AIR9, and potential AIR9/POK1 interacting proteins are recruited to the PPB. Upon disassembly of the PPB, POK1 is lost from the division site and during telophase aberrantly accumulates in the phragmoplast midline. Due to the loss of TAN1 and POK1 from the division site, the phragmoplast is not guided to the location defined by the PPB. C) In *tan1 air9* double mutants expressing *TAN1(28-33A)*, TAN1(28-33A) and POK1 are recruited to the PPB independently of one another. POK1 and TAN1(28-33A) are partially maintained in some metaphase and early telophase cells possibly by interactions with other proteins. However, due to the inability of TAN1(28-33A) and POK1 to interact with one another, both proteins are not efficiently maintained at the division site. The majority (90%) of late telophase cells contain both POK1 and TAN1(28-33A) at the division site. Late recruitment of POK1 and TAN1(28-33A) may help guide the phragmoplast to the correct division site in a majority of cells.

We demonstrate that the first region of the TAN1 protein, the first 132 amino acids which primarily accumulates at the division site during telophase (Rasmussen et al., 2011), is both necessary (Mir et al., 2018) and sufficient to largely rescue the *tan1 air9* double mutant (Figure 3.2). This suggests that TAN1₁₋₁₃₂ and its recruitment to the division site during telophase is critical for correct division plane orientation in the *tan1 air9* double mutant. Although full length TAN1 localizes to the division site throughout cell division, the ability of TAN1₁₋₁₃₂ to rescue the *tan1 air9* double mutant, suggests that TAN1, and possibly POK1, localization to the PPB and division site during metaphase may not be required for division site maintenance in Arabidopsis. Indeed, whether the PPB itself is required for division plane positioning has been raised by analysis of a triple mutant in three closely related *TONNEAU RECRUITING MOTIF6,7,8* genes (*trm6,7,8*). *trm678* mutants, which lacked well defined PPBs, had disrupted POK1 recruitment to the division site but only minor defects in division positioning (Schaefer et al., 2017). However, when amino acids critical for TAN1-POK1 interactions in the yeast two-hybrid system are disrupted by transforming *TAN1(28-33A)*₁₋₁₃₂-*YFP* into the *tan1 air9* double mutant, root growth and phragmoplast positioning are disrupted. *TAN1(28-33A)*₁₋₁₃₂-*YFP* accumulation at the division site during telophase was reduced compared to unaltered *TAN1*₁₋₁₃₂-*YFP*. This suggests that TAN1-POK1 interaction promotes, but is not strictly necessary, for TAN1 recruitment to the division site during telophase.

Full-length TAN1(28-33A) localizes to the division site throughout cell division and almost fully rescues the *tan1 air9* double mutant. TAN1, AIR9, and POK1 coclocalize at the PPB independently of one another, which may promote the formation of protein complexes required for division site maintenance.

Colocalizing with the PPB may provide an opportunity for proteins in close proximity to form stabilizing interactions before PPB disassembly. This suggests that recruitment of TAN1 and POK1 to the division site early in cell division may provide another temporally distinct way to promote correct division plane positioning. Phragmoplast positioning defects in TAN1(28-33A) *tan1 air9* plants may be the result of defects in phragmoplast guidance in cells that lacked TAN1(28-33A) and POK1 at the division site in metaphase or early telophase that were not corrected in late telophase.

The ability of TAN1(28-33A) and POK1 to remain at the division site in some cells after PPB disassembly in the *tan1 air9* double mutant suggests that there are other proteins that interact with TAN1 and/or POK1 that help stabilize them at the division site perhaps via the formation of multiprotein complexes. The pleckstrin homology GAPS, PHGAP1 and PHGAP2 (Stöckle et al., 2016), RANGAP1 (Xu et al., 2008), and IQ67 DOMAIN (IQD)^{6,7,8} proteins (Kumari et al., 2021) are division site localized proteins that may stabilize TAN1 and POK1 at the division site via their interaction with POK1. PHGAP1, PHGAP2, and RANGAP1 are dependent on POK1 and POK2 for division site recruitment. Like

TAN1, RANGAP1 colocalizes with the PPB and remains at the division site throughout cell division (Xu et al., 2008). PHGAP1 and PHGAP2 are uniformly distributed in the cytoplasm and on the plasma membrane in interphase cells and accumulate at the division site during metaphase. These proteins also have their own distinct roles in division site maintenance (Stöckle et al., 2016). PHGAP2 has a likely role in division site establishment by regulating ROP activity (Hwang et al., 2008). RANGAP1 regulation of local RAN-GTP levels has potential roles in microtubule organization and division site identity (Xu et al., 2008). IQD6, IQD7, and IQD8 interact with POK1 and play a role in PPB formation and POK1 recruitment to the division site. *iqd678* triple mutants have PPB formation defects and fail to recruit POK1 to the division site in cells lacking PPBs. However, POK1 localization to the division site in *iqd678* mutants recovers during telophase to wild-type levels (Kumari et al., 2021). We speculate that this IQD6-8 independent recruitment may depend on TAN1. Unlike the PHGAPs and RANGAP1, IQD8 localization to the division site is not dependent on POK1 and POK2. This suggests that IQD6-8 proteins work upstream of POK1 to establish the division site and are important for POK1 recruitment to the division site early in cell division. Although TAN1-POK1 interaction becomes critical for TAN1 and POK1 maintenance at the division site in the absence of AIR9, other division site localized proteins may provide additional stability and help maintain TAN1 and POK1 at the division site.

How AIR9 stabilizes POK1 at the division site in the absence of TAN1 is less clear. There is no information about whether POK1 and AIR9 interact directly with one another. Additionally, AIR9 localization, in contrast to TAN1 localization, is intermittent at the division site. When expressed in tobacco Bright Yellow2 (BY2) cells, AIR9 colocalizes with the PPB but is then lost from the division site until late telophase when the phragmoplast contacts the cortex (Buschmann et al., 2006). In Arabidopsis, AIR9 may localize to the division site during metaphase or telophase, but it is difficult to observe because AIR9 also strongly colocalizes with cortical microtubules which may obscure AIR9 localization in nearby cells (Buschmann et al., 2015). Rather than directly interacting with POK1, AIR9 may recruit other proteins to the division site during preprophase that help maintain POK1 at the division site in the absence of TAN1. One potential candidate is the kinesin-like calmodulin binding protein, KCBP, which interacts with AIR9 (Buschmann et al., 2015). KCBP is a minus-end-directed kinesin (Song et al., 1997) that localizes to the division site in Arabidopsis and moss (Miki et al., 2014; Buschmann et al., 2015). We speculate that other TAN1, AIR9, and POK1 interacting proteins that have not been identified yet may be key for TAN1-POK1 division site maintenance.

POK1 and POK2 have roles in phragmoplast guidance, but POK2 also has a role in phragmoplast dynamics (Lipka et al., 2014; Herrmann et al., 2018). Although POK1 does not frequently accumulate in the phragmoplast midline in wild-type

cells, POK2 showed striking dual localization to both the phragmoplast midline and the division site. Localization of POK2 to the phragmoplast midline required the N-terminal motor domain, while the C-terminal region was localized to the division site (Herrmann et al., 2018). Our hypothesis is that the “default” location of both POK1 and POK2 is at microtubule plus-ends at the phragmoplast midline, based on likely or confirmed plus-end directed motor activity (Chugh et al., 2018). Interactions with division site localized proteins, such as TAN1 and AIR9, may stabilize or recruit POK1 and POK2 at the division site away from the phragmoplast midline.

We demonstrate that AIR9 and TAN1 function redundantly to maintain POK1 at the division site to ensure correct cell wall placement. In the absence of AIR9, our data suggests that TAN1-POK1 interaction promotes, but is not required for, the maintenance of both proteins at the division site and disrupting this interaction partially disrupts their localization to the division site. This also suggests that other TAN1, POK1, and AIR9 interacting proteins are involved with stabilizing TAN1 and POK1 at the division site.

MATERIALS AND METHODS

Growth conditions, genotyping mutants, and root length measurements

Arabidopsis seedlings were grown on ½ strength Murashige and Skoog (MS) media (MP Biomedicals; Murashige and Skoog, 1962) containing 0.5 g/L MES (Fisher Scientific), pH 5.7, and 0.8% agar (Fisher Scientific). Seeds sown on plates were first stratified in the dark at 4°C for 2 to 5 days then grown vertically in a growth chamber (Percival) with 16/8-h light/dark cycles and temperature set to 22°C. For root length experiments, *tan1 air9* transgenic T3 lines expressing *p35S:TAN1-YFP*, *35S:TAN1₁₋₁₃₂-YFP*, *35S:TAN1(28-33A)₁₋₁₃₂-YFP*, or *35S:YFP-TAN1(28-33A)* were grown vertically, the plates were scanned (Epson) and root lengths were measured using FIJI (ImageJ, <http://fiji.sc/>) after 8 days.

Untransformed *tan1 air9* double mutants and *air9* single mutants were grown alongside the double mutant seeds expressing the TAN1 constructs in equal numbers on the same plates to ensure plants were grown under the same conditions. After plates were scanned, seedlings were screened by confocal microscopy to identify seedlings expressing YFP translational fusion transgenes and CFP-TUBULIN, if present in the transgenic lines. At least 3 biological replicates, grown on separate plates on separate days, and at least 28 plants of each genotype total across all replicates were analyzed for each root growth experiment. Welch's t-test was used to identify whether there were statistically significant differences between replicates before pooling the replicates for analysis. Root lengths were then plotted using Prism (GraphPad). Statistical

analysis of root length was performed with Prism (GraphPad) using t-test with Welch's correction. Welch's t-test (unequal variance t-test) is used to test the hypothesis that two populations have equal means. Unlike the Student's t-test, Welch's t-test is often used when two samples have unequal variances or sample sizes. This test was used due to the unequal sample sizes because the plants examined were often segregating for multiple transgenes and had lower sample sizes than control plants such as *air9* single mutants and *tan1 air9* double mutants which either lacked transgenes or were segregating fewer transgenes.

YFP translational fusion TAN1 constructs were analyzed in *csH-tan (TAN1, AT3G05330) air9-31 (AIR9, AT2G34680)* double mutants in *Landsberg erecta (Ler)* unless otherwise specified. The *pPOK1:YFP-POK1* transgene in Columbia, a kind gift from Sabine Müller (Lipka et al., 2014), was crossed into the *tan-mad* and *air9-5* Columbia/Wassilewskija double mutant previously described (Mir et al., 2018). *tan-mad* and *air9-5* mutants were genotyped with primers ATRP and ATLP (to identify wild-type *TAN1*), JL202 and ATLP (to identify T-DNA insertion in *TAN1*), AIR9-5RP and AIR9-5LP (to identify wild-type *AIR9*), and LBb1.3 and AIR9RP (to identify T-DNA insertion in *AIR9*) and by observation of the *tan1 air9* double mutant phenotype (Supplementary Table 3.1).

Generation of Transgenic Lines

Agrobacterium tumefaciens-mediated floral dip transformation was used as described (Clough and Bent, 1999). *csH-tan air9-31* double mutants were used

for all floral dip transformations unless otherwise specified. Transgenic plants were selected on 15 µg/mL glufosinate (Finale; Bayer) and screened by microscopy before being transferred to soil and selfed. *CFP-TUBULIN* was crossed into *35S:TAN1(28-33A)₁₋₁₃₂-YFP tan1 air9* plants using *tan1 air9 CFP-TUBULIN* plants (Mir et al., 2018) and progeny were subsequently screened by microscopy for CFP and YFP signal. *csH-tan1 air9-31* double mutants were confirmed by genotyping with primers ATLP and AtTAN 733-CDS Rw (to identify TAN1 wild-type), AtTAN 733-CDS Rw and Ds5-4 (to identify T-DNA insertion in TAN1), AIR9_cDNA 2230 F and AIR9 gnm7511 R (to identify AIR9 wild-type), and AIR9 gnm7511 R and Ds5-4 (to identify T-DNA insertion in AIR9).

Columbia expressing the microtubule marker *UBQ10:mScarlet-MAP4* (Pan et al., 2020), a kind gift from Xue Pan and Zhenbiao Yang (UCR), was crossed to *tan-mad* and *air9-5* Columbia/Wassilewskija double mutants expressing *pPOK1:YFP-POK1*. Progeny were screened for mScarlet-MAP4 and YFP-POK1 by confocal microscopy and then selfed to recover *air9-5* single mutants, *tanmad* single mutants, and *air9-5 tan-mad* double mutants expressing *mScarlet-MAP4* and *YFP-POK1*.

pTAN1:CFP-TAN1 and *pTAN1:CFP-TAN1(28-33A)* were introduced into *air9-5 tan-mad* double mutants expressing *mScarlet-MAP4* and *YFP-POK1* by *Agrobacterium tumefaciens*-mediated floral dip transformation. *pTAN1:CFP-*

TAN1 and *pTAN1:CFP-TAN1(28-33A)* transformants were selected on 100µg/mL gentamicin (Fisher Scientific) and the presence of mScarlet-MAP4, YFP-POK1, and either CFP-TAN1 or CFP-TAN1(28-33A) was confirmed by confocal microscopy. 4 independent transformed lines for *pTAN:CFP-TAN1(28-33A)* and 3 independent transformed lines for unaltered *pTAN:CFP-TAN1* were examined for division site localization cell counts.

Plasmid Construction

*TAN1*₁₋₁₃₂-*YFP* coding sequences were subcloned by EcoRI and BamHI double digestion from the plasmid *pEZRK-LNY-TAN1*₁₋₁₃₂-*YFP* described previously (Rasmussen et al., 2011) into *pEZT-NL* vector (a kind gift from David Ehrhardt, Carnegie Institute, Stanford University) and selected with glufosinate (Finale; Bayer). The CFP-TUBULIN (CFP-TUA6) vector was previously described, a kind gift from Viktor Kirik (Kirik et al., 2007).

Six amino acid alanine substitutions were generated using overlapping PCR (primers in Supplementary Table 3.1) beginning at amino acid 10 of *TAN1*₁₋₁₃₂. *TAN1*₁₋₁₃₂-*YFP* coding sequence from plasmids described previously was used as the PCR template (Rasmussen et al., 2011). *TAN1(28-33A)*₁₋₁₃₂-*YFP* was subcloned by EcoRI BamHI double digestion into *pEZT-NL*. To generate *YFP-TAN1(28-33A)*, alanine substitutions were first introduced into G22672 (*TAN1* cDNA in *pENTR223*, from the Arabidopsis Biological Resource Center) using overlapping PCR with the same primers to generate *TAN1(28-33A)*. Gateway LR

reaction (Fisher Scientific) was then used to subclone *TAN1(28-33A)* into pEarley104 (Earley et al., 2006).

pTAN:CFP-TAN1(28-33A) was generated using overlapping PCR. The TANGLED1 native promoter was amplified from *Np:AtTAN-YFP* (Walker et al., 2007) using the primers NpTANSaclFor and NpTANceruleanRev. Cerulean was amplified from the Cerulean CDS in pDONR221P4r/P3r using the primers NpTANceruleanFor and CeruleanpEarleyRev. *TAN1(28-33A)* in pEarley104 was amplified using CeruleanpEarleyFor and pEarleyOCSPstIRev. TANGLED1 native promoter, Cerulean, and *TAN1(28-33A)* were then combined using overlapping PCR using NpTANSacl and pEarleyOCSPstIRev. *pTAN:CFP-TAN1(28-33A)* was then subcloned into pJHA212G, a kind gift of Meng Chen (UCR), using SacI and PstI double digest. pTAN:CFP-TAN1 was generated the same way as pTAN:CFP-TAN1(28-33A) except unaltered *TAN1* in pEarley104 was amplified using CeruleanpEarleyFor and pEarleyOCSPstIRev.

Microscopy

An inverted Ti Eclipse (Nikon) with motorized stage (ASI Piezo) and spinning-disk confocal microscope (Yokogawa W1) built by Solamere Technology was used with Micromanager software (micromanager.org). Solid-state lasers (Obis) and emission filters (Chroma Technology) were used. For CFP translational fusions excitation 445, emission 480/40 was used; YFP translational fusions excitation 514, emission 540/30; and propidium iodide (PI), Alexa-568 goat anti-

mouse antibody, and mScarlet-MAP4 excitation 561, emission 620/60 were used. The 20x objective has 0.75 numerical aperture and the 60x objective has 1.2 numerical aperture which was used with perfluorocarbon immersion liquid (RIAAA-6788 Cargille). Excitation spectra for mScarlet-MAP4 and YFP-POK1 partially overlapped, which resulted in faint bleed through signal in the YFP channel for some dense microtubule structures (e.g. spindles and phragmoplasts). YFP-POK1 colocalization with PPBs was carefully determined based on distinct YFP-POK1 signal and the presence of cytosolic YFP-POK1.

The ratio of the division site versus cytosolic fluorescence intensity was determined by taking the median YFP fluorescence intensity from the center Z-stack of individual cells with PPBs or phragmoplasts. For each cell the median fluorescence intensity was measured for two cytosolic areas and the division site on each side of the cell using circles with areas of $0.875 \mu\text{m}^2$. The sum of the median intensity at the division site on each side was then divided by the sum of the median intensity of the two cytosolic areas to calculate the ratio of the division site versus cytosolic fluorescence intensity. Fluorescence intensities were measured in FIJI. All plants used for this analysis were grown on the same day and imaged using identical conditions, and at least 5 plants of each genotype were examined.

Measurements of PPB and phragmoplast angles and cell file rotation

At least 3 biological replicates, grown on separate plates on separate days, composed of at least 15 plants per genotype for PPB measurements and at least 8 plants per genotype for phragmoplast measurements were used to gather angle data. 8-day-old seedlings were stained with 10 μ M PI for 1 minute and then destained in distilled water before imaging by confocal microscopy using a 20x or 60x objective. PPB and phragmoplast angles were measured using FIJI. The angle was measured between the left-hand cell wall and the orientation of the PPB or phragmoplast in the root tips of *tan1 air9* double mutants expressing *CFP-TUBULIN* or immunostained microtubules (described in the next section). Cell file rotation was examined by measuring from the left-hand side of the transverse cell wall relative to the long axis of the root in images of the differentiation zone stained with PI. The differentiation zone was identified by the presence of root hairs. Prism (GraphPad) and Excel (Microsoft Office) were used to perform statistical analyses and to plot data. F-test was used to compare normally distributed variances (PPB and phragmoplast angles) and Levene's test was used to compare non-normally distributed variances (cell file rotation angle measurements). *tan1 air9* double mutants have non-normally distributed cell file twisting because the roots tend to twist to the left (Mir et al., 2018). Genotypes across biological replicates were compared to ensure there was no statistically significant difference between them before pooling data.

Immunostaining

air9, *tan1 air9 p35S:TAN1-YFP*, *tan1 air9 35S:YFP-TAN1(28-33A)*, and untransformed *tan1 air9* plants were stratified and then grown vertically on ½ MS plates in a growth chamber at 22°C with a 16/8-h light/dark cycle for 8 days. The seedlings were screened by microscopy for YFP and then fixed and processed for immunofluorescence microscopy using a 1:2000 dilution of monoclonal anti- α -tubulin B-5-1-2 antibody (Life Technologies; 32-2500) followed by 1:2000 dilution of Alexa-568 goat anti-mouse antibody (Thermo Fisher; A-11004) as described previously (Sugimoto et al., 2000).

Yeast two-hybrid

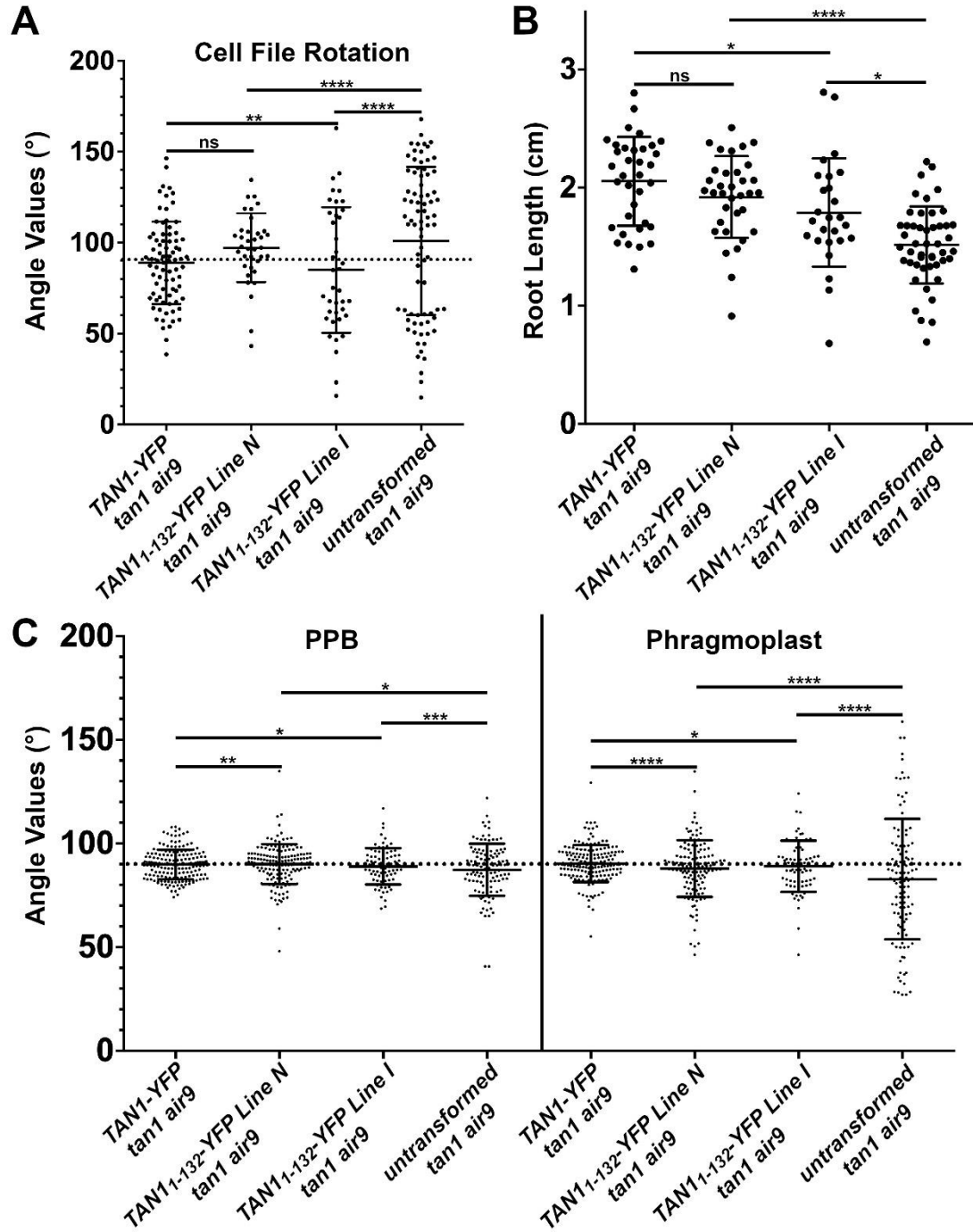
Six alanine substitutions were generated using overlapping PCR and TAN1 coding sequence in pEZRK-LNY-*TAN1*₁₋₁₃₂-YFP as a template beginning at amino acid 10 of TAN1 and continuing through amino acid 123 according to (Russell and Sambrook, 2001). All except amino acids substitutions for 64-69 and 106-111 were cloned into pAS vector (Fan et al., 1997) using EcoRI BamHI double digestion. pBD-TAN1(28-33A) was generated by using primers Ala_05_FOR and Ala_05_REV to perform DpnI mediated site-directed mutagenesis by PCR (Fisher and Pei, 1997). pBD-TAN1 (Walker et al., 2007), and pAS-*TAN1*₁₋₁₃₂ (Rasmussen et al., 2011) were used as positive controls, while pAD-MUT was used as a negative control for testing interaction with pAD-POK1 (Müller et al., 2006). *pAD-POK1* and *pAS-TAN1*₁₋₁₃₂ constructs were co-transformed into yeast strain YRG2 according to manufacturer instructions

(Stragene). Positive yeast two-hybrid interaction was determined by the presence of growth on plates cultured at 30°C lacking histidine after 3 days. Plates were then scanned (Epson).

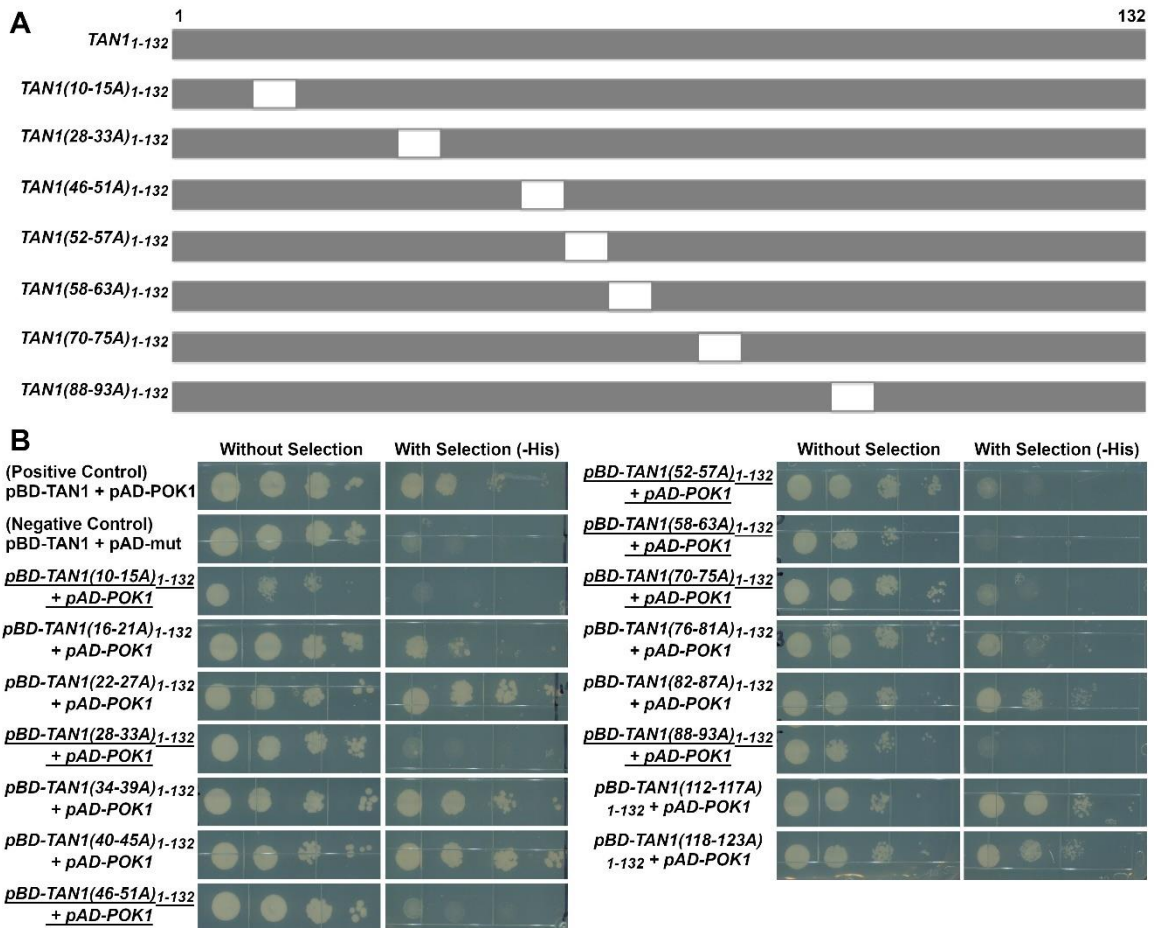
ACKNOWLEDGEMENTS

Thanks to Andrew Gomez (UCR, supported by USDA-NIFA 2017-38422-27135) for help with yeast two-hybrid experiments, Prof. Sabine Müller (University of Tübingen) for YFP-POK1 seeds, and Profs. Meng Chen and David Nelson (UCR) for their helpful comments on alanine scanning mutagenesis. Thanks to Prof. Henrik Buschmann (Osnabrück University) for original *tan1 air9* characterization. Thanks to Lindy Allsman, Stephanie Martinez, and Aimee Uyehara (UCR) for helpful comments on the manuscript. NSF-CAREER #1942734 and NSF-MCB #1716972, USDA-NIFA-CA-R-BPS-5108-H are gratefully acknowledged for funding.

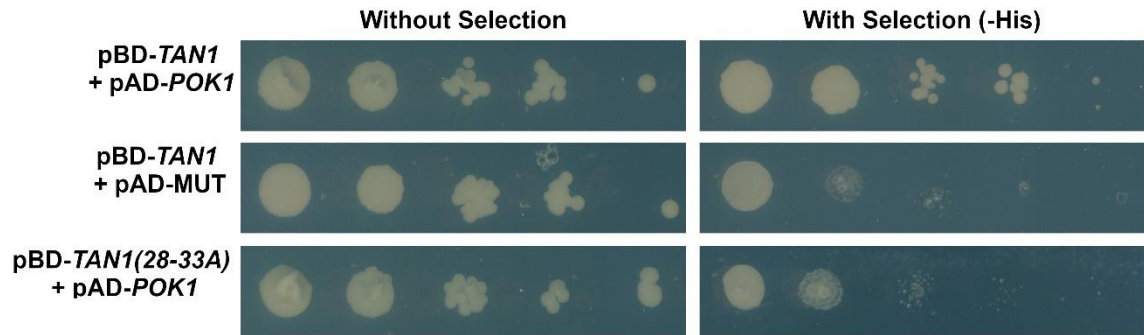
SUPPLEMENTAL FIGURES AND TABLES



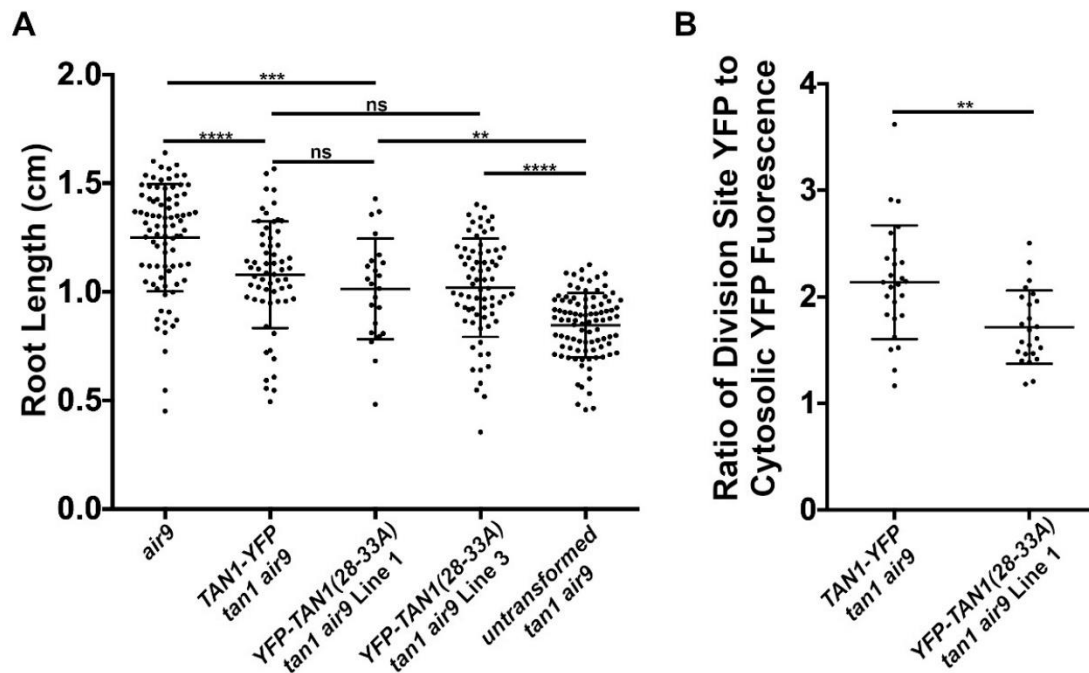
Supplementary Figure 3.1. *p35S:TAN1₁₋₁₃₂-YFP tan1 air9* lines show significant rescue compared to untransformed *tan1 air9* double mutants. A) Cell file rotation angles of *tan1 air9* double mutants expressing *p35S:TAN1-YFP* (left), two *p35S:TAN1₁₋₁₃₂-YFP* transgenic lines designated as line N (center left) and line I (center right) and untransformed *tan1 air9* plants (right) $n > 6$ plants for each genotype. Angle variances were compared with Levene's test. B) Root length measurements from 8 days after stratification of *tan1 air9* double mutants expressing *p35S:TAN1-YFP* (left), two *p35S:TAN1₁₋₁₃₂-YFP* transgenic lines (middle) and untransformed plants (right), $n > 13$ plants for each genotype, compared by two-tailed t-test with Welch's correction. C) PPB and phragmoplast angle measurements in dividing root cells of *tan1 air9* double mutants expressing *p35S:TAN1-YFP* (left), two *p35S:TAN1₁₋₁₃₂-YFP* transgenic lines (middle) and untransformed plants (right), $n > 23$ plants of each genotype. Angle variations compared with F-test. ns indicates not significant, * P-value <0.05 , ** P-value <0.01 , **** P-value <0.0001 .



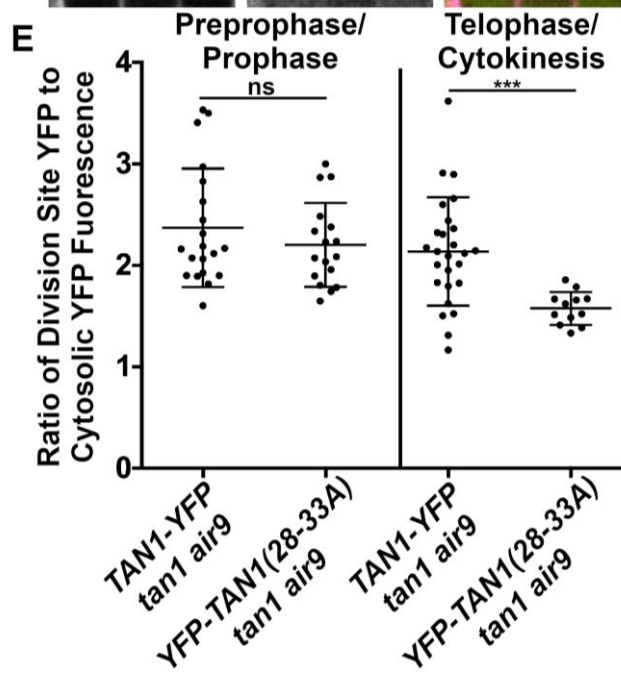
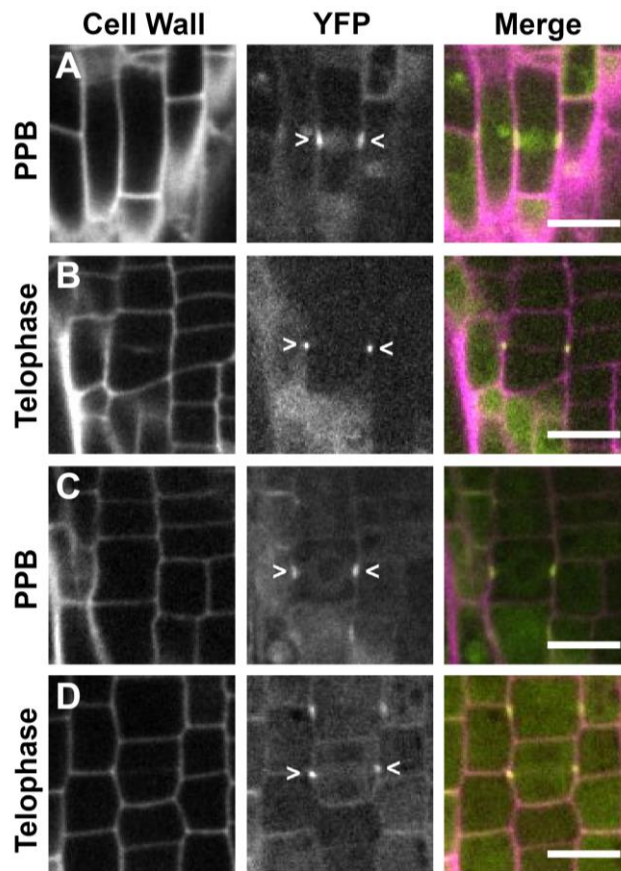
Supplementary Figure 3.2. Yeast two-hybrid interactions between POK1 (C-terminal amino acids 1683-2066, as previously described (Müller et al., 2006; Rasmussen et al., 2011; Lipka et al., 2014)) and TAN1₁₋₁₃₂ alanine scanning constructs. A) Diagram of alanine scanning constructs that showed loss of interaction with POK1 by yeast two-hybrid. The location of the six alanine substitutions within each TAN1₁₋₁₃₂ construct are represented by white boxes. B) Yeast two-hybrid results of screen for loss of interaction with POK1. Underlined constructs showed loss of interaction with POK1. Alanines 64-69 and 106-111 were not completed and not included in the yeast two-hybrid.



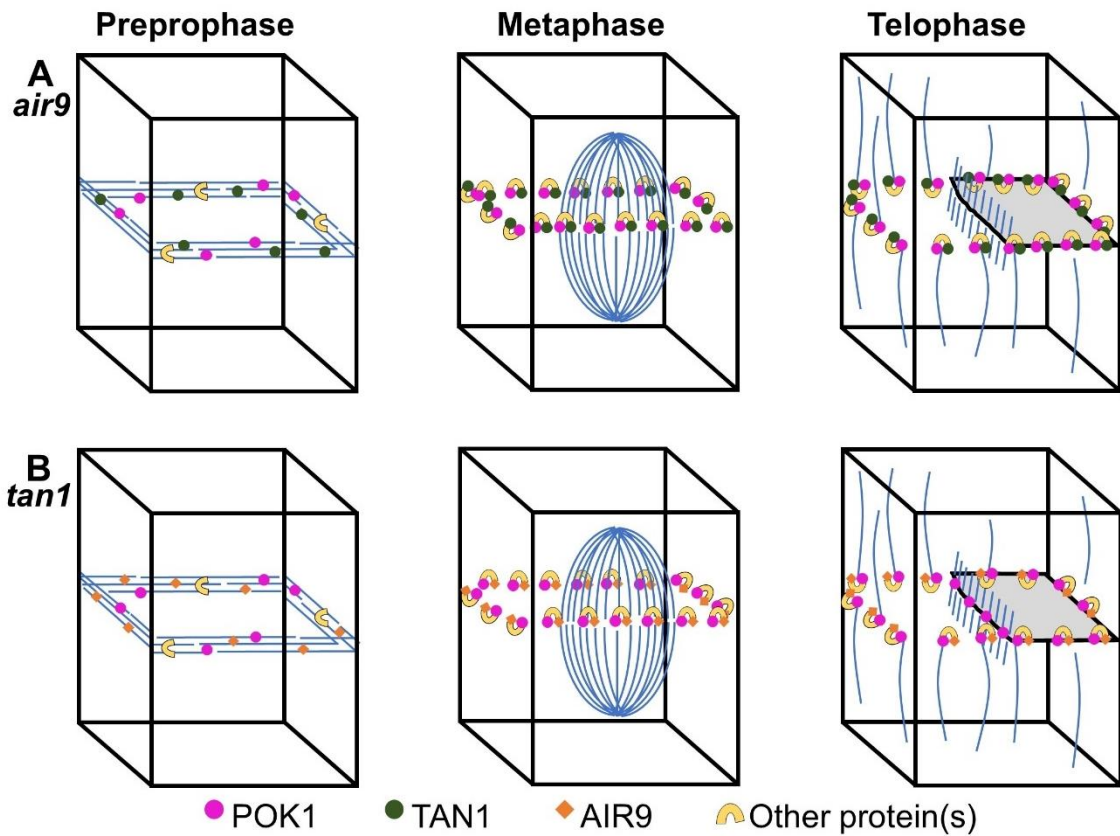
Supplementary Figure 3.3. Yeast two-hybrid interactions between TAN1 and POK1 (C-terminal amino acids 1683-2066, as previously described (Müller et al., 2006; Rasmussen et al., 2011; Lipka et al., 2014)) and TAN1(28-33A). Full-length TAN1(28-33A) does not interact with POK1 by yeast two-hybrid.



Supplementary Figure 3.4. *p35S:YFP-TAN1(28-33A) tan1 air9* lines show significant rescue compared to untransformed *tan1 air9*, but less accumulation of YFP-TAN1(28-33A) during telophase. A) Root length measurements from 8 days after stratification of *air9* single mutants (left), *tan1 air9* double mutants expressing *p35S:TAN1-YFP* (second from the left), two *p35S:YFP-TAN1(28-33A)-YFP* transgenic lines designated as line 1 (center) and line 3 (second from the right), and untransformed plants (right), $n > 22$ plants for each genotype, compared by two-tailed t-test with Welch's correction. B) Ratio of TAN1-YFP or TAN1(28-33A)-YFP fluorescence at the division site to cytosolic fluorescence from *tan1 air9* plants expressing *p35S:TAN1-YFP* (left) or *p35S:YFP-TAN1(28-33A)* (right) during telophase, $n > 12$ plants for each genotype. Asterisks indicate a significant difference as determined by Mann-Whitney U test. ns indicates not significant, ** P-value < 0.01 , *** P-value < 0.001 , **** P-value < 0.0001 . Note: TAN1-YFP fluorescence measurements are the same as those used for the telophase fluorescence measurements in supplementary figure 5E.



Supplementary Figure 3.5. YFP-TAN1(28-33A) localizes to the division site in preprophase or prophase and with reduced fluorescence during telophase in *tan1 air9* mutants. Propidium iodide stained *tan1 air9* plants expressing *p35S:TAN1-YFP* in (A) preprophase or prophase (B) telophase or cytokinesis. *tan1 air9* plants expressing *p35S:YFP-TAN1(28-33A)* in (C) preprophase or prophase (D) telophase or cytokinesis. The division site is indicated by arrowheads in the YFP panels. Bars = 10 μ m. E) TAN1-YFP or TAN1(28-33A)-YFP ratio of the division site versus cytosolic fluorescence intensity from *tan1 air9* plants expressing *p35S:TAN1-YFP* or *p35S:YFP-TAN1(28-33A)* during preprophase or prophase and telophase or cytokinesis, n >5 plants for each genotype. Ratios compared with Mann-Whitney U test. ns indicates not significant, *** P-value <0.001.



Supplementary Figure 3.6. A model of POK1 localization in *tan1* and *air9* single mutants. A) In *air9* single mutants TAN1 and POK1 are recruited to the PPB and their interaction with one another and other proteins stabilizes TAN1 and POK1 at the division site. B) In *tan1* single mutants AIR9 and POK1 are recruited to the PPB. POK1 is potentially stabilized at the division site either by interacting directly with AIR9 or another protein recruited to the division site by AIR9. POK1 tends to accumulate in the phragmoplast midline in *tan1* single mutants, which may reflect that POK1 is not as efficiently recruited to the division site in the absence of TAN1.

```

A. thaliana    MVARTPQKQRKVAM-----VVPPLNSDLLKETLNKVDKCMERLQELQYTIAGGTKVVS
O. sativa      MVARSPDARRSRQTAAAAAAAAALNPALVRETLKKVDFCMARLQELQYTVAGGAKVVS
Z. mays        MVARSPNAKPDRQKAAALAAAAALNPALLRETLKKVDFCMARLQELQYTVAGGAKVVS
S. bicolor     MVARSPNAKPDRQTAAALAAAAALNPALVRETLKKVDFCMARLQELQYTVAGGAKVVS
S. lycopersicum MVARTPPKLQNKKM-----VVPPLNPILLRETLNKVDKCMARLQELQYTVGGHKVIS
B. napus       MVARTPQMQRVAM-----VVPPLNTELLKETLNKVDKCMERLQELQYTIAGGTKVVS
****:*          ....** *:.**.:**.* ** *****:.* ** :.*

```

Supplementary Figure 3.7. Alignments of amino acids 1-55 of *A. thaliana* TAN1 with TAN1 homologs from other plant species. Amino acids 28-33 of Arabidopsis TAN1 and amino acids that align with them in other plant species are highlighted in green. “*” indicates residues are fully conserved, “:” indicates strong conservation of properties across species, and “.” indicates weak conservation of properties across species.

Supplementary Table 3.1. Primers used for cloning and genotyping.

Primer Name	Sequence
ATRP	ATCTCTTAGGAACCAAACCGGACGCTGT
ATLP	GATCCGTTACGAAAGTGAACACCTTTATC
JL202	CATTTTATAATAACGCTGCGGACATCTAC
AIR9-5RP	TGGATCAGCTGCAACATTATTC
AIR9-5LP	ATTAACATTTTGCAACGCAGG
Lb1.3	ATTTTGCCGATTTGGAAC
Ds5-4	TACGATAACGGTCGGTACGG
AtTAN 733-CDS Rw	AAATAGAGGGTTCGGAAAAAGAACC
AIR9 gnm7511 R	CCTCCAGTATATGAAGCAACAAAGC
AIR9_cDNA 2230 F	GATGAGGAATATATGTTATCTTTAGATG
Ala_Scan_FOR	GCCGTCACAGATAGATTGGCT
Ala_Scan_Rev	GAAAGCAACCTGACCTACAGG
Ala_02_FOR	GCTGCTGCCGCTGCCGCTGTGCCTCCTCTCAACTCAGAT
Ala_02_Rev	AGCGGCAGCGGCAGCAGCCTGCTTCTGTGGGTTCT
Ala_03_FOR	GCTGCTGCCGCTGCCGCTGATCTTCTCAAGGAAACGATCAAC
Ala_03_REV	AGCGGCAGCGGCAGCAGCCACCATCGCCACTTTCT
Ala_04_FOR	GCTGCTGCCGCTGCCGCTATCAACAAGGTTGATAAATGTATGGAA
Ala_04_REV	AGCGGCAGCGGCAGCAGCTGAGTTGAGAGGAGGCACCAC
Ala_05_FOR	GCTGCTGCCGCTGCCGCTTGTATGGAAAGACTGCAAGAGCTA
Ala_05_REV	AGCGGCAGCGGCAGCAGCCGTTTCTTGAGAAGATCTGAGTT
Ala_06_FOR	GCTGCTGCCGCTGCCGCTGAGCTACAGTACACAATTGCAGGA
Ala_06_REV	AGCGGCAGCGGCAGCAGCTTTATCAACCTTGTGATCGTTTCTT
Ala_07_FOR	GCTGCTGCCGCTGCCGCTGCAGGAGGAACCAAGTTGTC
Ala_07_REV	AGCGGCAGCGGCAGCAGCTTGCAGTCTTCCATACATTTATCAAC
Ala_08_FOR	GCTGCTGCCGCTGCCGCTGTCTCTGGTGTGAACCTTAGC
Ala_08_REV	AGCGGCAGCGGCAGCAGCAATTGTGTACTGTAGCTCTTGCAG
Ala_09_FOR	GCTGCTGCCGCTGCCGCTAGCCCTGAAGCACTAGA
Ala_09_REV	AGCGGCAGCGGCAGCAGCAACTTTGGTTCTCCTGCAAT
Ala_10_FOR	GCTGCTGCCGCTGCCGCTATTTACTTGAAGACTAGTCTTAGATGCAAG
Ala_10_REV	AGCGGCAGCGGCAGCAGCAAGGTTACACCAGAGACAAC
Ala_12_FOR	GCTGCTGCCGCTGCCGCTACTTTAAGGATCAAGAATGCTACTAATAAG
Ala_12_REV	AGCGGCAGCGGCAGCAGCACTAGTCTTCAAGTAAATCTAGTGCT
Ala_13_FOR	GCTGCTGCCGCTGCCGCTGCTACTAATAAGAAATCTCCAGTAGGG
Ala_13_REV	AGCGGCAGCGGCAGCAGCTTCTTGCTTGCATCTAAGACTAGT
Ala_14_FOR	GCTGCTGCCGCTGCCGCTCCAGTAGGGAAGTTTCTGCT
Ala_14_REV	AGCGGCAGCGGCAGCAGCATTCTTGATCCTTAAAGTTTCTTGCTT
Ala_15_FOR	GCTGCTGCCGCTGCCGCTGCTTCTCACCAGGAGATTGG
Ala_15_REV	AGCGGCAGCGGCAGCAGCAGATTTCTTATTAGTAGCATTCTTGATCCT
Ala_16_FOR	GCTGCTGCCGCTGCCGCTTGGAGGAAAATGCTACTCCCA
Ala_16_REV	AGCGGCAGCGGCAGCAGCAGGAACTTCCCTACTGGAGA
Ala_17_FOR	GCTGCTGCCGCTGCCGCTCCAGCAATGCTACTAGGAGAG
Ala_17_REV	AGCGGCAGCGGCAGCAGCATCTCCTGGTGAGGAAGCAGG
Ala_19_FOR	GCTGCTGCCGCTGCCGCTTTACAAGCCTCACAGGTCACA
Ala_19_REV	AGCGGCAGCGGCAGCAGCTCCTAGTAGCATTGCTGGGAG
Ala_20_FOR	GCTGCTGCCGCTGCCGCTACAAGAGACATTGTGGACGCC
Ala_20_REV	AGCGGCAGCGGCAGCAGCGATTTTACATTTACAGTCTCTCCTAGTAGCAT
NpTANSaclFor	gtatgagctccggtagagttgaaccag
NpTANceruleanRev	cctgccttgctcaccatcttctatatatattttctta
NpTANceruleanFor	taaagaaaatatatagaagatggtgagcaagggcgagg
CeruleanpEarleyRev	ggcccggtaccgtcctgtacagctgctccatgc
CeruleanpEarleyFor	gcatggacgagctgtacaaggacggtaccgcccc
pEarleyOCSpstIRev	ccatctgacgctgctgagcctgacat
AtExon1_1For	ctcaactcagatcttcaaggaaagc
At255AfterStopRev	gcatagtggtaccctcaattacacc

REFERENCES

- Bellinger, M.A., Uyehara, A.N., Martinez, P., McCarthy, M.C., and Rasmussen, C.G.** (2021). Cell cortex microtubules contribute to division plane positioning during telophase in maize. *bioRxiv* 2021.01.11.426230; doi: <https://doi.org/10.1101/2021.01.11.426230>.
- Buschmann, H., Chan, J., Sanchez-Pulido, L., Andrade-Navarro, M.A., Doonan, J.H., and Lloyd, C.W.** (2006). Microtubule-associated AIR9 recognizes the cortical division site at preprophase and cell-plate insertion. *Curr. Biol.* **16**: 1938–1943.
- Buschmann, H., Dols, J., Kopischke, S., Peña, E.J., Andrade-Navarro, M.A., Heinlein, M., Szymanski, D.B., Zachgo, S., Doonan, J.H., and Lloyd, C.W.** (2015). Arabidopsis KCBP interacts with AIR9 but stays in the cortical division zone throughout mitosis via its MyTH4-FERM domain. *J. Cell Sci.* **128**: 2033–2046.
- Chugh, M., Reißner, M., Bugiel, M., Lipka, E., Herrmann, A., Roy, B., Müller, S., and Schäffer, E.** (2018). Phragmoplast Orienting Kinesin 2 Is a Weak Motor Switching between Processive and Diffusive Modes. *Biophys. J.* **115**: 375–385.
- Cleary, A.L. and Smith, L.G.** (1998). The Tangled1 gene is required for spatial control of cytoskeletal arrays associated with cell division during maize leaf development. *Plant Cell* **10**: 1875–1888.
- Clough, S.J. and Bent, A.F.** (1999). Floral dip : a simplified method for *Agrobacterium*-mediated transformation of *Arabidopsis thaliana*. **16**: 735–743.
- Dixit, R. and Cyr, R.J.** (2002). Spatio-temporal relationship between nuclear-envelope breakdown and preprophase band disappearance in cultured tobacco cells. *Protoplasma* **219**: 116–121.
- Earley, K.W., Haag, J.R., Pontes, O., Opper, K., Juehne, T., Song, K., and Pikaard, C.S.** (2006). Gateway-compatible vectors for plant functional genomics and proteomics. *Plant J.* **45**: 616–629.
- Facette, M.R., Rasmussen, C.G., and Van Norman, J.M.** (2018). A plane choice: coordinating timing and orientation of cell division during plant development. *Curr. Opin. Plant Biol.* **47**: 47–55.

- Fan, H.Y., Hu, Y., Tudor, M., and Ma, H.** (1997). Specific interactions between the K domains of AG and AGLs, members of the MADS domain family of DNA binding proteins. *Plant J.* **12**: 999–1010.
- Fisher, C.L. and Pei, G.K.** (1997). Modification of a PCR-based site-directed mutagenesis method. *Biotechniques* **23**: 570–1, 574.
- Herrmann, A., Livanos, P., Lipka, E., Gadeyne, A., Hauser, M.-T., Van Damme, D., and Müller, S.** (2018). Dual localized kinesin-12 POK2 plays multiple roles during cell division and interacts with MAP65-3. *EMBO Rep.* **19**: e46085.
- Hoshino, H., Yoneda, A., Kumagai, F., and Hasezawa, S.** (2003). Roles of actin-depleted zone and preprophase band in determining the division site of higher-plant cells, a tobacco BY-2 cell line expressing GFP-tubulin. *Protoplasma* **222**: 157–165.
- Hwang, J.-U., Vernoud, V., Szumlanski, A., Nielsen, E., and Yang, Z.** (2008). A tip-localized RhoGAP controls cell polarity by globally inhibiting Rho GTPase at the cell apex. *Curr. Biol.* **18**: 1907–1916.
- Karahara, I., Suda, J., Tahara, H., Yokota, E., Shimmen, T., Misaki, K., Yonemura, S., Staehelin, L.A., and Mineyuki, Y.** (2009). The preprophase band is a localized center of clathrin-mediated endocytosis in late prophase cells of the onion cotyledon epidermis. *Plant J.* **57**: 819–831.
- Kirik, V., Herrmann, U., Parupalli, C., Sedbrook, J.C., Ehrhardt, D.W., and Hülskamp, M.** (2007). CLASP localizes in two discrete patterns on cortical microtubules and is required for cell morphogenesis and cell division in *Arabidopsis*.: 4416–4425.
- Kojo, K.H., Higaki, T., Kutsuna, N., Yoshida, Y., Yasuhara, H., and Hasezawa, S.** (2013). Roles of cortical actin microfilament patterning in division plane orientation in plants. *Plant Cell Physiol.* **54**: 1491–1503.
- Kumari, P., Dahiya, P., Livanos, P., Zergiebel, L., Kölling, M., Poeschl, Y., Stamm, G., Hermann, A., Abel, S., Müller, S., and Bürstenbinder, K.** (2021). IQ67 DOMAIN proteins facilitate preprophase band formation and division-plane orientation. *Nat Plants* **7**: 739–747.
- Lee, Y.-R.J., Hiwatashi, Y., Hotta, T., Xie, T., Doonan, J.H., and Liu, B.** (2017). The Mitotic Function of Augmin Is Dependent on Its Microtubule-Associated Protein Subunit EDE1 in *Arabidopsis thaliana*. *Curr. Biol.* **27**: 3891–3897.e4.
- Lee, Y.-R.J. and Liu, B.** (2019). Microtubule nucleation for the assembly of acentrosomal microtubule arrays in plant cells. *New Phytol.* **222**: 1705–1718.

- Lee, Y.-R.J., Li, Y., and Liu, B.** (2007). Two Arabidopsis phragmoplast-associated kinesins play a critical role in cytokinesis during male gametogenesis. *Plant Cell* **19**: 2595–2605.
- Lipka, E., Gadeyne, A., Stöckle, D., Zimmermann, S., De Jaeger, G., Ehrhardt, D.W., Kirik, V., Van Damme, D., and Müller, S.** (2014). The Phragmoplast-Orienting Kinesin-12 Class Proteins Translate the Positional Information of the Preprophase Band to Establish the Cortical Division Zone in Arabidopsis thaliana. *Plant Cell* **26**: 2617–2632.
- Li, S., Sun, T., and Ren, H.** (2015). The functions of the cytoskeleton and associated proteins during mitosis and cytokinesis in plant cells. *Front. Plant Sci.* **6**: 282.
- Livanos, P. and Müller, S.** (2019). Division Plane Establishment and Cytokinesis. *Annu. Rev. Plant Biol.*
- Martinez, P., Dixit, R., Balkunde, R.S., Zhang, A., O’Leary, S.E., Brakke, K.A., and Rasmussen, C.G.** (2020). TANGLED1 mediates microtubule interactions that may promote division plane positioning in maize. *J. Cell Biol.* **219**.
- Martinez, P., Luo, A., Sylvester, A., and Rasmussen, C.G.** (2017). Proper division plane orientation and mitotic progression together allow normal growth of maize. *Proc. Natl. Acad. Sci. U. S. A.* **114**: 2759–2764.
- McMichael, C.M. and Bednarek, S.Y.** (2013). Cytoskeletal and membrane dynamics during higher plant cytokinesis. *New Phytol.* **197**: 1039–1057.
- Miki, T., Naito, H., Nishina, M., and Goshima, G.** (2014). Endogenous localizome identifies 43 mitotic kinesins in a plant cell. *Proc. Natl. Acad. Sci. U. S. A.* **111**: E1053–E1061.
- Mills, A.M. and Rasmussen, C.** (2022). Action at a distance: Defects in division plane positioning in the root meristematic zone affect cell organization in the differentiation zone. *bioRxiv*: 2021.04.30.442137.
- Mir, R., Morris, V.H., Buschmann, H., and Rasmussen, C.G.** (2018). Division Plane Orientation Defects Revealed by a Synthetic Double Mutant Phenotype. *Plant Physiol.* **176**: 418–431.
- Müller, S., Han, S., and Smith, L.G.** (2006). Two kinesins are involved in the spatial control of cytokinesis in Arabidopsis thaliana. *Curr. Biol.* **16**: 888–894.

- Müller, S. and Jürgens, G.** (2016). Plant cytokinesis—No ring, no constriction but centrifugal construction of the partitioning membrane. *Semin. Cell Dev. Biol.* **53**: 10–18.
- Murata, T., Sano, T., Sasabe, M., Nonaka, S., Higashiyama, T., Hasezawa, S., Machida, Y., and Hasebe, M.** (2013). Mechanism of microtubule array expansion in the cytokinetic phragmoplast. *Nat. Commun.* **4**: 1967.
- Nakaoka, Y., Miki, T., Fujioka, R., Uehara, R., Tomioka, A., Obuse, C., Kubo, M., Hiwatashi, Y., and Goshima, G.** (2012). An inducible RNA interference system in *Physcomitrella patens* reveals a dominant role of augmin in phragmoplast microtubule generation. *Plant Cell* **24**: 1478–1493.
- van Oostende-Triplet, C., Guillet, D., Triplet, T., Pandzic, E., Wiseman, P.W., and Geitmann, A.** (2017). Vesicle Dynamics during Plant Cell Cytokinesis Reveals Distinct Developmental Phases. *Plant Physiol.* **174**: 1544–1558.
- Pan, R., Lee, Y.-R.J., and Liu, B.** (2004). Localization of two homologous Arabidopsis kinesin-related proteins in the phragmoplast. *Planta* **220**: 156–164.
- Panteris, E.** (2008). Cortical actin filaments at the division site of mitotic plant cells: a reconsideration of the “actin-depleted zone.” *New Phytol.* **179**: 334–341.
- Pan, X., Fang, L., Liu, J., Senay-Aras, B., Lin, W., Zheng, S., Zhang, T., Guo, J., Manor, U., Van Norman, J., Chen, W., and Yang, Z.** (2020). Auxin-induced signaling protein nanoclustering contributes to cell polarity formation. *Nat. Commun.* **11**: 3914.
- Rasmussen, C.G. and Bellinger, M.** (2018). An overview of plant division-plane orientation. *New Phytol.*
- Rasmussen, C.G., Sun, B., and Smith, L.G.** (2011). Tangled localization at the cortical division site of plant cells occurs by several mechanisms. *J. Cell Sci.* **124**: 270–279.
- Russell, D.W. and Sambrook, J.** (2001). *Molecular cloning: a laboratory manual* Third. (Cold Spring Harbor Laboratory Cold Spring Harbor, NY: Cold Spring Harbor).
- Schaefer, E., Belcram, K., Uyttewaal, M., Duroc, Y., Goussot, M., Pastuglia, M., and Bouchez, D.** (2017). The preprophase band of microtubules controls the robustness of division orientation in plants. *189*: 186–189.

- Smertenko, A. et al.** (2017). Plant Cytokinesis: Terminology for Structures and Processes. *Trends Cell Biol.* **27**: 885–894.
- Smertenko, A., Hewitt, S.L., Jacques, C.N., Kacprzyk, R., Liu, Y., Marcec, M.J., Moyo, L., Ogden, A., Oung, H.M., Schmidt, S., and Serrano-Romero, E.A.** (2018). Phragmoplast microtubule dynamics - a game of zones. *J. Cell Sci.* **131**: jcs203331.
- Song, H., Golovkin, M., Reddy, A.S., and Endow, S.A.** (1997). In vitro motility of AtKCBP, a calmodulin-binding kinesin protein of Arabidopsis. *Proc. Natl. Acad. Sci. U. S. A.* **94**: 322–327.
- Stöckle, D., Herrmann, A., Lipka, E., Lauster, T., Gavidia, R., Zimmermann, S., and Müller, S.** (2016). Putative RopGAPs impact division plane selection and interact with kinesin-12 POK1. *Nat Plants* **2**: 16120.
- Suetsugu, N., Yamada, N., Kagawa, T., Yonekura, H., Uyeda, T.Q.P., Kadota, A., and Wada, M.** (2010). Two kinesin-like proteins mediate actin-based chloroplast movement in Arabidopsis thaliana. *Proc. Natl. Acad. Sci. U. S. A.* **107**: 8860–8865.
- Sugimoto, K., Williamson, R.E., and Wasteneys, G.O.** (2000). New Techniques Enable Comparative Analysis of Microtubule Orientation, Wall Texture, and Growth Rate in Intact Roots of Arabidopsis. *Plant Physiology* **124**: 1493–1506.
- Van Damme, D.** (2009). Division plane determination during plant somatic cytokinesis. *Curr. Opin. Plant Biol.* **12**: 745–751.
- Vanstraelen, M., Torres Acosta, J.A., De Veylder, L., Inzé, D., and Geelen, D.** (2004). A plant-specific subclass of C-terminal kinesins contains a conserved a-type cyclin-dependent kinase site implicated in folding and dimerization. *Plant Physiol.* **135**: 1417–1429.
- Walker, K.L., Müller, S., Moss, D., Ehrhardt, D.W., and Smith, L.G.** (2007). Arabidopsis TANGLED identifies the division plane throughout mitosis and cytokinesis. *Curr. Biol.* **17**: 1827–1836.
- Wu, S.-Z., Yamada, M., Mallett, D.R., and Bezanilla, M.** (2018). Cytoskeletal discoveries in the plant lineage using the moss *Physcomitrella patens*. *Biophys. Rev.*
- Xu, X.M., Zhao, Q., Rodrigo-Peirís, T., Brkljacic, J., He, C.S., Müller, S., and Meier, I.** (2008). RanGAP1 is a continuous marker of the Arabidopsis cell division plane. *Proc. Natl. Acad. Sci. U. S. A.* **105**: 18637–18642.

Chapter 4: Action at a distance: Defects in division plane positioning in the root meristematic zone affect cell organization in the differentiation zone

ABSTRACT

Cell division plane orientation is critical for plant and animal development and growth. TANGLED1 (TAN1) and AUXIN-INDUCED-IN-ROOT-CULTURES9 (AIR9) are division-site localized microtubule-binding proteins required for division plane positioning. *tan1* and *air9 Arabidopsis thaliana* single mutants have minor or no noticeable phenotypes but the *tan1 air9* double mutant has synthetic phenotypes including stunted growth, misoriented divisions, and aberrant cell file rotation in the root differentiation zone. These data suggest that TAN1 plays a role in nondividing cells. To determine whether TAN1 is required in elongating and differentiating cells in the *tan1 air9* double mutant, we limited its expression to actively dividing cells using the G2/M specific promoter of the syntaxin *KNOLLE (pKN:TAN1-YFP)*. Unexpectedly, in addition to rescuing division plane defects, *pKN:TAN1-YFP* rescued root growth and the root differentiation zone cell file rotation defects in the *tan1 air9* double mutant. This suggests that defects that occur in the meristematic zone later affect the organization of elongating and differentiating cells.

INTRODUCTION

Correct division plane orientation is key for patterning and growth across kingdoms. Because plant cells are confined by cell walls, division positioning is

tightly regulated (Facette et al., 2018; Livanos and Müller, 2019; Rasmussen and Bellinger, 2018; Wu et al., 2018). Division plane determination begins during S or G2, when the nucleus is repositioned within the cell (Facette et al., 2018; Frey et al., 2010; Wada, 2018; Yi and Goshima, 2020). Polarity is often established and maintained by nuclear repositioning and polar localization of proteins during asymmetric division (Facette et al., 2018; Guo et al., 2021; Kimata et al., 2016; Muroyama and Bergmann, 2019; Shao and Dong, 2016; Wada, 2018). Next, land-plant cells typically form a structure around the nucleus at the cell cortex called the preprophase band (PPB). The PPB is a ring of microtubules, microfilaments and associated proteins that marks the future position of the new cell wall, called the division site (Li et al., 2015; Pickett-Heaps et al., 1999; Rasmussen and Bellinger, 2018; Smertenko et al., 2017; Van Damme, 2009). Nuclear and PPB positioning often match division predictions based on cell geometry (Martinez et al., 2018; Moukhtar et al., 2019). PPB disassembly upon nuclear envelope breakdown precedes spindle formation (Dixit and Cyr, 2002). After chromosome separation, the phragmoplast forms from the anaphase spindle to direct new cell wall synthesis. The phragmoplast is an antiparallel array of microtubules with plus-ends facing the cell center (Ho et al., 2012; McMichael and Bednarek, 2013; Müller and Jürgens, 2016). Kinesins transport vesicles to form the cell plate (Lee and Liu, 2013; Smertenko et al., 2018). New microtubule nucleation expands the phragmoplast outwards until the cell plate

contacts the division site (Gu and Rasmussen, 2022; Murata et al., 2013; van Oostende-Triplet et al., 2017).

Division-site localized proteins including TANGLED1 (TAN1), PHRAGMOPLAST ORIENTING KINESIN1 (POK1), POK2, MICROTUBULE-ASSOCIATED PROTEIN 65-4 (MAP65-4), RAN GTPASE ACTIVATING PROTEIN (RAN-GAP), MYOSIN VIII and KINESIN-LIKE CALMODULIN BINDING PROTEIN (KCBP) remain at the cell cortex at the division site throughout cell division (Buschmann et al., 2015; Herrmann et al., 2018; Li et al., 2017; Lipka et al., 2014; Morgan et al., 2008; Walker et al., 2007; Wu and Bezanilla, 2014). Many of these proteins are important for division plane positioning, often during telophase. TAN1 is a division-site-localized protein required for phragmoplast guidance to the division site in maize (Martinez et al., 2017; Smith et al., 2001; Walker et al., 2007). TAN1 organizes microtubules at the cell cortex called cortical telophase microtubules which are incorporated into the phragmoplast to direct its movement at the cell cortex (Bellinger et al.). TAN1 binds and bundles microtubules in vitro (Martinez et al., 2020). Although the *tan1* maize mutant has misplaced divisions and stunted growth, *tan1 Arabidopsis thaliana* (*Arabidopsis*) mutants grow as well as wild-type plants and have minor division placement defects (Walker et al., 2007). Another division-site-localized protein, AIR9, also binds microtubules. AIR9 localizes to interphase cortical microtubule arrays, as well as co-localizing with the PPB, the phragmoplast, and localizing to the division site during late

telophase (Buschmann et al., 2006). Similar to *tan1* single mutants, *air9* single mutants resemble wild-type plants (Buschmann et al., 2015). Due to their similar division-site localization, *tan1 air9* double mutants were generated in Arabidopsis. Combining mutations in both *tan1* and *air9* results in division-plane-positioning defects, stunted growth, and root twisting in the differentiation zone (Mir et al., 2018). While PPBs and phragmoplasts were both frequently misoriented in *tan1 air9* mutants, improper phragmoplast guidance is the primary defect (Mir et al. 2018). Transforming the *tan1 air9* double mutant with *TAN1-YFP* driven by the constitutive viral Cauliflower mosaic *CaMV35S* promoter rescues root growth, misoriented divisions, and cell-file-rotation defects (Mir et al., 2018).

We hypothesized that TAN1 may also have a role in organizing interphase microtubules in elongating and differentiated cells, because *tan1 air9* mutants had aberrant cell-file rotation in the root differentiation zone, minor defects in interphase microtubule organization, and root growth defects that were enhanced by the microtubule-depolymerizing-drug propyzamide (Mir et al., 2018). Cell file rotation phenotypes are often caused by mutations in microtubule-associated proteins or tubulin that alter the organization or stability of the interphase cortical microtubule array (Abe et al., 2004; Buschmann and Borchers, 2020; Buschmann et al., 2004; Hashimoto, 2015; Ishida et al., 2007; Nakajima et al., 2004; Sakai et al., 2008; Sedbrook et al., 2004; Shoji et al., 2004). For example,

in several *alpha-tubulin* mutants, cell file rotation occurred in hypocotyls and root differentiation zones and in isolated cultured mutant cells (Abe et al., 2004; Buschmann et al., 2009; Ishida et al., 2007; Thitamadee et al., 2002). Cell file twisting also occurs when cell elongation differs between epidermal and cortical cells. Arabidopsis treated with compounds that affect microtubule stability, such as oryzalin or propyzamide, have helical cell files due to cortical cell swelling and reduced longitudinal cell expansion (Furutani et al., 2000; Hashimoto, 2002). Therefore, defects in organ twisting are sometimes due to interphase microtubule disruption and likely independent of division-plane defects. However, several examples suggest that division-plane-orientation defects may lead to cell-file-rotation defects (Cnops et al., 2000; Wasteneys and Collings, 2009). Double mutants in two related receptor-like kinases have defects in division plane orientation near the quiescent center and in the endodermis and also have abnormal root skewing (Goff and Van Norman, 2021). Therefore, it is possible that either mitotic or non-mitotic defects lead to aberrant growth and root twisting defects.

To determine whether mitotic *TAN1* expression was sufficient to rescue root twisting in the differentiation zone of *tan1 air9* double mutants, we drove *TAN1* expression using the G2/M-phase-specific *KNOLLE* promoter (Lukowitz et al., 1996; Menges et al., 2005). *KNOLLE* is a syntaxin/Qa-SNARE required for cell-plate vesicle fusion (Strompen et al., 2002; Völker et al., 2001). The *KNOLLE*

promoter drove *TAN1* expression in mitotic cells which rescued root growth and cell-file-rotation defects in the *tan1 air9* double mutant. Our results suggest that cell-file-rotation defects in the *tan1 air9* double mutant are likely due to defects that occur in actively dividing meristematic cells, and not due to a lack of TAN1 in nondividing cells.

RESULTS AND DISCUSSION

We generated two independent native-promoter TAN1 fluorescent protein fusions to determine whether *TAN1-YFP* or *CFP-TAN1* expressed by its native promoter would rescue the *tan1 air9* double mutant. Both constructs rescued the *tan1 air9* mutant. Previous studies showed that 35S-driven *TAN1* expression rescued *tan1 air9* mutants (Mir et al., 2018). We drove expression of *CFP-TAN1* and *TAN1-YFP* using 1263 bp upstream of the start codon, *pTAN:CFP-TAN1* and *pTAN:TAN1-YFP*, and transformed or crossed them into the *tan1 air9* double mutant. Cell shape in the root tip (Figure 4.1A) and cell file rotation in the differentiation zone of *pTAN:CFP-TAN1 tan1 air9* plants was restored to *air9* single mutant levels (Figure 4.1B, 4.1C). Single *air9* mutants are indistinguishable from wild-type plants (Buschmann et al., 2015; Mir et al., 2018). Root cell division primarily occurs at the root tip (the meristematic zone). Above that, non-dividing cells elongate in the elongation zone. Root hairs mark the differentiation zone, where root cells mature and differentiate into different cell types (Wachsman et al. 2015). Transverse cell-wall angles in the differentiation

zone indicate cell-file rotation. *tan1 air9* mutant roots tend to twist left with variable cell file angle values that skew above 90° (Mir et al., 2018). *pTAN:CFP-TAN1* rescued *tan1 air9* root growth, with *pTAN:CFP-TAN1* expressing plants growing slightly longer than *air9* single mutants (Figure 4.1D). *pTAN:TAN1-YFP* also fully rescued *tan1 air9* root growth and restored normal root tip patterning (Supplementary Figure 4.1). Measuring PPB and phragmoplast angles is a metric for division plane orientation. PPB and phragmoplast angles were measured relative to the left-hand cell wall. *pTAN:CFP-TAN1* fully rescued PPB and phragmoplast positioning defects in *tan1 air9* mutants, restoring angle variances close to 90° (Figure 4.1E). This shows that mitotic expression of *TAN1* by its native promoter and fluorescent protein fusion at either end of the *TAN1* protein is sufficient for normal plant growth, including the expansion and patterning of nondividing cells in the *tan1 air9* double mutant.

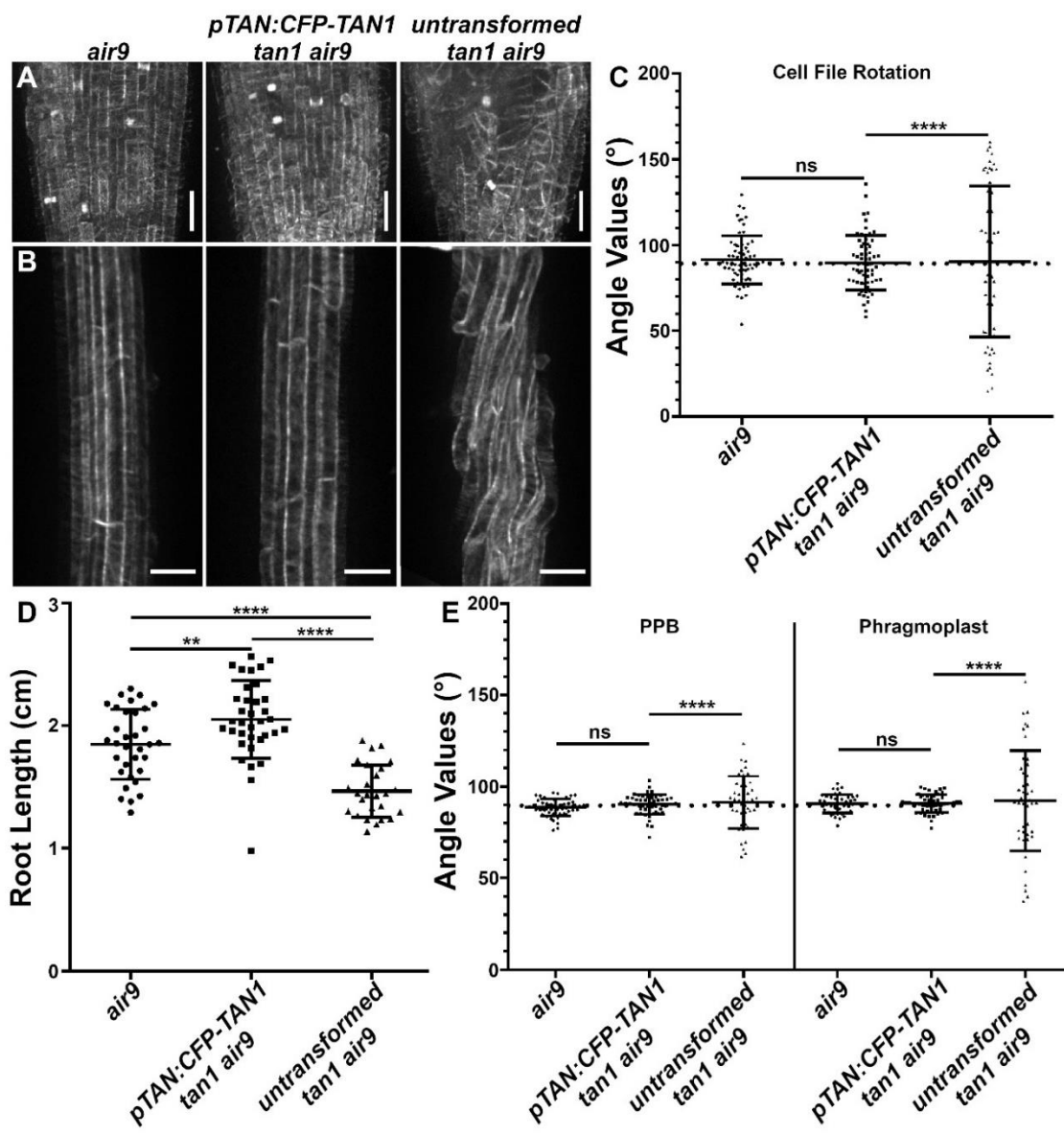


Figure 4.1: The TAN1 native promoter fused to TAN1 (*pTAN:CFP-TAN1*) rescues the *tan1 air9* double mutant. A) Maximum projections of 20 1- μ m Z-stacks of root tips of an *air9* mutant (left), *pTAN:CFP-TAN1* (magenta) *tan1 air9* mutant (middle), and untransformed *tan1 air9* mutant (right) expressing microtubule marker *UBQ10:mScarlet-MAP4* (green in the top middle panel). Bars = 25 μ m. B) Maximum projections of 15 1- μ m Z-stacks of the differentiation zone of an *air9* mutant (left), *pTAN:CFP-TAN1 tan1 air9* mutant (middle), and untransformed *tan1 air9* mutant (right) expressing *UBQ10:mScarlet-MAP4*. Bars = 50 μ m. C) Cell-file-rotation angles of *air9* mutants (left), *pTAN:CFP-TAN1 tan1 air9* mutants (middle), and untransformed *tan1 air9* mutants (right), $n > 11$ plants for each genotype and $n > 57$ cells for angle measurements. Cell-file-angle variances were compared with Levene's test due to the non-normal distribution. D) Root-length measurements from 8 days after stratification of *air9* mutants (left), *pTAN:CFP-TAN1 tan1 air9* mutants (middle), and untransformed *tan1 air9* mutants (right), $n > 25$ plants for each genotype, compared by two-tailed t-test with Welch's corrections. E) PPB and phragmoplast angle measurements in *air9* single mutants (left), *pTAN:CFP-TAN1 tan1 air9* mutants (middle), and untransformed *tan1 air9* mutants (right), $n > 9$ plants for each genotype. $N > 41$ cells for angle measurements. PPB and phragmoplast angle variations compared with F-test. ns indicates not significant, ** P-value < 0.01 , **** P-value < 0.0001 .

Previous fluorescence measurements of TAN1-YFP in wild-type lines expressing *pTAN:TAN1-YFP* demonstrated that fluorescent signal above background was limited to the meristematic zone (Mir et al., 2018). We hypothesized that TAN1 accumulated at low but undetectable levels in interphase cells when driven by its native promoter. To test whether *TAN1* expression limited to mitotic cells influenced root growth and suppressed root twisting in the *tan1 air9* double mutant, we fused the *KNOLLE* promoter to *TAN1-YFP* (*pKN:TAN1-YFP*) and transformed it into the *tan1 air9* double mutant. The *KNOLLE* promoter is specifically expressed in G2/M and is contingent on the MYB (myeloblastosis) transcription factors MYB3R1 and MYB3R4 which promote mitosis-specific gene expression (Haga et al., 2011; Yang et al., 2021). Our prediction was that *pKN:TAN1-YFP* would fully rescue mitotic defects but not restore root growth or suppress aberrant cell file rotation within the root differentiation zone in the *tan1 air9* mutant.

pKN:TAN1-YFP fully rescued the defects in *tan1 air9* mutants (Figure 4.2, other independent lines in Supplementary Figure 4.2). This includes rescuing cell patterning and cell file rotation defects (Figure 4.2A-C), root growth (Figure 4.2D), and PPB and phragmoplast positioning (Figure 4.2E). In addition, *pKN*-driven TAN1-YFP localized to the division site during mitotic stages similar to *pTAN1*-driven CFP-TAN1 (Supplementary Figure 4.3). We compared phenotypes of *pKN:TAN1-YFP* to the *35S:TAN1-YFP* lines which rescue the *tan1*

air9 mutant (Mir et al. 2018). Both *35S:TAN1-YFP* and *pKN:TAN1-YFP* significantly rescued the *tan1 air9* double mutant (Figure 4.3A & 4.3B). Root growth and PPB and phragmoplast angles were equivalent in *tan1 air9* plants expressing *pKN:TAN1-YFP* or *35S:TAN1-YFP* (Figure 4.3D & 4.3E). However, *pKN:TAN1-YFP* reduced cell-file-rotation variability slightly more than *35S:TAN1-YFP* (Figure 4.3C). This suggests that expressing *TAN1* in dividing cells is sufficient to fully rescue the *tan1 air9* double mutant. To determine why rescue with the *KNOLLE* promoter resulted in less cell-file-rotation variance, we measured TAN1-YFP fluorescence intensities in the *35S:TAN1-YFP* and *pKN:TAN1-YFP* lines. *pKN:TAN1-YFP* was expressed strongly in the meristematic zone of root tips (Figure 4.4B), often showing TAN1-YFP fluorescence in recently divided cells, similar to native promoter driven accumulation (Figure 4.1, Supplementary Figure 4.1, (Mir et al., 2018)). Indeed, TAN1-YFP accumulated at higher levels in the meristematic zone when expression was driven by the *KNOLLE* promoter (Figure 4.4G). However, unlike TAN1-YFP from *p35S:TAN1-YFP*, TAN1-YFP did not accumulate above background levels in the elongation and differentiation zone of roots expressing *pKN:TAN1-YFP* (Figure 4.4F & 4.4G). Lack of TAN1-YFP outside the meristematic zone and more complete rescue of *tan1 air9* cell file rotation by *pKN:TAN1-YFP* suggests that TAN1 is not required in elongating and differentiating cells. In other words, cell-file-rotation defects may be a

consequence of defects that occur within the root meristematic zone either during mitosis or shortly afterwards.

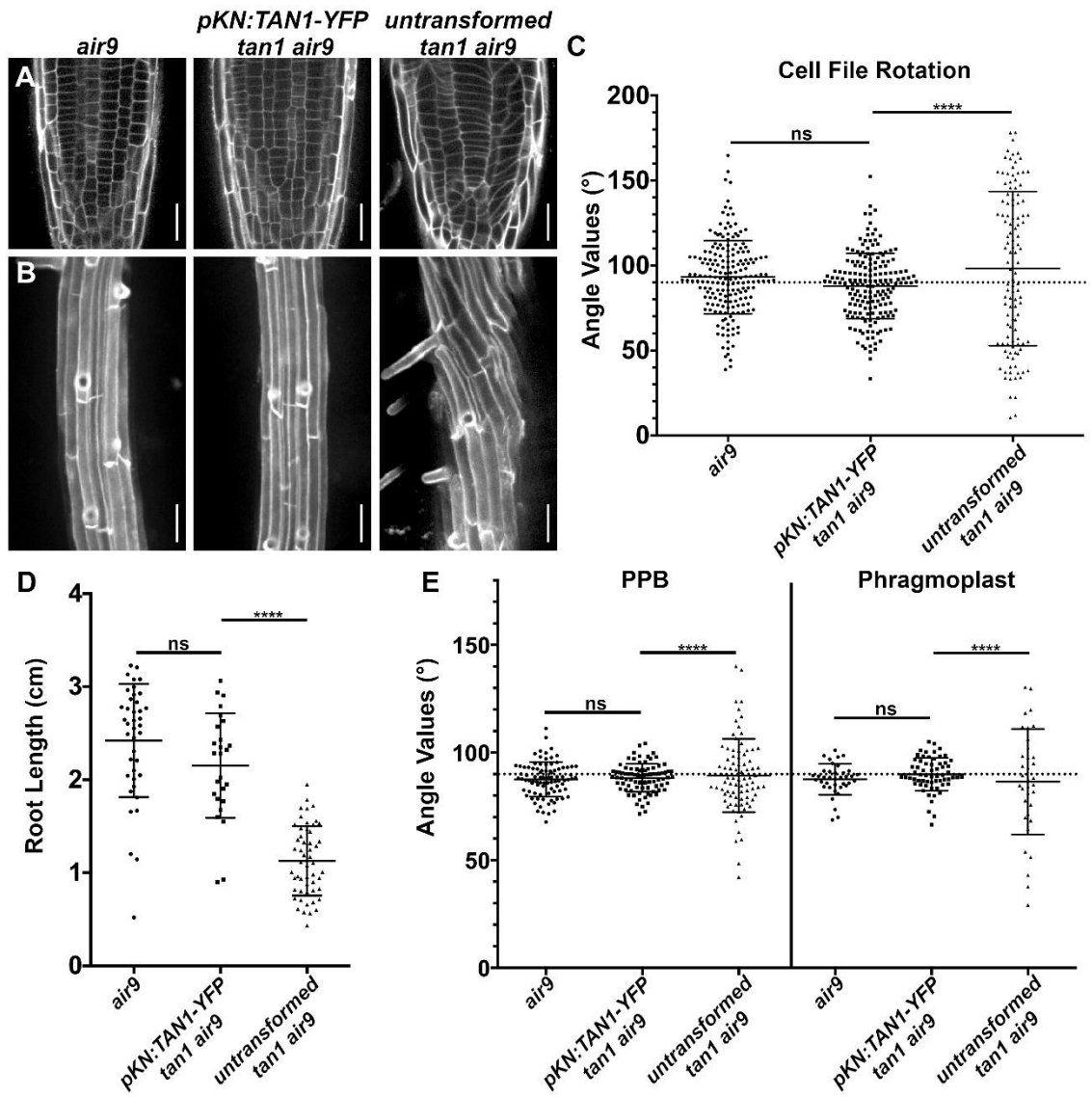


Figure 4.2: Full rescue of the *tan1 air9* double mutant with the G2/M-specific *KNOLLE* promoter fused to *TAN1* (*pKN:TAN1-YFP*). A) Propidium iodide (PI) stained cell walls in root tips of an *air9* single mutant (left), *pKN:TAN1-YFP tan1 air9* mutant (middle), and untransformed *tan1 air9* mutant (right). Bars = 25 μ m. B) Maximum projections of 10 1- μ m Z-stacks of PI-stained differentiation zone root cell walls. Bars = 50 μ m. C) Cell-file-rotation angles of *air9* mutants (left), *pKN:TAN1-YFP tan1 air9* mutants (middle), and untransformed *tan1 air9* mutants (right), n > 23 plants for each genotype. N > 114 cells for angle measurements. Cell-file-rotation angle variances were compared with Levene's test due to the non-normal distribution. D) Root-length measurements from 8 days after stratification of *air9* mutants (left), *pKN:TAN1-YFP tan1 air9* mutants (middle), and untransformed *tan1 air9* mutants (right), n > 25 plants for each genotype, compared by two-tailed t-test with Welch's corrections. E) PPB and phragmoplast angle measurements in *air9* mutants (left), *pKN:TAN1-YFP tan1 air9* mutants (middle), and untransformed *tan1 air9* mutants (right), n > 20 plants for each genotype. N > 34 cells for angle measurements. PPB and phragmoplast angle variations compared with F-test. ns indicates not significant, **** P-value <0.0001.

35S:TAN1-YFP *tan1 air9* pKN:TAN1-YFP *tan1 air9* untransformed *tan1 air9*

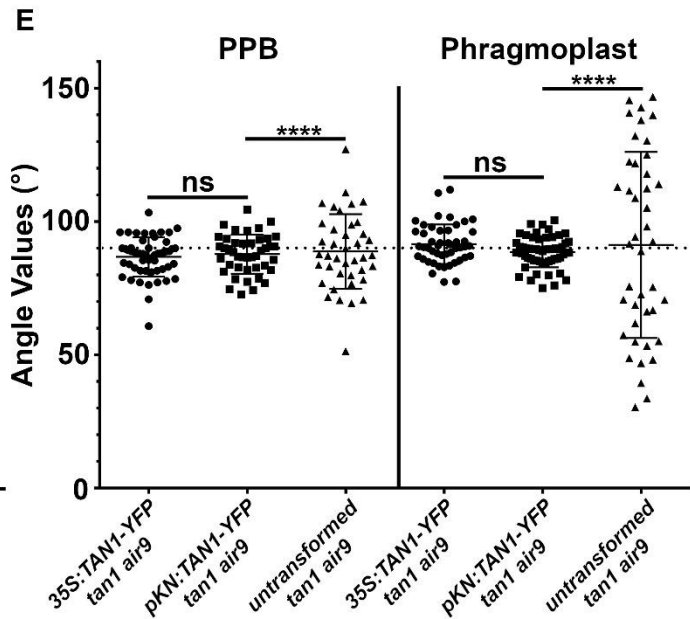
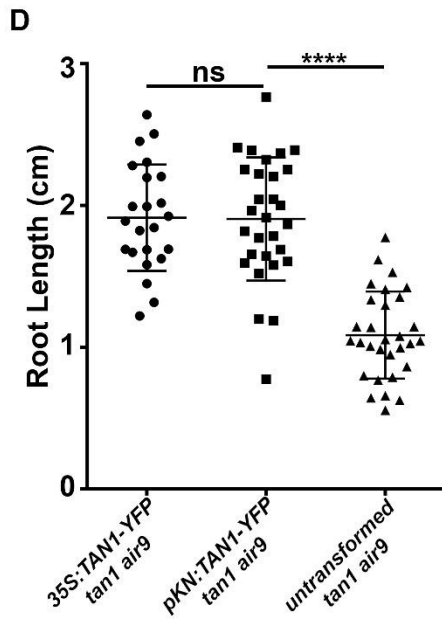
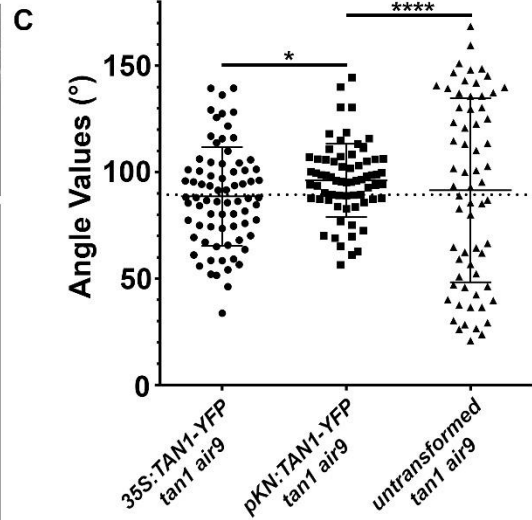
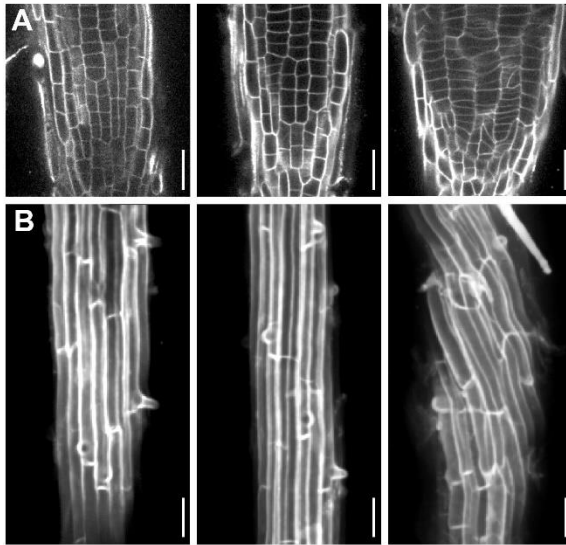


Figure 4.3: Comparison between *KNOLLE* promoter driven (*pKN:TAN1-YFP*) and 35S driven *TAN1* (*p35S:TAN1-YFP*) rescue of the *tan1 air9* double mutants. A) Propidium iodide (PI) stained root tips of a *tan1 air9* mutant expressing *p35S:TAN1-YFP* (left), *pKN:TAN1-YFP* (middle), and untransformed *tan1 air9* mutant (right). Bars = 25 μ m. B) Maximum projections of 10 1- μ m Z-stacks of PI-stained differentiation-zone root cell walls of a *tan1 air9* mutant expressing *p35S:TAN1-YFP* (left), *pKN:TAN1-YFP* (middle), and untransformed *tan1 air9* mutant (right). Bars = 50 μ m. C) Cell-file-rotation angles of *tan1 air9* mutants expressing *p35S:TAN1-YFP* (left), *pKN:TAN1-YFP* (middle), and untransformed plants (right), n > 13 plants for each genotype. N > 64 cells for angle measurements. Angle variances were compared with Levene's test. D) Root-length measurements from 8 days after stratification of *tan1 air9* mutants expressing *p35S:TAN1-YFP* (left), *pKN:TAN1-YFP* (middle), and untransformed plants (right), n > 17 plants for each genotype, compared by two-tailed t-test with Welch's corrections. E) PPB and phragmoplast angle measurements in *tan1 air9* double mutants expressing *p35S:TAN1-YFP* (left), *pKN:TAN1-YFP* (middle), and untransformed plants (right), n > 12 plants for each genotype. N > 39 cells for angle measurements. PPB and phragmoplast angle variations compared with F-test. ns indicates not significant, * P-value <0.05, **** P-value <0.0001.

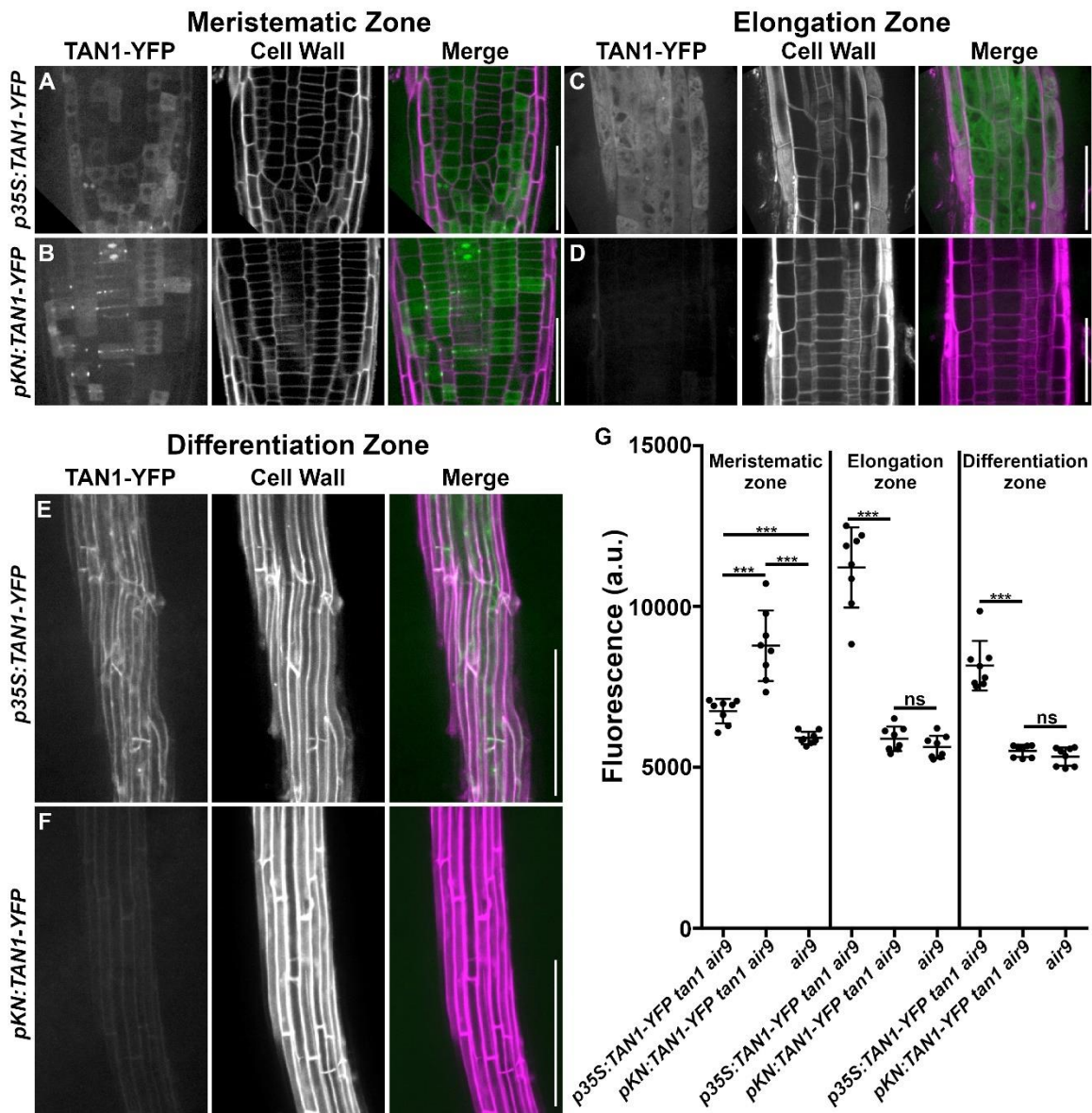


Figure 4.4: Comparison of TAN1-YFP fluorescence intensity when driven by the constitutive 35S promoter (*p35S:TAN1-YFP*) and G2/M-specific *KNOLLE* promoter (*pKN:TAN1-YFP*) in *tan1 air9* roots. (A and B) Micrographs of the meristematic zone, (C and D) maximum projections of 3 1- μ m Z-stacks of the elongation zone, and (E and F) maximum projections of 10 1- μ m Z-stacks of the differentiation zone of *tan1 air9* mutants expressing (A, C, E) *p35S:TAN1-YFP* or (B, D, F) *pKN:TAN1-YFP*. Cell walls were stained with propidium iodide. Root tip and elongation zone, bars = 50 μ m. Differentiation zone, bars = 200 μ m. G) TAN1-YFP fluorescence-intensity measurements (arbitrary units, a.u.) from the meristematic zone, elongation zone, and differentiation zone of *tan1 air9* mutants expressing *p35S:TAN1-YFP* (left), *pKN:TAN1-YFP* (middle), and *air9* mutants, n = 8 plants for each genotype, fluorescence compared with Mann-Whitney U test. *** P-value <0.001. ns indicates not significant.

Another example of defects in mitotic expression and division plane positioning affecting nondividing cell organization occurs in the MYB activated GRAS-type (GIBBERELLIC-ACID INSENSITIVE, REPRESSOR of GAI and SCARECROW-type) transcription factor *scarecrow-like 28-3 (sc/28-3)* mutant. G2/M specific gene expression controlled by SCL28 is important for mitotic progression and division-plane positioning. *sc/28-3* mutants have both misoriented divisions and root twisting (Goldy et al., 2021).

How do defects that occur within the meristematic zone influence the patterning or shape of nondividing, differentiating root cells and root growth? Our hypothesis is that misshapen cells and improper division plane orientation in *tan1 air9* double mutants cause the uneven distribution of mechanical stresses across the root, which then triggers cell wall integrity responses that limit growth and alter root organization. Cell wall stress patterns depend on cell geometry and the mechanical properties of cell walls (Cosgrove, 2018; Hamant and Haswell, 2017). Plant cell growth is coordinated by cell wall polymer extension and addition of cell wall material in response to internal cell turgor pressure and supracellular mechanical stress (Mirabet et al., 2011; Schopfer, 2006; Whitewoods and Coen, 2017).

Division-plane positioning is another way plants may respond to mechanical stress (Chakraborty et al., 2018; Louveaux et al., 2016). Cell division relieves

mechanical stress by creating smaller cells with less surface; further, divisions along maximal tensile stress promote growth homogeneity (Alim et al., 2012; Sapala et al., 2018). Microtubules often align parallel to maximal tensile stress (Hamant et al., 2008; Heisler et al., 2010; Sampathkumar et al., 2014; Uyttewaal et al., 2012) and cortical-microtubule alignment often influences PPB placement (Louveaux et al., 2016; Rasmussen et al., 2013; Wick and Duniec, 1983). However, division plane positioning is disrupted in mutants with division plane orientation defects. Although *tan1 air9* cells may perceive mechanical stress, phragmoplast guidance defects prevent construction of new cell walls in an orientation that minimizes mechanical stress. Abnormal stresses are perceived by receptor-like kinases involved in the cell-wall-integrity response. Cell-wall-integrity responses trigger slow growth, upregulation of stress responses, and changes in cell morphogenesis, (Buschmann and Borchers, 2020; Caño-Delgado et al., 2003; Gonneau et al., 2018; Hématy et al., 2007; Wolf et al., 2014), which may also contribute to the stunted growth and twisted cell files observed in the *tan1 air9* double mutant.

MATERIALS AND METHODS

Plasmid Construction

pKN:TAN1-YFP was generated by amplifying 2152 bp of the 5' *KNOLLE* (AT1G08560) promoter from Columbia with primers pKN-5'SacI Fw and pKN-5'EcoRI Rw. EcoRI and StuI double digestion was used to introduce the *KNOLLE* promoter into pEZT-NL containing the TAN1 coding sequence. Primers 35SpKN5' Fw and YFP XhoI Rw were used to amplify *pKN:TAN1-YFP* then XhoI and StuI double digestion was used to clone *pKN:TAN1-YFP* into pEGAD, a gift from Professor Sean Cutler (University of California, Riverside).

pTAN:CFP-TAN1 was created by overlapping PCR. The 1263bp 5' sequence upstream of genomic *TAN1* was amplified using *Np:AtTAN-YFP* (Walker et al., 2007) as a template with the primers NpTANSacIFor and NpTANceruleanRev. Cerulean fluorescent protein (CFP) was amplified using Cerulean CDS in pDONR221P4r/P3r, a kind gift from Professor Anne Sylvester (University of Wyoming), as template with the primers NpTANceruleanFor and CeruleanpEarleyRev. TAN1 CDS was amplified using *35S:YFP-TAN1* in pEarley104 as a template with the primers CeruleanpEarleyFor and pEarleyOCSPstIRev. The 1263bp TAN1 native promoter, CFP, and TAN1 CDS were combined to create *pTAN:CFP-TAN1* by overlapping PCR with the primers NpTANSacI and pEarleyOCSPstIRev. SacI and PstI double digest was used to

subclone *pTAN:CFP-TAN1* into pJHA212G, a kind gift from Professor Meng Chen (University of California, Riverside).

Generation of Transgenic Lines

Transgenic Arabidopsis lines were generated using *Agrobacterium tumefaciens*-mediated floral dip transformation as described (Clough and Bent, 1999).

Previously described *tan1 air9* mutants (Mir et al., 2018), *csH-tan (TAN1, AT3G05330* (Walker et al., 2007)) and *air9-31 (AIR9, AT2G34680* (Buschmann et al., 2015)), were used for floral dip transformation of *pKN:TAN1-YFP* and T1 transgenic plants were subsequently selected on 1/2 MS plates containing 15 µg/mL glufosinate (Finale; Bayer). TAN1-YFP signal in T1 plants was confirmed by confocal microscopy before being transferred to soil and selfed. The genotypes of *csH-tan1 air9-31* transformants was confirmed using the primers AIR9_cDNA 2230 F and AIR9 gnm7511 R (to identify *AIR9* wild-type), AIR9 gnm7511 R and Ds5-4 (to identify T-DNA insertion in *AIR9*), ATLP and AtTAN 733-CDS Rw (to identify TAN1 wild-type), and AtTAN 733-CDS Rw and Ds5-4 (to identify T-DNA insertion in *TAN1*). The microtubule marker *CFP-TUBULIN* (Kirik et al., 2007), a kind gift from Professor David Erhardht (Stanford University) was crossed into *pKN:TAN1-YFP tan1 air9* plants using *tan1 air9 CFP-TUBULIN* plants (Mir et al., 2018).

air9-5 tan-mad Columbia/Wassilewskija double mutants (Mir et al., 2018) expressing the microtubule marker *UBQ10:mScarlet-MAP4* (Pan et al., 2020), a

kind gift from Professor Zhenbiao Yang (University of California, Riverside), was used for floral dip transformation of *pTAN1:CFP-TAN1* and selected on 1/2 MS plates containing 100 µg/mL gentamicin (Fisher Scientific). T1 seedlings were screened for mScarlet and CFP signal and then transferred to soil to self.

Growth conditions and root length measurements

Plates containing ½ strength Murashige and Skoog (MS) media (MP Biomedicals; Murashige and Skoog, 1962) containing 0.5 g/L MES (Fisher Scientific), pH 5.7, and solidified with 0.8% agar (Fisher Scientific) were used to grow *Arabidopsis* seedlings. *tan1 air9* transgenic lines expressing T3 *p35S:TAN1-YFP*, T2 *pKN:TAN1-YFP*, and T2 *pTAN:CFP-TAN1* were used for root length experiments. At least 3 biological replicates were used for each root growth assay. 5-7 1/2 MS plates were used for each replicate. 12-15 seeds were sown in a single level line on each plate with untransformed *tan1 air9* double mutants and *air9* single mutants sown on plates alongside double mutants expressing *TAN1* constructs. Seeds were stratified on plates in the dark at 4°C for 2 to 5 days. After stratifying, plates were positioned vertically in a growth chamber (Percival) with a 16/8-h light/dark cycle and temperature set to 22°C. Each biological replicate was placed in the growth chamber on different days. 8 days after stratification, plates were scanned (Epson) and root lengths were measured using FIJI (ImageJ, <http://fiji.sc/>). Transgenic seedlings were screened for fluorescence by confocal microscopy to identify seedlings expressing YFP, CFP and mScarlet translational fusion transgenes when present. Each root

growth experiment had a minimum of 3 biological replicates. Statistical analysis of root length was determined using Welch's t-test with Prism (GraphPad) and replicates were checked for discrepancies in statistical significance before pooling replicates for analysis. Root length plots were created using Prism (GraphPad).

To assess the ability of *TAN1* driven by its native promoter to rescue the *tan1 air9* double mutant, *Np:AtTAN-YFP* (Walker et al., 2007) was crossed to *tan-mad air9-5* double mutants. The progeny of *pTAN1:TAN1-YFP tan-mad/+ air9-5/+* plants were sown on 1/2 MS media and grown as described above. The seedlings were screened by confocal microscopy for the presence of TAN1-YFP and then collected for genotyping. Seedlings were genotyped with primers AtExon1_1For and At255AfterStopRev (to identify TAN wild-type), JL202 and ATLP (to identify T-DNA insertion in *TAN1*), AIR9-5RP and AIR9-5LP (to identify wild-type *AIR9*), and LBb1.3 and AIR9RP (to identify T-DNA insertion in *AIR9*) (Supplementary Table 4.1). The length of *tan1 air9* double mutants expressing *pTAN1:TAN1-YFP* was compared to *tan1 air9* double mutants and *air9* single mutant siblings lacking *pTAN1:TAN1-YFP*. *air9* single mutants used for root length analysis included *air9/air9 TAN1/TAN1* and *air9/air9 TAN1/tan1* plants.

Confocal Microscopy

Imaging and screening was performed using Micromanager software (micromanager.org) running an inverted Ti Eclipse (Nikon) with motorized stage

(ASI Piezo) and spinning-disk confocal microscope (Yokogawa W1) built by Solamere Technology. Solid-state lasers (Obis) were used with standard emission filters (Chroma Technology). Excitation 445, emission 480/40 (for CFP-translational fusions); excitation 514, emission 540/30 (for YFP-translational fusions); and excitation 561, emission 620/60 (for propidium iodide and mScarlet-MAP4) were used. The 20x objective has a 0.75 numerical aperture. The 60x objective was used with perfluorocarbon immersion liquid (RIAAA-6788, Cargille) and has a 1.2 numerical aperture objective.

Measurements of PPB and phragmoplast angles and cell file rotation

All angle data was gathered from at least 3 biological replicates. Each replicate consisted of 5-7 1/2 MS plates with 12-15 seeds sown on each plate. 4-5 seeds of each genotype were sown on each plate to ensure growing conditions were identical. Each replicate was moved from stratifying to the growth chamber on independent days. Seedlings were then imaged at 8 days after stratification. Images were collected by confocal microscopy using the 20x objective to collect images of the differentiation zone for cell file angles and the 60x objective to collect images of root tips expressing a microtubule marker (*CFP-TUBULIN* or *mScarlet-MAP4*) for PPB and phragmoplast angles. The differentiation zone was identified by the presence of root hairs. Angles were measured using FIJI. Cell file angles were measured from the left hand side of the cell taking the angle between the long axis of the root and the transverse cell wall using images of root cells in the differentiation zone. PPB and phragmoplast angles were

measured by taking the angle between the left-hand cell wall and the PPB or phragmoplast. Because CFP-TUBULIN was faint and poorly marked cell boundaries, the cell walls of *CFP-TUBULIN* expressing seedlings were stained with 10 μ M PI for 1 minute before destaining in distilled water prior to imaging. Each angle measurement represents a single angle measured from one cell.

Statistical analyses were performed using Excel (Microsoft Office) and Prism (GraphPad). To compare normally distributed variance of PPB and phragmoplast angles F-test was used. Levene's test was used to compare variances of cell file angle measurements because *tan1 air9* cell file angles are non-normally distributed due to left hand twisting of the roots. Angle variance across biological replicates was checked before pooling data.

Fluorescence Intensity Measurements

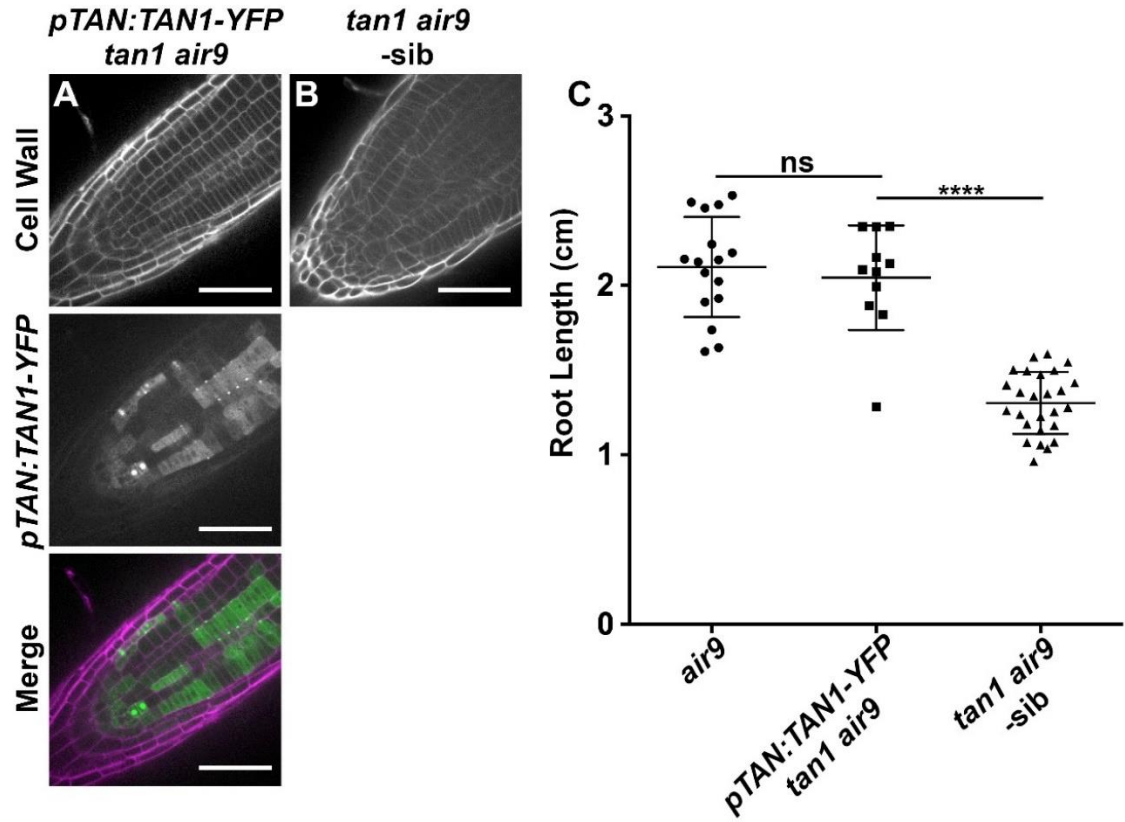
air9, *35S:TAN1-YFP tan1 air9*, and *pKN:TAN1-YFP tan1 air9* plants were grown on 1/2 MS plates as described above. 8 days after stratification, plants were imaged by confocal microscopy using identical settings. Root tips were imaged using the 60X objective. The median fluorescence intensity of an 116,001.5 μ m² area was measured from multiple individual plants of each genotype. Each fluorescence measurement represents the median fluorescence from a single meristematic zone from one plant. Elongation zone and differentiation zone images were taken with the 20x objective and the median fluorescence intensity of an 12,323.4 μ m² area was measured from multiple individual plants of each

genotype. Each fluorescence measurement represents the median fluorescence from a single elongation or differentiation zone from one plant.

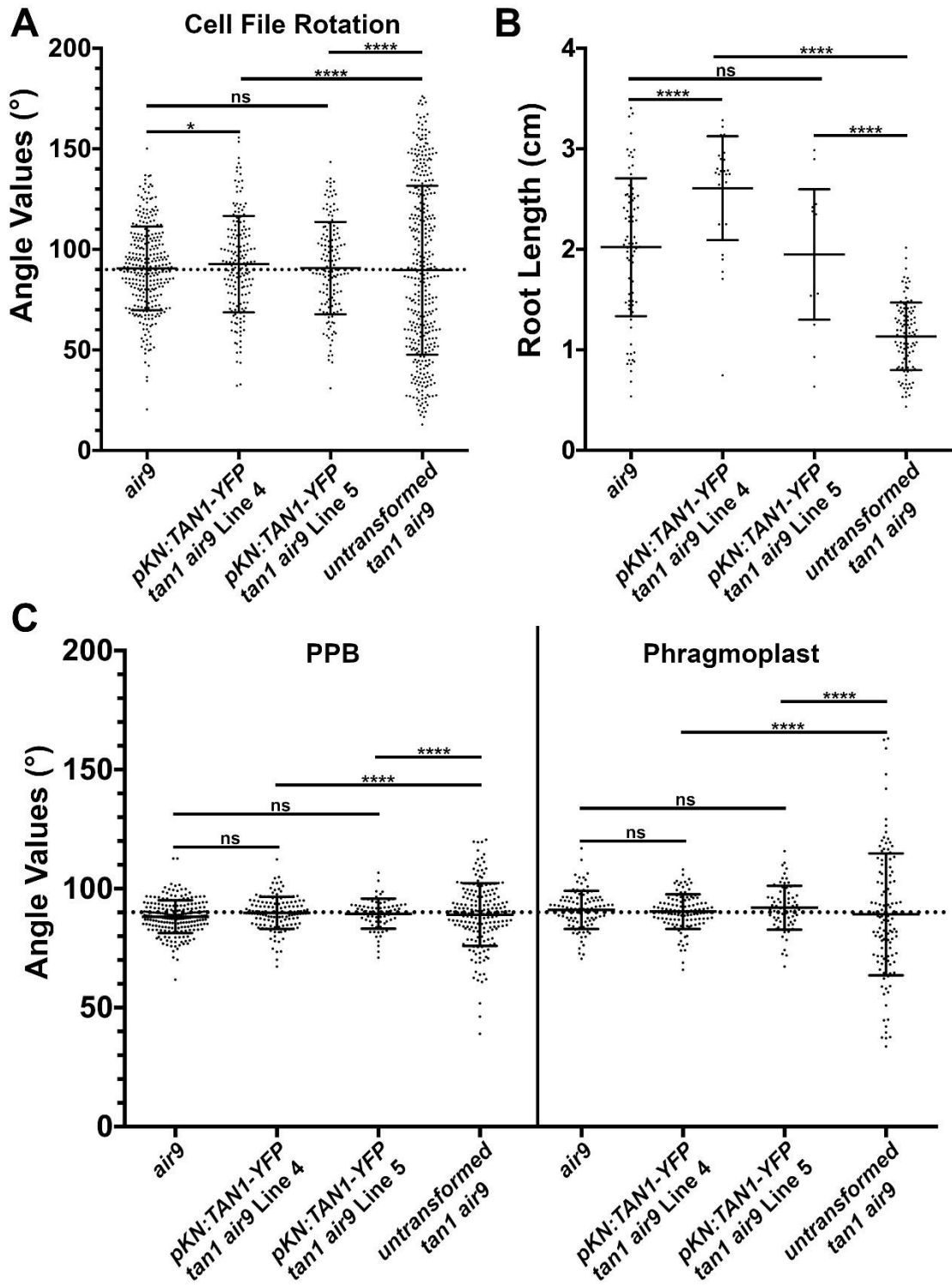
ACKNOWLEDGEMENTS

We thank Stephanie Martinez (University of California, Riverside, UCR) and Aimee Uyehara (UCR) for improving manuscript clarity, Professors Henrik Buschmann (Osnabruck University), Meng Chen (UCR), Zhenbio Yang (UCR), Sean Cutler (UCR), David Ehrhardt (Carnegie Institute), Anne Sylvester (University of Wyoming) and Dr. Ricardo Mir (UCR) for materials or facilities, and Professor Jaimie Van Norman (UCR) for cloning advice.

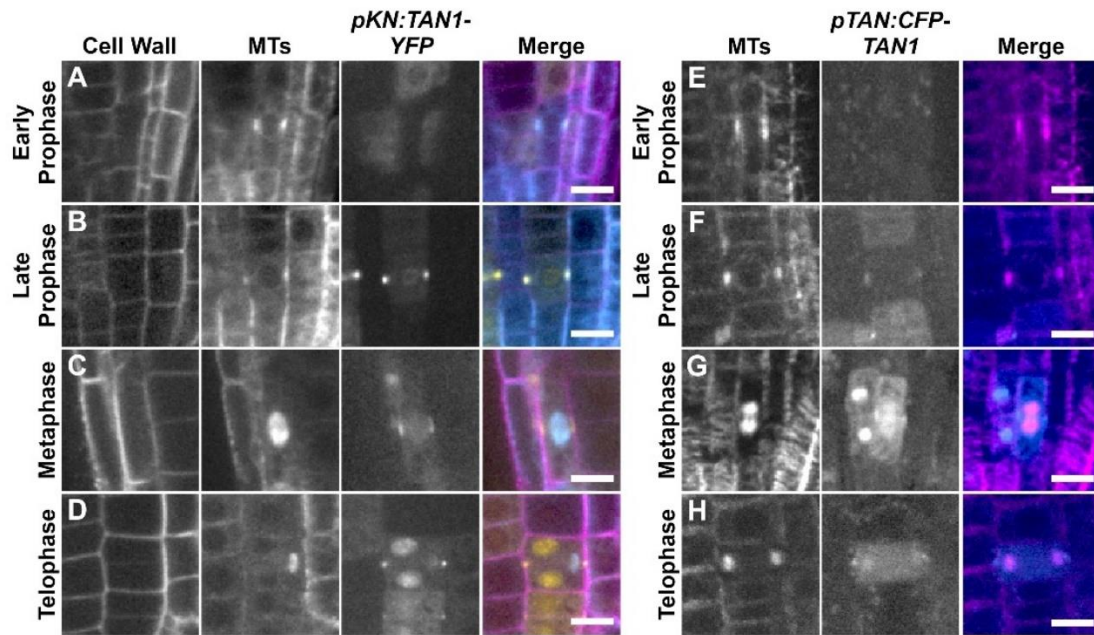
SUPPLEMENTAL FIGURES AND TABLES



Supplementary Figure 4.1. *TAN1-YFP* expressed by its native promoter (*pTAN:TAN1-YFP*) rescues *tan1 air9* double mutant root growth. Confocal images of propidium iodide-stained roots of *tan1 air9* plants. A) A *tan1 air9* plant expressing *pTAN:TAN1-YFP*. B) A negative sibling *tan1 air9* plant. Bars = 50 μ m. C) Root length measurements from 8 days after stratification of *air9* single mutants (left), *pTAN:TAN1-YFP tan1 air9* double mutants (middle), and *tan1 air9* double mutants (right). $n > 10$ plants for each genotype, compared by two-tailed t-test with Welch's correction. ns indicates not significant, **** P-value < 0.0001 .



Supplementary Figure 4.2. *pKN:TAN1-YFP tan1 air9* lines show significant rescue compared to untransformed *tan1 air9*. A) Cell file rotation angles of *air9* single mutants (left), two transgenic lines expressing *pKN:TAN1-YFP* in the *tan1 air9* double mutant designated as line 4 (center left) and line 5 (center right) and untransformed plants (right), $n > 17$ plants for each genotype. $N > 146$ cells for angle measurements. Angle variances were compared with Levene's test. B) Root length measurements from 8 days after stratification of *air9* single mutants (left), two transgenic lines expressing *pKN:TAN1-YFP* in the *tan1 air9* double mutant (middle), and untransformed plants (right), $n > 21$ plants for each genotype, compared by two-tailed t-test with Welch's correction. C) PPB and phragmoplast angle measurements in dividing root cells of *air9* single mutants (left), two transgenic lines expressing *pKN:TAN1-YFP* in the *tan1 air9* double mutant (middle), and untransformed plants (right), $n > 15$ plants for each genotype. $N > 69$ cells for angle measurements. Angle variations compared with F-test. ns indicates not significant, * P-value < 0.05 , **** P-value < 0.0001 .



Supplementary Figure 4.3. Division site localization of TAN1-YFP driven by the *KNOLLE* promoter (*pKN:TAN1-YFP*) and CFP-TAN1 driven by the *TAN1* promoter (*pTAN:CFP-TAN1*) in *tan1 air9* double mutants. A-D) Confocal images of propidium iodide-stained (Cell Wall) roots of *tan1 air9* plants expressing *pKN:TAN1-YFP* and *CFP-TUBULIN* (MTs) in dividing root tip cells. E-F) Maximum projections of 3 1- μ m Z-stacks of *tan1 air9* plants expressing *pTAN:CFP-TAN1* and the microtubule (MTs) marker *UBQ10:mScarlet-MAP4* in dividing root tip cells. Representative images of cells with (A&E) broad early PPBs, (B&F) late narrow PPBs, (C&G) metaphase spindles, and (D&H) phragmoplasts. Bars = 10 μ m.

Supplementary Table 4.1. Primers used for cloning and genotyping.

Primer Name	Sequence
ATRP	ATCTCTTAGGAACCAAACCGGACGCTGT
ATLP	GATCCGTTACGAAAGTGAACACCTTTATC
JL202	CATTTTATAATAACGCTGCCGGACATCTAC
AIR9-5RP	TGGATCAGCTGCAACATTATTC
AIR9-5LP	ATTAACATTTTGCAACGCAGG
LBb1.3	ATTTTGCCGATTTGGAAC
Ds5-4	TACGATAACGGTCGGTACGG
AtTAN 733-CDS Rw	AAATAGAGGGTTCGGAAAAAGAACC
AIR9 gnm7511 R	CCTCCAGTATATGAAGCAACAAAGC
AIR9_cDNA 2230 F	GATGAGGAATATATGTTATCTTTAGATG
pKN-5'SacI Fw	GAGGAGCTCCAGAAGAAAAAGAAAAAGTTCTC
pKN-5'EcoRI Rw	TAAGCGGAATTCCTTTTTACCTGAAA
35SpKN5' Fw	ACCCACAGATGGTTAGAGagg
YFP XhoI Rw	ATAATGCTCGAGAGAGTCGCG
NpTANSacIFor	GTATGAGCTCCGGTAGAGTTGAACCAG
NpTANceruleanRev	CCTCGCCCTTGCTCACCATCTTCTATATATATTTCTTTA
NpTANceruleanFor	TAAAGAAAATATATATAGAAGATGGTGAGCAAGGGCGAGG
CeruleanpEarleyRev	GGCCCGCGGTACCGTCCTTGTACAGCTCGTCCATGC
CeruleanpEarleyFor	GCATGGACGAGCTGTACAAGGACGGTACCGCGGGCC
pEarleyOCSpStIRev	CCATCTGCAGCTGCTGAGCCTCGACAT
AtExon1_1For	CTCAACTCAGATCTTCTCAAGGAAACG
At255AfterStopRev	GCATAGTGGTACCCTCAAATTACACC

REFERENCES

- Abe, T., Thitamadee, S. and Hashimoto, T.** (2004). Microtubule defects and cell morphogenesis in the lefty1lefty2 tubulin mutant of *Arabidopsis thaliana*. *Plant Cell Physiol.* **45**, 211–220.
- Alim, K., Hamant, O. and Boudaoud, A.** (2012). Regulatory role of cell division rules on tissue growth heterogeneity. *Front. Plant Sci.* **3**, 174.
- Bellinger, M.A., Uyehara, A.N., Martinez, P., McCarthy, M.C., and Rasmussen, C.G.** (2021). Cell cortex microtubules contribute to division plane positioning during telophase in maize. bioRxiv 2021.01.11.426230; doi: <https://doi.org/10.1101/2021.01.11.426230>.
- Buschmann, H. and Borchers, A.** (2020). Handedness in plant cell expansion: a mutant perspective on helical growth. *New Phytol.* **225**, 53–69.
- Buschmann, H., Fabri, C. O., Hauptmann, M., Hutzler, P., Laux, T., Lloyd, C. W. and Schäffner, A. R.** (2004). Helical Growth of the *Arabidopsis* Mutant *tortifolia1* Reveals a Plant-Specific Microtubule-Associated Protein. *Curr. Biol.* **14**, 1515–1521.
- Buschmann, H., Chan, J., Sanchez-Pulido, L., Andrade-Navarro, M. A., Doonan, J. H. and Lloyd, C. W.** (2006). Microtubule-associated AIR9 recognizes the cortical division site at preprophase and cell-plate insertion. *Curr. Biol.* **16**, 1938–1943.
- Buschmann, H., Hauptmann, M., Niessing, D., Lloyd, C. W. and Scha, A. R.** (2009). Helical Growth of the *Arabidopsis* Mutant *tortifolia2* Does Not Depend on Cell Division Patterns but Involves Handed Twisting of Isolated Cells. *The Plant Cell.* **21**, 2090–2106.
- Buschmann, H., Dols, J., Kopischke, S., Pen, E. J., Andrade-navarro, M. A., Heinlein, M., Szymanski, D. B., Zachgo, S., Doonan, J. H. and Lloyd, C. W.** (2015). *Arabidopsis* KCBP interacts with AIR9 but stays in the cortical division zone throughout mitosis via its MyTH4-FERM domain. *J Cell Sci.* **128**(11): 2033–2046.
- Caño-Delgado, A., Penfield, S., Smith, C., Catley, M. and Bevan, M.** (2003). Reduced cellulose synthesis invokes lignification and defense responses in *Arabidopsis thaliana*. *Plant J.* **34**, 351–362.

- Chakraborty, B., Willemsen, V., de Zeeuw, T., Liao, C.-Y., Weijers, D., Mulder, B. and Scheres, B.** (2018). A Plausible Microtubule-Based Mechanism for Cell Division Orientation in Plant Embryogenesis. *Curr. Biol.* **28**, 3031–3043.e2.
- Clough, S. J. and Bent, A. F.** (1999). Floral dip : a simplified method for Agrobacterium-mediated transformation of *Arabidopsis thaliana*. **16**, 735–743.
- Cnops, G., Wang, X., Linstead, P., Van Montagu, M., Van Lijsebettens, M. and Dolan, L.** (2000). Tornado1 and tornado2 are required for the specification of radial and circumferential pattern in the *Arabidopsis* root. *Development* **127**, 3385–3394.
- Cosgrove, D. J.** (2005). Growth of the plant cell wall. *Nat. Rev. Mol. Cell Biol.* **6**, 850–861.
- Cosgrove, D. J.** (2018). Diffuse Growth of Plant Cell Walls. *Plant Physiol.* **176**, 16–27.
- Dixit, R. and Cyr, R. J.** (2002). Spatio-temporal relationship between nuclear-envelope breakdown and preprophase band disappearance in cultured tobacco cells. *Protoplasma* **219**, 116–121.
- Facette, M. R., Rasmussen, C. G. and Van Norman, J. M.** (2018). A plane choice: coordinating timing and orientation of cell division during plant development. *Curr. Opin. Plant Biol.* **47**, 47–55.
- Fache, V., Gaillard, J., Van Damme, D., Geelen, D., Neumann, E., Stoppin-Mellet, V. and Vantard, M.** (2010). *Arabidopsis* kinetochore fiber-associated MAP65-4 cross-links microtubules and promotes microtubule bundle elongation. *Plant Cell* **22**, 3804–3815.
- Frey, N., Klotz, J. and Nick, P.** (2010). A kinesin with calponin-homology domain is involved in premitotic nuclear migration. *J. Exp. Bot.* **61**, 3423–3437.
- Furutani, I., Watanabe, Y., Prieto, R., Masukawa, M., Suzuki, K. and Naoi, K.** (2000). The SPIRAL genes are required for directional control of cell elongation in *Arabidopsis thaliana*. **4453**, 4443–4453.
- Goff, J. and Van Norman, J. M.** (2021). Polarly localized receptor-like kinases PXC2 and IRK act redundantly during *Arabidopsis* root development in the radial axis. *bioRxiv* 2021.02.11.429611.

- Goldy, C., Pedroza-Garcia, J.-A., Breakfield, N., Cools, T., Vena, R., Benfey, P. N., De Veylder, L., Palatnik, J. and Rodriguez, R. E.** (2021). The Arabidopsis GRAS-type SCL28 transcription factor controls the mitotic cell cycle and division plane orientation. *Proc. Natl. Acad. Sci. U. S. A.* **118**,.
- Gonneau, M., Desprez, T., Martin, M., Doblaz, V. G., Bacete, L., Miart, F., Sormani, R., Hématy, K., Renou, J., Landrein, B., et al.** (2018). Receptor Kinase THESEUS1 Is a Rapid Alkalinization Factor 34 Receptor in Arabidopsis. *Curr. Biol.* **28**, 2452–2458.e4.
- Gu, Y. and Rasmussen, C. G.** (2022). Cell biology of primary cell wall synthesis in plants. *Plant Cell* **34**, 103–128.
- Guo, X., Wang, L. and Dong, J.** (2021). Establishing asymmetry: stomatal division and differentiation in plants. *New Phytol.* **232**, 60–67.
- Haga, N., Kobayashi, K., Suzuki, T., Maeo, K., Kubo, M., Ohtani, M., Mitsuda, N., Demura, T., Nakamura, K., Jürgens, G., et al.** (2011). Mutations in MYB3R1 and MYB3R4 cause pleiotropic developmental defects and preferential down-regulation of multiple G2/M-specific genes in Arabidopsis. *Plant Physiol.* **157**, 706–717.
- Hamant, O. and Haswell, E. S.** (2017). Life behind the wall: sensing mechanical cues in plants. *BMC Biol.* **15**, 59.
- Hamant, O., Heisler, M. G., Jönsson, H., Krupinski, P., Uyttewaal, M., Bokov, P., Corson, F., Sahlin, P., Boudaoud, A., Meyerowitz, E. M., et al.** (2008). Developmental patterning by mechanical signals in Arabidopsis. *Science* **322**, 1650–1655.
- Hashimoto, T.** (2002). Molecular genetic analysis of left-right handedness in plants. *Philos. Trans. R. Soc. Lond. B Biol. Sci.* **357**, 799–808.
- Hashimoto, T.** (2015). Microtubules in plants. *Arabidopsis Book* **13**, e0179.
- Heisler, M. G., Hamant, O., Krupinski, P., Uyttewaal, M., Ohno, C., Jönsson, H., Traas, J. and Meyerowitz, E. M.** (2010). Alignment between PIN1 polarity and microtubule orientation in the shoot apical meristem reveals a tight coupling between morphogenesis and auxin transport. *PLoS Biol.* **8**, e1000516.
- Hématy, K., Sado, P.-E., Van Tuinen, A., Rochange, S., Desnos, T., Balzergue, S., Pelletier, S., Renou, J.-P. and Höfte, H.** (2007). A Receptor-like Kinase Mediates the Response of Arabidopsis Cells to the Inhibition of Cellulose Synthesis. *Current Biology* **17**, 922–931.

- Herrmann, A., Livanos, P., Lipka, E., Gadeyne, A., Hauser, M.-T., Van Damme, D. and Müller, S.** (2018). Dual localized kinesin-12 POK2 plays multiple roles during cell division and interacts with MAP65-3. *EMBO Rep.* **19**, e46085.
- Ho, C.-M. K., Lee, Y.-R. J., Kiyama, L. D., Dinesh-Kumar, S. P. and Liu, B.** (2012). Arabidopsis microtubule-associated protein MAP65-3 cross-links antiparallel microtubules toward their plus ends in the phragmoplast via its distinct C-terminal microtubule binding domain. *Plant Cell* **24**, 2071–2085.
- Ishida, T., Kaneko, Y., Iwano, M. and Hashimoto, T.** (2007). Helical microtubule arrays in a collection of twisting tubulin mutants of *Arabidopsis thaliana*. *Proc. Natl. Acad. Sci. U. S. A.* **104**, 8544–8549.
- Kimata, Y., Higaki, T., Kawashima, T., Kurihara, D., Sato, Y. and Yamada, T.** (2016). Cytoskeleton dynamics control the first asymmetric cell division in *Arabidopsis* zygote.
- Kirik, V., Herrmann, U., Parupalli, C., Sedbrook, J. C., Ehrhardt, D. W. and Hülskamp, M.** (2007). CLASP localizes in two discrete patterns on cortical microtubules and is required for cell morphogenesis and cell division in *Arabidopsis*. *J. Cell Sci.* **120**, 4416–4425.
- Lee, Y.-R. J. and Liu, B.** (2013). The rise and fall of the phragmoplast microtubule array. *Curr. Opin. Plant Biol.* **16**, 757–763.
- Li, S., Sun, T. and Ren, H.** (2015). The functions of the cytoskeleton and associated proteins during mitosis and cytokinesis in plant cells. *Front. Plant Sci.* **6**, 282.
- Li, H., Sun, B., Sasabe, M., Deng, X., Machida, Y., Lin, H., Lee, Y. J. and Liu, B.** (2017). Arabidopsis MAP 65-4 plays a role in phragmoplast microtubule organization and marks the cortical cell division site. *New Phytologist* **215**, 187–201.
- Lipka, E., Gadeyne, A., Stöckle, D., Zimmermann, S., De Jaeger, G., Ehrhardt, D. W., Kirik, V., Van Damme, D. and Müller, S.** (2014). The Phragmoplast-Orienting Kinesin-12 Class Proteins Translate the Positional Information of the Preprophase Band to Establish the Cortical Division Zone in *Arabidopsis thaliana*. *Plant Cell* **26**, 2617–2632.
- Livanos, P. and Müller, S.** (2019). Division Plane Establishment and Cytokinesis. *Annu. Rev. Plant Biol.*

- Louveaux, M., Julien, J.-D., Mirabet, V., Boudaoud, A. and Hamant, O.** (2016). Cell division plane orientation based on tensile stress in *Arabidopsis thaliana*. *Proc. Natl. Acad. Sci. U. S. A.* **113** (30) E4294-E4303.
- Lukowitz, W., Mayer, U. and Jürgens, G.** (1996). Cytokinesis in the *Arabidopsis* embryo involves the syntaxin-related KNOLLE gene product. *Cell* **84**, 61–71.
- Martinez, P., Luo, A., Sylvester, A. and Rasmussen, C. G.** (2017). Proper division plane orientation and mitotic progression together allow normal growth of maize. *Proc. Natl. Acad. Sci. U. S. A.* **114**, 2759–2764.
- Martinez, P., Allsman, L. A., Brakke, K. A., Hoyt, C., Hayes, J., Liang, H., Neher, W., Rui, Y., Roberts, A. M., Moradifam, A., et al.** (2018). Predicting Division Planes of Three-Dimensional Cells by Soap-Film Minimization. *Plant Cell* **30**, 2255–2266.
- Martinez, P., Dixit, R., Balkunde, R. S., Zhang, A., O’Leary, S. E., Brakke, K. A. and Rasmussen, C. G.** (2020). TANGLED1 mediates microtubule interactions that may promote division plane positioning in maize. *J. Cell Biol.* **219**,.
- McMichael, C. M. and Bednarek, S. Y.** (2013). Cytoskeletal and membrane dynamics during higher plant cytokinesis. *New Phytol.* **197**, 1039–1057.
- Menges, M., de Jager, S. M., Gruissem, W. and Murray, J. A. H.** (2005). Global analysis of the core cell cycle regulators of *Arabidopsis* identifies novel genes, reveals multiple and highly specific profiles of expression and provides a coherent model for plant cell cycle control. *Plant J.* **41**, 546–566.
- Mir, R., Morris, V. H., Buschmann, H. and Rasmussen, C. G.** (2018). Division Plane Orientation Defects Revealed by a Synthetic Double Mutant Phenotype. *Plant Physiol.* **176**, 418–431.
- Mirabet, V., Das, P., Boudaoud, A. and Hamant, O.** (2011). The role of mechanical forces in plant morphogenesis. *Annu. Rev. Plant Biol.* **62**, 365–385.
- Morgan, X., Zhao, Q., Rodrigo-peiris, T., Brkljacic, J., Sylvia, C., Mu, S. and Meier, I.** (2008). RanGAP1 is a continuous marker of the *Arabidopsis* cell division plane. **105**, 18637–18642.
- Moukhtar, J., Trubuil, A., Belcram, K., Legland, D., Khadir, Z., Urbain, A., Palauqui, J.-C. and Andrey, P.** (2019). Cell geometry determines symmetric and asymmetric division plane selection in *Arabidopsis* early embryos. *PLoS Comput. Biol.* **15**, e1006771.

- Müller, S. and Jürgens, G.** (2016). Plant cytokinesis—No ring, no constriction but centrifugal construction of the partitioning membrane. *Semin. Cell Dev. Biol.* **53**, 10–18.
- Murata, T., Sano, T., Sasabe, M., Nonaka, S., Higashiyama, T., Hasezawa, S., Machida, Y. and Hasebe, M.** (2013). Mechanism of microtubule array expansion in the cytokinetic phragmoplast. *Nat. Commun.* **4**, 1967.
- Muroyama, A. and Bergmann, D.** (2019). Plant Cell Polarity: Creating Diversity from Inside the Box. *Annu. Rev. Cell Dev. Biol.* **35**, 309–336.
- Nakajima, K., Furutani, I., Tachimoto, H., Matsubara, H. and Hashimoto, T.** (2004). SPIRAL1 encodes a plant-specific microtubule-localized protein required for directional control of rapidly expanding Arabidopsis cells. *Plant Cell* **16**, 1178–1190.
- Pan, X., Fang, L., Liu, J., Senay-Aras, B., Lin, W., Zheng, S., Zhang, T., Guo, J., Manor, U., Van Norman, J., et al.** (2020). Auxin-induced signaling protein nanoclustering contributes to cell polarity formation. *Nat. Commun.* **11**, 3914.
- Pickett-Heaps, J. D., Gunning, B. E. S., Brown, R. C., Lemmon, B. E. and Cleary, A. L.** (1999). The cytoplasmic concept in dividing plant cells: cytoplasmic domains and the evolution of spatially organized cell division. *Am. J. Bot.* **86**, 153–172.
- Rasmussen, C. G. and Bellinger, M.** (2018). An overview of plant division-plane orientation. *New Phytol.*
- Rasmussen, C. G., Wright, A. J. and Müller, S.** (2013). The role of the cytoskeleton and associated proteins in determination of the plant cell division plane. *Plant J.* **75**, 258–269.
- Sakai, T., Honing, H. van der, Nishioka, M., Uehara, Y., Takahashi, M., Fujisawa, N., Saji, K., Seki, M., Shinozaki, K., Jones, M. A., et al.** (2008). Armadillo repeat-containing kinesins and a NIMA-related kinase are required for epidermal-cell morphogenesis in Arabidopsis. *Plant J.* **53**, 157–171.
- Sampathkumar, A., Krupinski, P., Wightman, R., Milani, P., Berquand, A., Boudaoud, A., Hamant, O., Jönsson, H. and Meyerowitz, E. M.** (2014). Subcellular and supracellular mechanical stress prescribes cytoskeleton behavior in Arabidopsis cotyledon pavement cells. *Elife* **3**, e01967.
- Sapala, A., Runions, A., Routier-Kierzkowska, A.-L., Das Gupta, M., Hong, L., Hofhuis, H., Verger, S., Mosca, G., Li, C.-B., Hay, A., et al.** (2018). Why plants make puzzle cells, and how their shape emerges. *Elife* **7**,.

- Schopfer, P.** (2006). Biomechanics of plant growth. *Am. J. Bot.* **93**, 1415–1425.
- Sedbrook, J. C., Ehrhardt, D. W., Fisher, S. E., Scheible, W.-R. and Somerville, C. R.** (2004). The Arabidopsis SKU6/SPIRAL1 gene encodes a plus end-localized microtubule-interacting protein involved in directional cell expansion. *Plant Cell* **16**, 1506–1520.
- Shao, W. and Dong, J.** (2016). Polarity in plant asymmetric cell division: Division orientation and cell fate differentiation. *Dev. Biol.* **419**, 121–131.
- Shoji, T., Narita, N. N., Hayashi, K., Hayashi, K., Asada, J., Hamada, T., Sonobe, S., Nakajima, K. and Hashimoto, T.** (2004). Plant-specific microtubule-associated protein SPIRAL2 is required for anisotropic growth in Arabidopsis. *Plant Physiol.* **136**, 3933–3944.
- Smertenko, A. P., Kaloriti, D., Chang, H.-Y., Fiserova, J., Opatrny, Z. and Hussey, P. J.** (2008). The C-terminal variable region specifies the dynamic properties of Arabidopsis microtubule-associated protein MAP65 isotypes. *Plant Cell* **20**, 3346–3358.
- Smertenko, A., Assaad, F., Baluška, F., Bezanilla, M., Buschmann, H., Drakakaki, G., Hauser, M.-T., Janson, M., Mineyuki, Y., Moore, I., et al.** (2017). Plant Cytokinesis: Terminology for Structures and Processes. *Trends Cell Biol.* **27**, 885–894.
- Smertenko, A., Hewitt, S. L., Jacques, C. N., Kacprzyk, R., Liu, Y., Marcec, M. J., Moyo, L., Ogden, A., Oung, H. M., Schmidt, S., et al.** (2018). Phragmoplast microtubule dynamics - a game of zones. *J. Cell Sci.* **131**, jcs203331.
- Smith, L. G., Gerttula, S. M., Han, S. and Levy, J.** (2001). Tangled1: a microtubule binding protein required for the spatial control of cytokinesis in maize. *J. Cell Biol.* **152**, 231–236.
- Song, H., Golovkin, M., Reddy, A. S. and Endow, S. A.** (1997). In vitro motility of AtKCBP, a calmodulin-binding kinesin protein of Arabidopsis. *Proc. Natl. Acad. Sci. U. S. A.* **94**, 322–327.
- Strompen, G., El Kasmi, F., Richter, S., Lukowitz, W., Assaad, F. F., Jürgens, G. and Mayer, U.** (2002). The Arabidopsis HINKEL gene encodes a kinesin-related protein involved in cytokinesis and is expressed in a cell cycle-dependent manner. *Curr. Biol.* **12**, 153–158.
- Thitamadee, S., Tuchiara, K. and Hashimoto, T.** (2002). Microtubule basis for left-handed helical growth in Arabidopsis. *Nature* **417**, 193–196.

- Uyttewaal, M., Burian, A., Alim, K., Landrein, B., Borowska-Wykręt, D., Dedieu, A., Peaucelle, A., Ludynia, M., Traas, J., Boudaoud, A., et al.** (2012). Mechanical stress acts via katanin to amplify differences in growth rate between adjacent cells in *Arabidopsis*. *Cell* **149**, 439–451.
- Van Damme, D.** (2009). Division plane determination during plant somatic cytokinesis. *Curr. Opin. Plant Biol.* **12**, 745–751.
- van Oostende-Triplet, C., Guillet, D., Triplet, T., Pandzic, E., Wiseman, P. W. and Geitmann, A.** (2017). Vesicle Dynamics during Plant Cell Cytokinesis Reveals Distinct Developmental Phases. *Plant Physiol.* **174**, 1544–1558.
- Völker, A., Stierhof, Y. D. and Jürgens, G.** (2001). Cell cycle-independent expression of the *Arabidopsis* cytokinesis-specific syntaxin KNOLLE results in mistargeting to the plasma membrane and is not sufficient for cytokinesis. *J. Cell Sci.* **114**, 3001–3012.
- Wachsman, G., Sparks, E. E. and Benfey, P. N.** (2015). Genes and networks regulating root anatomy and architecture. *New Phytol.* **208**, 26–38.
- Wada, M.** (2018). Nuclear movement and positioning in plant cells. *Semin. Cell Dev. Biol.* **82**, 17–24.
- Walker, K. L., Müller, S., Moss, D., Ehrhardt, D. W. and Smith, L. G.** (2007). *Arabidopsis* TANGLED identifies the division plane throughout mitosis and cytokinesis. *Curr. Biol.* **17**, 1827–1836.
- Wasteneys, G. O. and Collings, D. A.** (2009). 3 Expanding beyond the great divide: the cytoskeleton and axial growth. *Differentiation and Development* **10**, 83.
- Whitewoods, C. D. and Coen, E.** (2017). Growth and Development of Three-Dimensional Plant Form. *Curr. Biol.* **27**, R910–R918.
- Wick, S. M. and Duniec, J.** (1983). Immunofluorescence microscopy of tubulin and microtubule arrays in plant cells. I. Preprophase band development and concomitant appearance of nuclear envelope-associated tubulin. *J. Cell Biol.* **97**, 235–243.
- Wolf, S., van der Does, D., Ladwig, F., Sticht, C., Kolbeck, A., Schürholz, A.-K., Augustin, S., Keinath, N., Rausch, T., Greiner, S., et al.** (2014). A receptor-like protein mediates the response to pectin modification by activating brassinosteroid signaling. *Proc. Natl. Acad. Sci. U. S. A.* **111**, 15261–15266.

- Wu, S.-Z. and Bezanilla, M.** (2014). Myosin VIII associates with microtubule ends and together with actin plays a role in guiding plant cell division. *Elife* **3**, e03498.
- Wu, S.-Z., Yamada, M., Mallett, D. R. and Bezanilla, M.** (2018). Cytoskeletal discoveries in the plant lineage using the moss *Physcomitrella patens*. *Biophys. Rev.* **10**(6), 1683–1693.
- Yang, W., Cortijo, S., Korsbo, N., Roszak, P., Schiessl, K., Gurzadyan, A., Wightman, R., Jönsson, H. and Meyerowitz, E.** (2021). Molecular mechanism of cytokinin-activated cell division in *Arabidopsis*. *Science* **371**, 1350–1355.
- Yi, P. and Goshima, G.** (2020). Rho of Plants GTPases and Cytoskeletal Elements Control Nuclear Positioning and Asymmetric Cell Division during *Physcomitrella patens* Branching. *Curr. Biol.* **30**, 2860–2868.e3.
- Yi, P. and Goshima, G.** (2022). Division site determination during asymmetric cell division in plants. *Plant Cell.* **34**, 6, 2120-2139.

Chapter 5: Discussion and Future Directions

In the studies described here, I highlight how protein interactions and the timing of expression of *TANGLED1* (*TAN1*) influence division plane positioning and plant growth. The *tan1 auxin-induced-in-root-cultures9 (air9) Arabidopsis thaliana* (*Arabidopsis*) double mutant has stunted growth, division plane orientation defects, and abnormal cell file twisting. Performing experiments that assess the ability of TAN1 and various altered TAN1 constructs to rescue these phenotypes has made the *tan1 air9* double mutant invaluable for studying the role of TAN1 and other proteins in division plane orientation. The *tan1 air9* double mutant will also be key in future experiments to identify TAN1 interactors, investigate mechanisms of division plane establishment and maintenance, and determine how mitotic defects alter plant growth and morphogenesis.

The ability of TAN1 with alanine substitutions at amino acids 28-33 (TAN1(28-33A)) and PHRAGMOPLAST ORIENTING KINESIN 1 (POK1) to localize to the division site in the *tan1 air9* double mutant despite their inability to interact in the yeast two-hybrid system suggests that there are likely other proteins that promote their recruitment to the division site. It is also likely that distinct mechanisms and proteins mediate POK1 and TAN1 recruitment to the division site at different stages of cell division. This is supported by evidence showing TAN1(28-33A) and POK1 are recruited to the division site in late telophase despite being absent at the division site in some metaphase and early telophase

cells and previous studies demonstrating that TAN1 recruitment to the division site is mediated by distinct mechanisms that involve different regions of the TAN1 protein (Rasmussen et al., 2011). There are many potential candidate proteins, some of which are known interactors of either TAN1, AIR9, POK1, or POK2, that likely help stabilize POK1 and TAN1 at the division site. How and when these proteins stabilize POK1-TAN1 interaction is an open question.

Teaching students molecular biology while conducting a high throughput screen for TAN1 interactors

Working with undergraduate students to develop CRISPR-Cas9 mutants of candidate genes has been a powerful tool in our initial steps to identify key TAN1 interacting proteins (Mills et al., 2021). In Spring quarter 2020, during required remote instruction due to the COVID pandemic, students designed 245 guide RNA pairs to specifically target 46 candidate genes. Even though students couldn't perform the cloning of the CRISPR-Cas9 constructs themselves, these guide RNAs will be useful for future experiments. The cloning procedure we designed for our course-based undergraduate research experience (CURE) is very straightforward and replicable, so a future undergraduate working in the lab could readily create many CRISPR-Cas9 constructs simultaneously using the predesigned guide RNAs. In Fall of 2021, with access to lab facilities, students designed guide RNAs and transformed *Arabidopsis air9* single mutant plants with CRISPR-Cas9 constructs targeting 39 candidate genes. However, following

through to screen, examine, and characterize these newly generated mutants presents a new challenge.

Designing a follow up CURE activity is one potential solution to carry the project forward. With this goal in mind, we chose pYUU as our destination vector when students created their CRISPR-Cas9 constructs. pYUU allows for selection of Cas9 positive seeds using blue light to screen for YFP expression in the seed coat without the need for antibiotic or herbicide selection plates (Angulo et al., 2020). This will allow undergraduate students to screen the dry T0 seeds for transformants without the material and labor cost associated with sterilizing and plating large quantities of seeds. Selected transformant seeds will then be transferred to soil to grow. Students will observe the seedlings for any severe growth or morphological phenotypes. Although it occurs less frequently, homozygous mutations can sometimes occur in the first generation (Wang et al., 2015). While the seedlings grow, students will design primers that flank their targeted gene to detect deletions. The gene locus and sequence of all designed guide RNAs was carefully recorded so students that continue the project can design their primers to detect the predicted deletion. Once the seedlings are large enough, students can extract DNA from their plants and then perform PCR with their primers to screen for transformants with large gene deletions. We are interested in recovering mutants with large deletions to ensure we have complete knockouts of the target gene and for ease of genotyping. Transformants with

large deletions would be selfed and the seeds would be collected. The next step would be to examine the progeny for homozygous mutants to determine if there are any phenotypes of interest, particularly division plane orientation defects. We hope to identify previously unknown TAN1 interactors which will become new areas of investigation for the lab.

Live cell imaging of fluorescent tagged proteins in the *tan1 air9* double mutant

Examining how other known division site localized proteins such as RAN GTPase ACTIVATING PROTEIN, PLECKSTRIN HOMOLOGY GTPase ACTIVATING PROTEINS (PHGAPS), KINESIN-LIKE CALMODULIN BINDING PROTEIN, and IQ67 DOMAIN proteins localize in the *tan1 air9* double mutant is another avenue to determine if these proteins act upstream of TAN1, AIR9, POK1, and POK2 in division site maintenance (Stöckle et al., 2016; Buschmann et al., 2015; Kumari et al., 2021; Xu et al., 2008). Proteins that localize to the division site in the *tan1 air9* double mutant may function upstream as anchors that help stabilize POK1 and TAN1 at the division site. Some proteins, such as the PHGAPS, which are recruited to the division site during metaphase, localize to the division site at specific stages of the cell cycle. Observing temporal changes in protein localization could provide clues on when certain protein interactions are occurring in division site maintenance. Many proteins of interest with fluorescent tags have already been generated in Arabidopsis and could

readily be crossed into the *tan1 air9* double mutant expressing the *mScarlet-MAP4* microtubule marker. Because I observed loss of POK1 at the division site in the *tan1 air9* double mutant, I crossed *p35S::GFP-POK2* (Herrmann et al., 2018) into the *tan1 air9* double mutant to see if POK2 localization is similarly altered in the *tan1 air9* double mutant.

Like POK1, POK2 colocalized with the preprophase band (PPB) in the absence of TAN1 and AIR9 but was lost from the division site after PPB disassembly (Figure 5.1A & 5.1C). This supports the hypothesis that POK1, POK2, TAN1, and AIR9 colocalize with the PPB independently of one another, likely via interaction with microtubules, but are dependent on protein-protein interactions to remain at the division site upon entry into metaphase. Unlike POK1, POK2 accumulates in the phragmoplast midline in addition to at the division site in wild-type telophase cells (Figure 5.1F) and has an additional role stabilizing the phragmoplast midzone via interactions with MAP65-3 (Herrmann et al., 2018). POK2 frequently accumulated in the phragmoplast midline but was absent at the division site in *tan1 air9* telophase cells (Figure 5.1E & 5.1G). This observation suggests that POK2 localization to the division site, but not the phragmoplast midline, is dependent on TAN1 and AIR9. POK2 was sometimes visible at the division site in late telophase cells where the cell plate had contacted the cortex (Figure 5.1I & 5.1J). POK2 division site localization in late telophase cells was often patchy, rather than a clear continuous ring like those observed in wild-type late telophase

cells (Figure 5.1H). I hypothesize that division site localized POK2 in *tan1 air9* late telophase cells is likely a result of phragmoplast midline associated POK2 being delivered to the division site as the phragmoplast contacts the cell cortex rather than normal recruitment of POK2 to the division site. Overall, these data suggest that, like POK1, POK2 maintenance at the division site is dependent on the presence of AIR9 or TAN1.

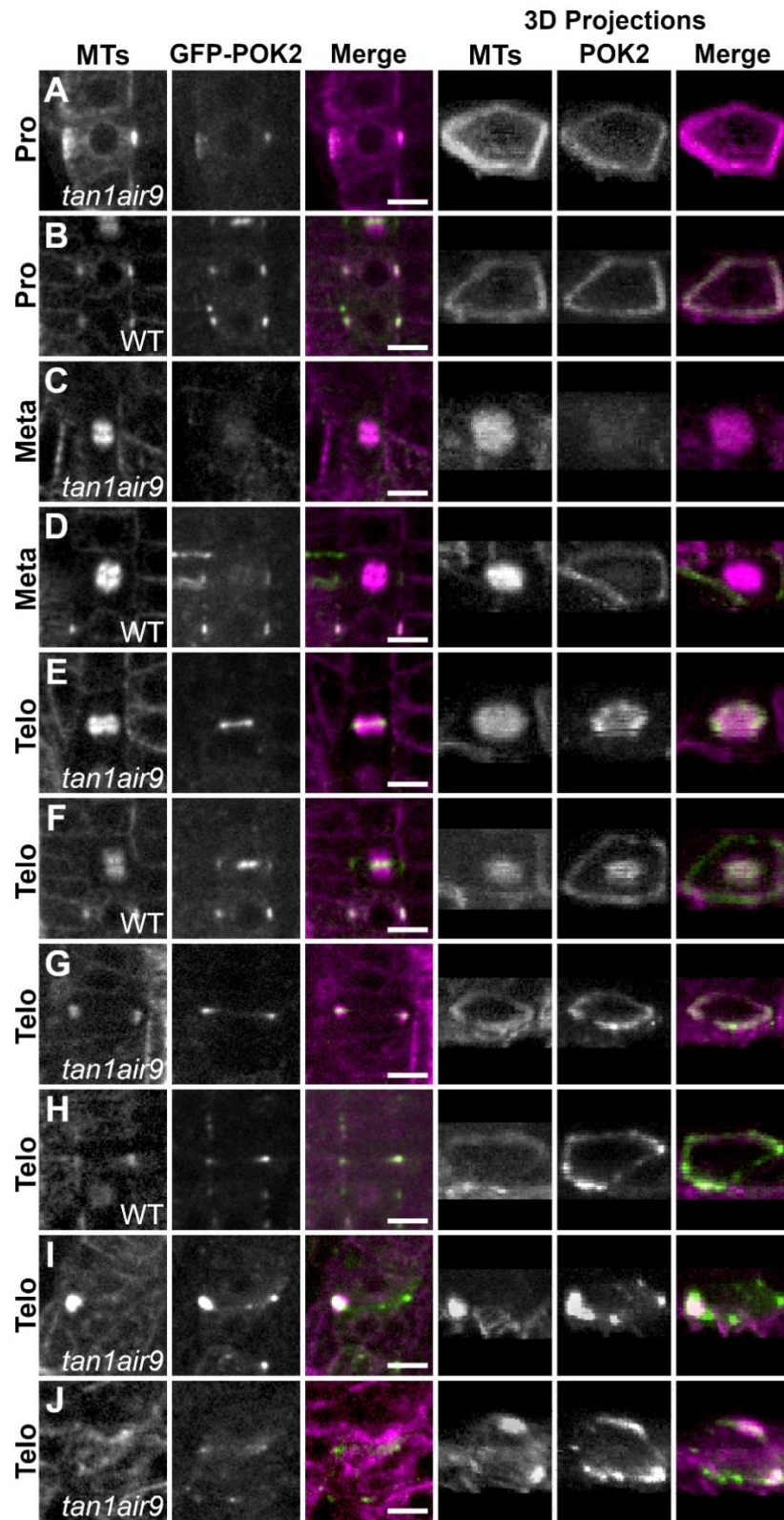


Figure 5.1: TAN1 and AIR9 promote POK2 maintenance at the division site. GFP-POK2 localization in wild-type and *tan1 air9* double mutants expressing *UBQ10:mScarlet-MAP4* to mark microtubules and *p35S:GFP-POK2*. N=19 double mutant plants. Scale bars = 10 μ m. A) GFP-POK2 localization during preprophase/prophase in *tan1 air9* mutants. In 84% of cells (n=74/88 cells) GFP-POK2 colocalized with the PPB. B) Representative image of GFP-POK2 colocalizing with the PPB in wild-type cells. C) GFP-POK2 was absent from the division site in 95% of cells in metaphase (19/20 cells). D) GFP-POK2 is maintained at the division site in wild-type metaphase cells. E) GFP-POK2 strongly accumulates in the phragmoplast midline of barrel phragmoplasts in early telophase, and remains absent from the division site (89%, n=17/19 cells). F) GFP-POK2 localizes to the phragmoplast midline and division site in wild-type telophase cells. G) During late telophase, GFP-POK2 is often visible in the phragmoplast midline, but NOT at the division site (66%, n=42/64 cells). H) GFP-POK2 persists as a continuous ring at the division site through telophase and cytokinesis in wild-type cells. I & J) During late cytokinesis as the cell plate contacts the cell cortex, GFP-POK2 is sometimes visible at the cell plate insertion site (19%, n=12/64 cells).

Whether POK2 localization to the division site and phragmoplast midline in *tan1* and *air9* single mutants is altered remains to be determined. I hypothesize that, like POK1, POK2 will localize to the division site in *tan1* and *air9* single mutants. Because POK1 and POK2 are homologs and they both interact with TAN1 (Figure 5.2), it is likely they localize to the division site via similar mechanisms. However, I expect there may be subtle changes in POK2 localization to the phragmoplast midline. In *tan1* single mutants, POK1 accumulated more frequently in the phragmoplast midline. This increased midline accumulation was likely caused by inefficient recruitment of POK1 to the division site by AIR9, which caused POK1 to accumulate at the plus ends of microtubules in the phragmoplast (Mills et al., 2022). POK2 localization to the phragmoplast midline is partially dependent on MAP65-3, and POK2 midline accumulation is reduced but not abolished in *map65-3* mutants (Herrmann et al., 2018). TAN1 and AIR9 both colocalize with the phragmoplast where they could potentially influence POK2 accumulation in the phragmoplast midline (Martinez et al., 2017; Buschmann et al., 2006). If POK2 localization to the phragmoplast midline is partially dependent on AIR9 and/or TAN1, I may see reduced POK2 accumulation in the phragmoplast midlines of the single mutants. Determining if loss of TAN1 or AIR9 influences POK2 midline accumulation could provide insight into potential unexplored roles for TAN1 or AIR9 in phragmoplast organization.

Yeast two-hybrid as a tool to identify protein interaction motifs

Alanine scanning mutagenesis followed by yeast two-hybrid screening was useful for quickly identifying possible TAN1-POK1 interaction motifs. I identified multiple regions within *TAN1*₁₋₁₃₂ required for interaction with POK1 in the yeast two-hybrid system but focused on the highly conserved amino acids 28-33 of TAN1. Interestingly, when expressed in the *tan1 air9* double mutant TAN1(28-33A) and POK1 showed impaired maintenance at the division site during metaphase and early telophase but were still efficiently recruited to the division site in late telophase. Additionally, recruitment during late telophase was sufficient to almost fully rescue the *tan1 air9* double mutant. Together this data suggests that POK1 and TAN1 are stabilized and/or recruited to the division site via interaction with other protein(s). This yeast two-hybrid screening approach has the potential to identify motifs within TAN1 that mediate interaction with other known interacting proteins such as RAB GTPase-activating protein, CALCIUM-DEPENDENT PROTEIN KINASE1 ADAPTOR PROTEIN2, and MYOSIN BINDING PROTEIN3 (Su, 2012). Determining which domains in TAN1 are important for mediating protein-protein interactions will be useful for developing a model of protein interactions involved in division site maintenance. Because TAN1₁₋₁₃₂ interacts with so many different proteins, it is also possible that interaction motifs for different proteins may overlap. This information would be useful for determining if TAN1 maintenance at the division site may involve proteins competing for interaction with TAN1

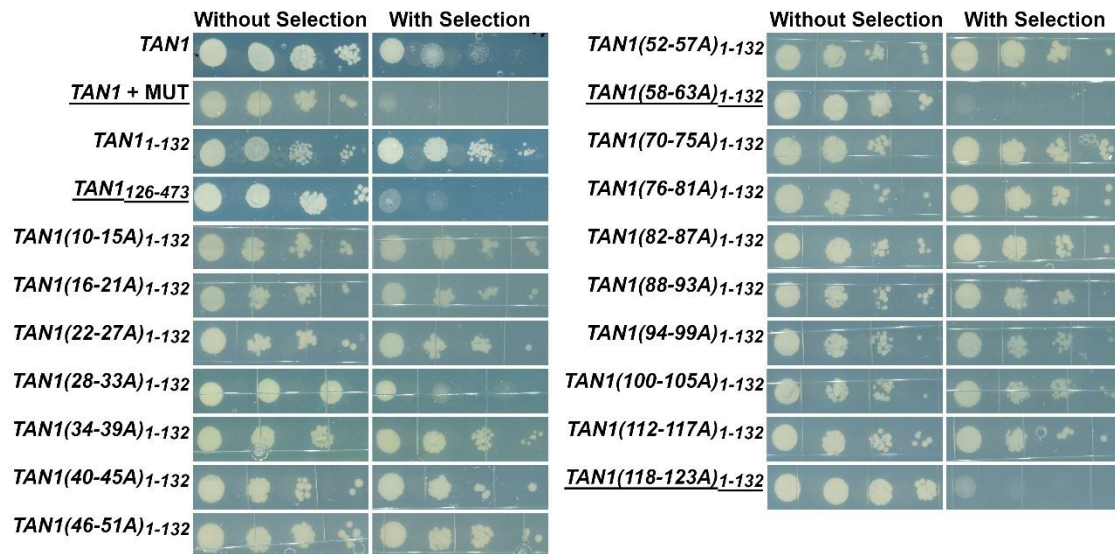


Figure 5.2: Yeast two-hybrid testing pAD-*POK2* 2083-2771 interaction with pBD-*TAN1* and alanine scanning pAS-*TAN1*₁₋₁₃₂ constructs. pBD-*TAN1*+pAD-MUT served as a control for loss of interaction. Underlined constructs showed loss of interaction. Alanines 64-69 and 106-111 were not completed and not included in the yeast two-hybrid.

I applied the same yeast two-hybrid screen approach to demonstrate that POK2 specifically interacts with *TAN1*₁₋₁₃₂ and identify POK2 interaction sites within *TAN1*₁₋₁₃₂ (Figure 5.2). Unlike POK1, which had several interaction sites within *TAN1*₁₋₁₃₂, there were only two POK2 interaction sites. Interestingly, one of these sites at amino acids 58-63 of TAN1 mediated interaction with both POK1 and POK2. Additionally, serine 58 is a conserved phosphorylated residue in TAN1, which suggests that phosphorylation may play a role in mediating protein interactions with TAN1 (Walley et al., 2016). I hypothesized that TAN1 with alanine substitutions at amino acids 58-63 (*TAN1*(58-63A)) would fail to be maintained at the division site after PPB disassembly, similar to TAN1 localization in *pok1 pok2* double mutants (Lipka et al., 2014). However, when I introduced *YFP-TAN1*(58-63A) into the *tan1 air9* double mutant I saw that *YFP-TAN1*(58-63A) localized to the division site during both preprophase/prophase and telophase (Figure 5.3C & 5.3D). *TAN1*(58-63A) also partially rescues the *tan1 air9* double mutant as evidenced by the visible rescue of root tip patterning and root twisting (Figure 5.3A and 5.3B). However, root growth rescue and PPB and phragmoplast positioning in *tan1 air9 TAN1*(58-63A) plants remains to be examined. It will also be informative to examine the mechanism by which *CFP-TAN1*(58-63A) colocalizes with *YFP-POK1* and *GFP-POK2* in the presence of a microtubule marker in dividing cells of the *tan1 air9* double mutant. I hypothesize that *TAN1*(58-63A) likely will have division site maintenance defects that are more severe than those observed for *TAN1*(28-33A), which loses interaction with

POK1 but not POK2, but that TAN1(58-63A), POK1, and POK2 will still be recruited to the division site during late telophase by other mechanisms. The study presented here demonstrates that identification of regions that specifically mediate protein interactions and examination of changes in localization and function in planta using the *tan1 air9* mutant can be used to dissect the role of specific protein interactions. It also suggests that there are yet to be discovered interactions and mechanisms that influence division site maintenance.

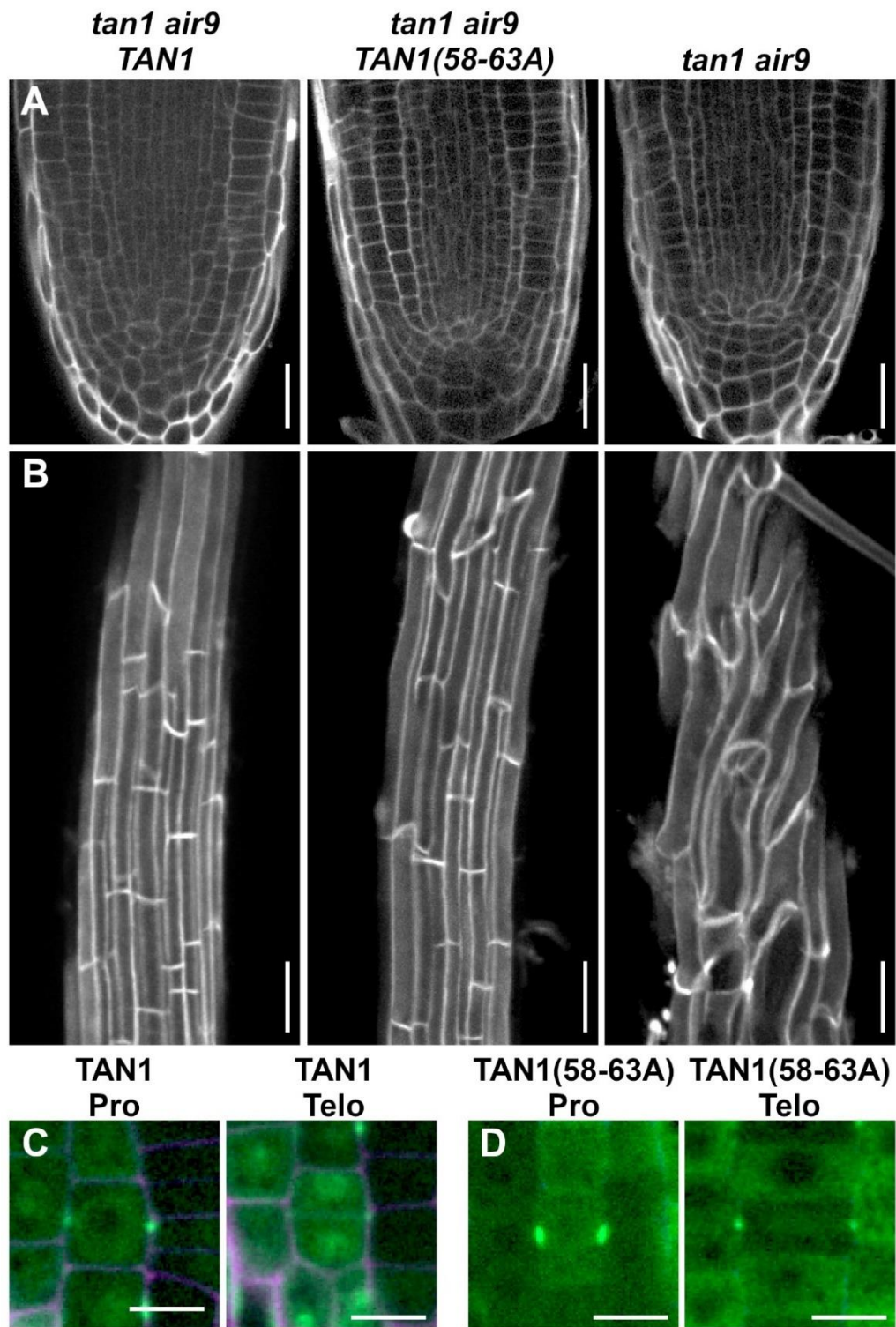


Figure 5.3: TAN1(58-63A) partly rescues the *tan1 air9* double mutant and localizes to the division site during preprophase/prophase, and telophase.

A) Cell walls of Arabidopsis *tan1 air9* double mutant root tips stained with propidium iodide (PI) of plants expressing *p35S:YFP-TAN1* (left), *p35S:YFP-TAN1(58-63A)* (middle), and untransformed *tan1 air9* double mutants (right). Scale bars = 25 μm . B) Maximum projections of 10 1- μm Z-stacks of PI-stained differentiation zone root cell walls. Scale bars = 50 μm . C) Propidium iodide stained *tan1 air9* plants expressing (C) *p35S:YFP-TAN1* or ((D) *p35S:YFP-TAN1(58-63A)* during preprophase/prophase (Pro) and telophase/cytokinesis (Telo). Scale bars = 10 μm .

Determining if defects in the nondividing cells of the *tan1 air9* double mutant are caused by cell wall integrity responses

Mitotic expression of *TAN1*, driven by the *KNOLLE* promoter (*pKNOLLE*) or *TAN1* native promoter, was sufficient to rescue the *tan1 air9* double mutant (Mills and Rasmussen, 2022). Furthermore, *pKNOLLE* driven *TAN1* rescued cell file rotation defects better than *TAN1* expressed under the constitutively active viral cauliflower mosaic *CaMV35S* promoter. This suggests that having sufficient *TAN1* in dividing cells is important for restoring the *tan1 air9* double mutant phenotype to wild-type levels, whereas expression in nondividing cells (driven by *pCaMV35S*) is not sufficient. These results further suggest that defects in the organization and growth of nondividing cells in the *tan1 air9* double mutant are the result of defects that occurred during mitosis.

I hypothesize that abnormal mechanical stresses that arise from cell wall positioning defects trigger stress responses that alter the growth and morphology of cells in the *tan1 air9* double mutant. Division plane positioning and mechanical stress are linked. Cortical microtubules align along the region of maximal stress, which can influence PPB positioning, and altering cell wall signaling responses can cause division plane orientation defects (Louveaux et al., 2016; Rasmussen et al., 2013; Wick and Duniec, 1983; Li et al., 2021). It is possible that cell wall stresses are heightened in the *tan1 air9* double mutant because phragmoplast guidance defects in the *tan1 air9* mutant prevent construction of new cell walls in

positions that minimize mechanical stress. This in turn could lead to increased stresses across the *tan1 air9* plant that trigger cell wall integrity responses which leads to slow growth and altered cell morphogenesis (Caño-Delgado et al., 2003; Wolf et al., 2014; Chaudhary et al., 2021; Li et al., 2021).

How cell wall stress and cell wall signaling may affect the *tan1 air9* double mutant remains to be studied. There are many cell wall integrity signaling pathways that allow plants to respond to mechanical stress (Rui and Dinneny, 2019). Pharmacological treatments that block or induce cell wall signaling pathways or mutants with altered cell wall signaling responses could be used to examine which pathways, if any, are active in the *tan1 air9* double mutant. If cell wall integrity signaling is heightened in *tan1 air9* double mutants, blocking certain signaling pathways may rescue growth and cell file twisting phenotypes. One receptor-like kinase of interest is THESEUS1 (THE1). Mutating *THE1* is sufficient to partially rescue the stunted growth of some cellulose deficient mutants (Hématy et al., 2007). Another example of how blocking cell wall signaling stress response can rescue stunted plant growth is the O-fucosyltransferase *esmeralda1* mutant which rescues the Wall Associated Kinase (WAK) hyperactive allele WAK2cTAP (Kohorn et al., 2021). Brassinosteroid (BR) hormone signaling plays a part in altering plant growth by mediating changes in the cell wall. Reduction of pectin methylesterase (PME) activity, which alters the mechanical property of the cell wall via de-methylesterification of the cell wall

component homogalacturonan, activates BR signaling (Wolf et al., 2014). BR signaling also influences division plane positioning and impairing BR signaling or overexpressing PME inhibitors (PMEI) alters cell wall orientation (Li et al., 2021). The potential role of BR signaling in the *tan1 air9* double mutant could be examined by reducing BR signaling by treating with the BR biosynthesis inhibitor propiconazole or by increasing BR signaling using PMEI overexpression lines (Hartwig et al., 2012; Li et al., 2021). Identifying specific cell wall integrity signaling responses that may be responsible for phenotypes observed in nondividing cells of *tan1 air9* double mutants will establish pathways that link division plane orientation, cell wall signaling, and plant morphogenesis.

REFERENCES

- Angulo, J., Astin, C.P., Bauer, O., Blash, K.J., Bowen, N.M., Chukwudinma, N.J., Dinofrio, A.S., Faletti, D.O., Ghulam, A.M., Gusinde-Duffy, C.M., Horace, K.J., Ingram, A.M., Isaack, K.E., Jeong, G., Kiser, R.I., Kobylanski, J.S., Long, M.R., Manning, G.A., Morales, J.M., Nguyen, K.H., Pham, R.T., Phillips, M.H., Reel, T.W., Seo, J.E., Vo, H.D., Wukuson, A.M., Yeary, K.A., Zheng, G.Y., Lukowitz, W. (2020).** Targeted mutagenesis of the Arabidopsis GROWTH-REGULATING FACTOR (GRF) gene family suggests competition of multiplexed sgRNAs for Cas9 apoprotein. *bioRxiv*. doi.org/10.1101/2020.08.16.253203.
- Buschmann, H., Chan, J., Sanchez-Pulido, L., Andrade-Navarro, M. A., Doonan, J. H. and Lloyd, C. W. (2006).** Microtubule-associated AIR9 recognizes the cortical division site at preprophase and cell-plate insertion. *Curr. Biol.* **16**, 1938–1943.
- Buschmann, H., Dols, J., Kopischke, S., Pen, E. J., Andrade-Navarro, M. A., Heinlein, M., Szymanski, D. B., Zachgo, S., Doonan, J. H. and Lloyd, C. W. (2015).** Arabidopsis KCBP interacts with AIR9 but stays in the cortical division zone throughout mitosis via its MyTH4-FERM domain. *J Cell Sci.* **128**(11): 2033–2046.
- Caño-Delgado, A., Penfield, S., Smith, C., Catley, M., and Bevan, M. (2003).** Reduced cellulose synthesis invokes lignification and defense responses in Arabidopsis thaliana. *Plant J.* **34**: 351–362.
- Chaudhary, A., Chen, X., Leśniewska, B., Boikine, R., Gao, J., Wolf, S., and Schneitz, K. (2021).** Cell wall damage attenuates root hair patterning and tissue morphogenesis mediated by the receptor kinase STRUBBELIG. *Development* **148**.
- Hartwig, T., Corvalan, C., Best, N.B., Budka, J.S., Zhu, J.-Y., Choe, S., and Schulz, B. (2012).** Propiconazole is a specific and accessible brassinosteroid (BR) biosynthesis inhibitor for Arabidopsis and maize. *PLoS One* **7**: e36625.
- Hématy, K., Sado, P.-E., Van Tuinen, A., Rochange, S., Desnos, T., Balzergue, S., Pelletier, S., Renou, J.-P., and Höfte, H. (2007).** A Receptor-like Kinase Mediates the Response of Arabidopsis Cells to the Inhibition of Cellulose Synthesis. *Current Biology* **17**: 922–931.

- Herrmann, A., Livanos, P., Lipka, E., Gadeyne, A., Hauser, M.-T., Van Damme, D., and Müller, S.** (2018). Dual localized kinesin-12 POK2 plays multiple roles during cell division and interacts with MAP65-3. *EMBO Rep.* **19**.
- Kohorn, B.D., Greed, B.E., Mouille, G., Verger, S., and Kohorn, S.L.** (2021). Effects of Arabidopsis wall associated kinase mutations on ESMERALDA1 and elicitor induced ROS. *PLoS One* **16**: e0251922.
- Kumari, P., Dahiya, P., Livanos, P., Zergiebel, L., Kölling, M., Poeschl, Y., Stamm, G., Hermann, A., Abel, S., Müller, S., and Bürstenbinder, K.** (2021). IQ67 DOMAIN proteins facilitate preprophase band formation and division-plane orientation. *Nat Plants* **7**: 739–747.
- Lipka, E., Gadeyne, A., Stöckle, D., Zimmermann, S., De Jaeger, G., Ehrhardt, D.W., Kirik, V., Van Damme, D., and Müller, S.** (2014). The Phragmoplast-Orienting Kinesin-12 Class Proteins Translate the Positional Information of the Preprophase Band to Establish the Cortical Division Zone in Arabidopsis thaliana. *Plant Cell* **26**: 2617–2632.
- Li, Z., Sela, A., Fridman, Y., Garstka, L., Höfte, H., Savaldi-Goldstein, S., and Wolf, S.** (2021). Optimal BR signalling is required for adequate cell wall orientation in the Arabidopsis root meristem. *Development* **148**.
- Louveaux, M., Julien, J.-D., Mirabet, V., Boudaoud, A. and Hamant, O.** (2016). Cell division plane orientation based on tensile stress in Arabidopsis thaliana. *Proc. Natl. Acad. Sci. U. S. A.* **113** (30) E4294-E4303.
- Martinez, P., Luo, A., Sylvester, A., and Rasmussen, C.G.** (2017). Proper division plane orientation and mitotic progression together allow normal growth of maize. *Proc. Natl. Acad. Sci. U. S. A.* **114**: 2759–2764.
- Mills, A., Jaganatha, V., Cortez, A., Guzman, M., Burnette, J.M., Collin, M., Lopez-Lopez, B., Wessler, S.R., Van Norman, J.M., Nelson, D.C., and Rasmussen, C.G.** (2021). A Course-Based Undergraduate Research Experience in CRISPR-Cas9 Experimental Design to Support Reverse Genetic Studies in Arabidopsis thaliana. *Journal of Microbiology & Biology Education.* **22**, (2) e00155-21.

- Mills, A.M., Morris, V.H., and Rasmussen, C.G.** (2022). The localization of PHRAGMOPLAST ORIENTING KINESIN1 at the division site depends on two microtubule binding proteins TANGLED1 and AUXIN-INDUCED-IN-ROOT-CULTURES9 in Arabidopsis. bioRxiv doi.org/10.1101/2022.04.27.489732
- Mills, A.M. and Rasmussen, C.G.** (2022). Action at a distance: Defects in division plane positioning in the root meristematic zone affect cell organization in the differentiation zone. bioRxiv doi.org/10.1101/2021.04.30.442137
- Rasmussen, C.G., Sun, B., and Smith, L.G.** (2011). Tangled localization at the cortical division site of plant cells occurs by several mechanisms. *J. Cell Sci.* **124**: 270–279.
- Rasmussen, C. G., Wright, A. J. and Müller, S.** (2013). The role of the cytoskeleton and associated proteins in determination of the plant cell division plane. *Plant J.* **75**, 258–269.
- Rui, Y., and Dinneny, J.R.** (2019). A wall with integrity: surveillance and maintenance of the plant cell wall under stress. *New Phytologist.* **225**: 1428-1439.
- Stöckle, D., Herrmann, A., Lipka, E., Lauster, T., Gavidia, R., Zimmermann, S., and Müller, S.** (2016). Putative RopGAPs impact division plane selection and interact with kinesin-12 POK1. *Nat Plants* **2**: 16120.
- Su, T.** (2012). Proteins that Interact with Arabidopsis TANGLED. UC San Diego. ProQuest ID: Su_ucsd_0033M_12339. Merritt ID: ark:/20775/bb3926230d. Retrieved from <https://escholarship.org/uc/item/5bx9v4v9>
- Walley, J.W., Sartor, R.C., Shen, Z., Schmitz, R.J., Wu, K.J., Urich, M.A., Nery, J.R., Smith, L.G., Schnable, J.C., Ecker, J.R., and Briggs, S.P.** (2016). Integration of omic networks in a developmental atlas of maize. *Science* **353**: 814–818.
- Wang, Z.-P., Xing, H.-L., Dong, L., Zhang, H.-Y., Han, C.-Y., Wang, X.-C., and Chen, Q.-J.** (2015). Egg cell-specific promoter-controlled CRISPR/Cas9 efficiently generates homozygous mutants for multiple target genes in Arabidopsis in a single generation. *Genome Biology* **16**.

- Wick, S.M. and Duniec, J.** (1983). Immunofluorescence microscopy of tubulin and microtubule arrays in plant cells. I. Preprophase band development and concomitant appearance of nuclear envelope-associated tubulin. *J. Cell Biol.* **97**: 235–243.
- Wolf, S. et al.** (2014). A receptor-like protein mediates the response to pectin modification by activating brassinosteroid signaling. *Proc. Natl. Acad. Sci. U. S. A.* **111**: 15261–15266.
- Xu, X.M., Zhao, Q., Rodrigo-Peiris, T., Brkljacic, J., He, C.S., Müller, S., and Meier, I.** (2008). RanGAP1 is a continuous marker of the Arabidopsis cell division plane. *Proc. Natl. Acad. Sci. U. S. A.* **105**: 18637–18642.